



UNIVERSITY OF
BIRMINGHAM

EVALUATION OF POLY-ETHER-ETHER-KETONE
(PEEK) FOR CERVICAL DISC REPLACEMENT

DEVICES

by

HUA XIN

A thesis submitted to the
University of Birmingham for the degree of
DOCTOR OF PHILOSOPHY

School of Mechanical Engineering

University of Birmingham

October 2013

UNIVERSITY OF
BIRMINGHAM

University of Birmingham Research Archive

e-theses repository

This unpublished thesis/dissertation is copyright of the author and/or third parties. The intellectual property rights of the author or third parties in respect of this work are as defined by The Copyright Designs and Patents Act 1988 or as modified by any successor legislation.

Any use made of information contained in this thesis/dissertation must be in accordance with that legislation and must be properly acknowledged. Further distribution or reproduction in any format is prohibited without the permission of the copyright holder.

ABSTRACT

Poly-ether-ether-ketone (PEEK) is a high performance aromatic thermoplastic with proven biocompatibility. Recently, it has been proposed as a promising bearing material for cervical total disc replacement (TDR). A new bearing combination of PEEK-on-PEEK based self-mating articulation has been used, which may overcome current bearing materials related complications.

For ball-on-socket based cervical TDR designs, PEEK based bearing articulation is expected to operate under a boundary lubrication regime regardless of the radial clearance used. The contact stress encountered by the bearing surfaces is insufficient to result in either material yield or fatigue failure.

High-cycle fatigue tests were performed on PEEK 450G specimens via three-point flexural bending. The obtained fatigue results (104.1 ± 5.8 MPa) show superiority over the historical polymeric bearing material UHMWPE (31 MPa). Moreover, it demonstrates a good resistance to sterilisation and thermal ageing. Laboratory wear simulation was also conducted, using spine simulators and following ISO 18192-1 standard. For PEEK-on-PEEK self-mating articulation, a steady state wear rate of 1.0 ± 0.9 mg/million cycles is

obtained, which is comparable as the historical bearing combination (UHMWPE against CoCrMo). The results of this work suggest that PEEK-on-PEEK based articulation is a possible alternative for future cervical TDR designs.

ACKNOWLEDGEMENT

I take this opportunity to extend my sincere and heartfelt gratitude to my supervisors Dr. Duncan Shepherd and Dr. Karl Dearn. Without their active guidance, selfless help, encouragement and inspiration, this work would not have materialized.

I am extremely thankful to Dr William Murray, Mr Carl Hingley and Dr James Bowen for their valuable suggestions and technical supports on the completion of the experimental aspect of this thesis.

My special thanks are extended to my friends Miss Jing Jin and Mr Lu Cao for their support and companionship.

At last but not least, I express my deepest appreciation to my parents for their endless love, spiritual encouragement and financial support. Without them, I wouldn't be where I am today.

TABLE OF CONTENT

Chapter 1: Introduction.....	1
Chapter 2: Background.....	6
2.1 Chapter overview.....	6
2.2 Cervical spine.....	7
2.2.1 Anatomy of the spine.....	7
2.2.2 Intervertebral disc.....	9
2.2.3 Biomechanics of the cervical spine.....	12
2.2.3.1 Anatomic coordinates.....	12
2.2.3.2 Motion of the cervical spine.....	13
2.2.3.3 Loading of the cervical spine.....	14
2.2.3.4 Standard test method for spinal implants.....	15
2.2.4 Spinal pain.....	17
2.2.4.1 Introduction.....	17
2.2.4.2 Nature of disc degeneration & ageing.....	18
2.2.4.3 General treatments.....	19
2.3 Total disc replacement.....	21
2.3.1 Introduction.....	21
2.3.2 Contemporary cervical disc designs.....	22

2.3.3 Wear debris induced issues (bearing material combinations).....	26
2.4 PEEK as a biomaterial.....	28
2.4.1 Introduction.....	28
2.4.2 Chemical structure.....	29
2.4.3 Fabrication of PEEK based devices.....	31
2.4.4 Mechanical properties of PEEK.....	31
2.4.5 Biocompatibility of PEEK.....	34
2.4.5.1 Introduction.....	34
2.4.5.2 Implant form.....	35
2.4.5.3 Particulate form.....	36
2.5 Basic tribology.....	37
2.5.1 Introduction.....	37
2.5.2 Friction.....	38
2.5.3 Wear.....	39
2.5.4 Lubrication.....	41
2.6 Chapter summary.....	42
Chapter 3: General Materials & Methods.....	43
3.1 Chapter overview.....	43
3.2 Materials.....	44
3.2.1 PEEK 450G.....	44

3.2.2 NuNec [®] cervical discs.....	45
3.3 Equipments.....	47
3.3.1 Coordinate Measuring Machine (CMM).....	47
3.3.2 Talysurf 120L.....	48
3.3.3 Lloyd 6000R.....	51
3.3.4 Bose ELF-3300 test machine.....	52
3.3.5 Bose spine simulator.....	54
3.3.6 Bose ELF-3330 test machine.....	58
3.3.7 Interferometer.....	59
3.3.8 Rheometer.....	62
3.4 Methods.....	64
3.4.1 Preparation of the disc samples.....	64
3.4.2 Clean, dry & weighing protocol.....	64
3.4.3 Lubricant preparation.....	65
3.5 Chapter summary.....	66
Chapter 4: Contact Stress & Lubrication Analysis...67	
4.1 Chapter overview.....	67
4.2 Introduction.....	68
4.3 Materials & Methods.....	70
4.3.1 Disc Model.....	70
4.3.2 Contact Stress.....	71

4.3.2.1 <i>Hertzian contact model</i>	71
4.3.2.2 <i>Johnson-Kendall-Roberts contact model</i>	72
4.3.3 Lubrication regimes	73
4.3.3.1 <i>Lambda ratio</i>	73
4.3.3.2 <i>Minimum effective film thickness</i>	73
4.3.4 Parameters	74
4.3.4.1 <i>Radii of the socket & ball</i>	74
4.3.4.2 <i>Contact surface roughness measurement</i>	75
4.3.4.3 <i>Other parameters</i>	75
4.4 Results	77
4.4.1 Contact stress	77
4.4.2 Lubrication	79
4.5 Discussion	84
4.6 Chapter summary	86

Chapter 5: Strength of PEEK – Effects of Thermal Ageing & Gamma Sterilisation.....87

5.1 Chapter overview	87
5.2 Background	88
5.2.1 Introduction	88
5.2.2 Polymer fatigue	89
5.2.3 Fatigue assessment approach	89

5.2.4 Historical studies of PEEK fatigue.....	90
5.2.5 Accelerated ageing of PEEK.....	92
5.2.6 Sterilisation.....	94
5.3 Materials & Methods.....	94
5.3.1 PEEK specimen preparation.....	94
5.3.2 Annealing, sterilisation & ageing.....	95
5.3.3 Testing rig (three-point bending).....	97
5.3.4 Static tests.....	97
5.3.5 Dynamic tests.....	98
5.3.6 Scanning electron microscopy.....	99
5.3.7 Statistical analysis.....	100
5.4 Results.....	101
5.4.1 Static tests.....	101
5.4.2 Dynamic tests.....	103
5.4.3 Scanning electron microscopy.....	104
5.5 Discussion.....	107
5.5.1 Static results.....	107
5.5.2 Fatigue results.....	108
5.5.3 Thermal ageing.....	110
5.6 Chapter summary.....	111

Chapter 6: Tribological Assessment of NuNec[®] Cervical Disc Replacement.....112

6.1 Chapter overview.....	112
6.2 Introduction.....	113
6.2.1 Historical review of PEEK tribological studies.....	113
6.2.2 Lubricant.....	116
6.3 Materials & Methods.....	119
6.3.1 Test specimens.....	119
6.3.2 Disc fixture.....	119
6.3.3 Wear testing	122
6.3.3.1 Fixation & alignment.....	123
6.3.3.2 Loading & motions.....	123
6.3.3.3 Bovine serum based lubricate.....	125
6.3.3.4 Gravimetric wear measurement.....	125
6.3.3.5 Surface characterization.....	126
6.3.4 Frictional torque.....	126
6.3.5 Statistical analysis.....	129
6.4 Results.....	130
6.4.1 Wear results.....	130
6.4.2 Surface topology.....	134
6.4.3 Frictional results.....	136

6.4.4 Stribeck plot.....	139
6.5 Discussion.....	142
6.5.1 Wear.....	142
6.5.2 Frictional torque.....	145
6.5.3 Hydroxyapatite.....	148
6.6 Chapter summary.....	148
Chapter 7: Overall Discussion & Conclusions.....	150
Glossary.....	155
Appendix A.....	159
Appendix B.....	161
Appendix C.....	165
References.....	168

LIST OF FIGURES

Fig. 2.1: Anatomy structure of the spine (author's own photograph, adapted from Kurtz & Edidin, 2006).....	8
Fig. 2.2: The essential structure of a typical cervical vertebra (adapted from Louis-Ugbo <i>et al.</i> , 2012).....	9
Fig. 2.3: The essential components of intervertebral disc (Guerin & Elliott, 2006).....	11
Fig. 2.4: Anatomic coordinate system (author's own photographs, adapted from Kurtz & Edidin, 2006).....	12
Fig. 2.5: The kinematic motions of the spine a) extension, b) flexion, c) lateral bend, and d) axial rotation.....	13
Fig. 2.6: Contemporary cervical disc designs a) Prodisc-C, b) PCM, c) Prestige [®] ST and d) Bryan (adapted from Kurtz, 2006).....	23
Fig. 2.7: a) PEEK chemical structure unit and b) Orthorhombic crystal unit cell for PEEK (adapted from Kurtz & Devine, 2007).....	30
Fig. 2.8: Schematic diagram of a) boundary lubrication, b) mixed lubrication and c) fluid-film lubrication (author's own drawing, adapted from Jin & Fisher, 2008).....	42
Fig. 3.1: PEEK 450G sheet.....	44
Fig. 3.2: The NuNec [®] cervical disc arthroplasty system a) assembled and b) disassembled.....	46
Fig. 3.3: DEA-Swift CMM. The measuring ranges are 510 mm (X-axis: lateral direction), 410 mm (Y-axis: anterior-posterior direction) and 330 mm (Z-axis: inferior-superior direction).....	48
Fig. 3.4: Taylsurf-120L. The measuring range is 10 mm and the measuring speed is 0.5 mm/s.....	50

Fig. 3.5: The 3D surface roughness for convex surface (ball component) after separation of waviness, using a cut-off length 0.8mm.....	51
Fig. 3.6: Lloyd 6000R materials testing machine. The vertical travel length of the crosshead is roughly equal to 1000 mm.....	52
Fig. 3.7: Bose ELF 3300 material test machine.....	54
Fig. 3.8: Bose SDWS-1single station spine simulator equipped with a multi-axial load cell. Black dashed lines represent the x, y, and z axes. The red dot is the location of the centre of rotation of this spine simulator.....	56
Fig. 3.9: a) uni-axial load cell and b) multi-axial load cell.....	57
Fig. 3.10: Essential components of Bose Spine Simulator. A) actuator, C) computer, T) temperature module, P) power tower, and W) main test chamber.....	57
Fig. 3.11: a) Enlarged view of the main test chamber, b) thermal chamber with lower adaptor and c) heating block.....	58
Fig. 3.12: Bose ELF-3330 II material test machine.....	59
Fig. 3.13: The KLA-Tencor MicroXAM2 interferometer.....	61
Fig. 3.14: An example of the 3D surface roughness image. Scanning area is 639 x 859 μm , at the centre of the sample.....	62
Fig. 3.15: Picture of AR-G2 rheometer.....	63
Fig. 4.1: Schematic diagram showing the geometry of the ball-and-socket joint (adapted from Wenzel & Shepherd, 2007).....	70
Fig. 4.2: Variation of maximum contact stress with force, for radial clearance values of 0.05, 0.10, 0.15 and 0.7 mm.....	78
Fig. 4.3: Variation of maximum contact stress with force for a radial clearance value of 0.7 mm, calculated using the Hertz and JKR contact model.....	79
Fig. 4.4: a) Variation of minimum film thickness with angular velocity; b) Variation of Lambda ratio with angular velocity. Each figure is plotted for a	

cervical disc arthroplasty under 150 N load, using interstitial fluid as the lubricant.....	81
Fig. 4.5: a) Variation of minimum film thickness with angular velocity; b) Variation of Lambda ratio with angular velocity. Each figure is plotted for a cervical disc arthroplasty at a radial clearance value of 0.7 mm, using interstitial fluid as the lubricant.....	82
Fig. 4.6: a) Variation of minimum film thickness with angular velocity; b) Variation of Lambda ratio with angular velocity. Each figure is plotted for a cervical disc arthroplasty at a radial clearance value of 0.7 mm, under 150 N load.....	83
Fig. 5.1: PEEK 450G rectangular specimens (nominal thickness is 6 mm).....	95
Fig. 5.2: Three-point bend test rig.....	97
Fig. 5.3: Load-displacement curve for Group 3, specimen 2.....	102
Fig. 5.4: Stress against number of cycles to failure (or run out); x-axis is on a logarithmic scale, base 10.....	104
Fig. 5.5: SEM image for Group 3 dynamic, specimen 10 (the large white arrow indicates the fracture direction from right to left).....	105
Fig. 5.6: a) Enlarged beech mark region, b) Void nucleation site and c) Fine fatigue striation.....	106
Fig. 6.1: Vertical distances from the top plate to the COR of the spine simulator (16 mm) and the lower plate (23.5 mm). Black dashed lines represent the top and lower plate levels, respectively. The red dashed line represents the level of the COR.....	121
Fig. 6.2: Schematic diagram of the disc fixtures. The red dot represents the COR of the ball component.....	122
Fig. 6.3: a) lower ball fixture, b) locking pins and c) upper socket fixture...	122
Fig. 6.4: Angular displacement and load curves of the spine simulator (adapted from ISO 18192-1, 2011).....	124

Fig. 6.5: A typical Stribeck curve (author’s own drawing, adapted from Jin & Fisher, 2008). Region a) indicates boundary lubrication; b) indicates mixed lubrication; and c) indicates fluid-film lubrication.....127

Fig. 6.6: Variation of viscosity against shear rate. Axes are on log 10 based scale.....129

Fig. 6.7: Cumulative mass loss against number of cycles, for each disc. Discs 1-3 are the testing specimens and disc 4 is the load soak control specimen.....132

Fig. 6.8: Disc 1 superior end plate a) pre-wear and b) after 5 million cycles wear test. Note the light grey hydroxyapatite coating was completely removed.....132

Fig. 6.9: Mean PEEK mass loss against number of cycles for discs 1 to 3. Error bars represent the standard deviation. Two regression lines have been fitted by $y = 4.7x - 0.3$ ($R^2 = 0.98$) and $y = x + 7.8$ ($R^2 = 0.91$) to show the initial run-in phase and steady-state phase.....133

Fig. 6.10: Disc 1 ball part a) pre-wear and b) after 5 million cycles.....135

Fig. 6.11: Surface scan of disc 1 a) ball pre-wear, b) socket pre-wear, c) ball after 5 million cycles, and d) socket after 5 million cycles. Area of view is 639 x 859 μm at the pole of the specimen.....135

Fig. 6.12: Mean frictional torques of discs (1 to 3), under flexion motion (0 to $+7.5^\circ$), before and after wear testing, plotted against frequency. Error bars represent 95% confidence intervals.....137

Fig. 6.13: Mean frictional torques of discs(1 to 3), under lateral bending motion (0 to $+4^\circ$), before and after wear testing, plotted against frequency. Error bars represent 95% confidence intervals.....138

Fig. 6.14: Mean frictional torques of discs (1 to 3), under rotation motion (0 to $+2^\circ$), before and after wear testing, plotted against frequency. Error bars represent 95% confidence intervals.....139

Fig. 6.15: Stribeckplot for disc samples under flexion motion (0 to $+7.5^\circ$). A third order polynomial has been fitted to the data points.....140

Fig. 6.16: Stribeck plot for disc samples under lateral bending motion (0 to +4°). A third order polynomial has been fitted to the data points.....141

Fig. 6.17: Stribeck plot for disc samples under axial rotation motion (0 to +2°). A third order polynomial has been fitted to the data points.....142

LIST OF TABLES

Table 2.1: Range of motion (mean \pm standard deviation) for each cervical spine segment (Panjabi <i>et al.</i> , 2001)	14
Table: 2.2: Range of motion for cervical spine as defined by ASTM F2423 (2005) and ISO 18192-1 (2011).....	16
Table: 2.3: Recommended axial loading for wear testing of cervical disc prosthesis as defined by ASTM F2423 (2005) and ISO 18192-1(2011).....	16
Table 2.4: Typical material properties of PEEK 450G and PEEK Optima-LT1, compared with ASTM PEEK biomaterial specification and UHMWPE (Kurtz & Devine, 2007; ASTM F2026, 2010; PEEK TM 450G datasheet, 2012; PEEK Optima-LT1 product specification, 2012).....	33
Table 4.1: Summary of constant parameters and variables used.....	77
Table 5.1: Test conditions of historical PEEK fatigue studies.....	91
Table 5.2: Pre-treatments and subsequent static and dynamic test methods for all PEEK 450G specimens.....	96
Table 5.3: Load at yield, deflection at yield and flexural strength for the static tests on the five groups of specimens. (All values mean \pm standard deviation).....	102
Table 5.4: Coefficients of linear regression lines.....	104
Table 6.1: PEEK self-mating wear performance (Historical control bearing combination of UHMWPE against CoCrMo is also included for comparison purpose).....	114
Table 6.2: Essential testing conditions for studies shown in Table 6.1.....	115
Table 6.3: Some of the major composition of human interstitial fluid, blood plasma, bovine serum, and human synovial fluid (Fogh-Andersen <i>et al.</i> , 1995; Joshi & Joshi-Mendhurwar, 2005; Harsha & Joyce, 2011; Aaronson <i>et al.</i> , 2012).....	117

Table 6.4: The mass loss rate for each individual disc, under different wear stages. The mean mass loss and mean volume loss are also presented ...134

Table 6.5: Surface roughness values (mean \pm SD.) during wear testing for discs 1 to 3.....136

Chapter 1

Introduction

Cervical total disc replacement (TDR) is a motion preserving surgical intervention, which is used to treat disc degeneration, radiculopathy and myelopathy (Kurtz, 2006; Auerbach *et al.*, 2008). Among the contemporary disc replacement designs, a variety of bearing materials has been used which includes ultra high molecular weight polyethylene (UHMWPE), cobalt chromium molybdenum alloy (CoCrMo) and stainless steel. Wear debris generated by these materials may lead to a series of complications (e.g. osteolysis and hypersensitivity) (Brown, 2006) and significantly reduce the intended longevity of the disc replacement device.

Recently, a novel all polymer based cervical TDR design NuNec[®] disc arthroplasty system (Pioneer Surgical Technology Inc., Driebergen, Netherlands) has been introduced into the market. A poly-ether-ether-ketone (PEEK) based self-mating bearing combination is used, due to a combination of good mechanical strength (Jones *et al.*, 1985) and proven biocompatibility (Jeffery, 2012).

This PEEK-on-PEEK based cervical TDR design is brand new. There is lack of information regarding its likely lubrication regime and contact stress, under natural cervical spine operating conditions. A comprehensive theoretical

lubrication regime and contact stress analysis is needed, which provides a rationale for the design of cervical TDR using PEEK.

Polymers are susceptible to the effect of radiation sterilisation and ageing. For example, UHMWPE shows a significantly reduced fatigue strength after sterilisation in air (Sauer *et al.*, 1996). Moreover, the ageing of a polymer occurs both *in-vivo* and *in-vitro*, which may lead to a change of polymer properties over time (White, 2006; Ratner, 2012). Investigation of the effects of sterilisation and ageing on the mechanical strength of PEEK is necessary.

Since wear debris induced complications are a major failure mode for cervical TDRs, assessment of wear performance of a new bearing combination is necessary. Normally, cervical TDRs are expected to function for over two decades (Kurtz & Edidin, 2006), therefore good durability (*i.e.* low wear rate) of the bearing material is crucial.

In this thesis, PEEK was evaluated, based on its tribological and fatigue performance. The aim of the research work was to provide a complete understanding of PEEK biomaterial for the application of cervical TDR designs.

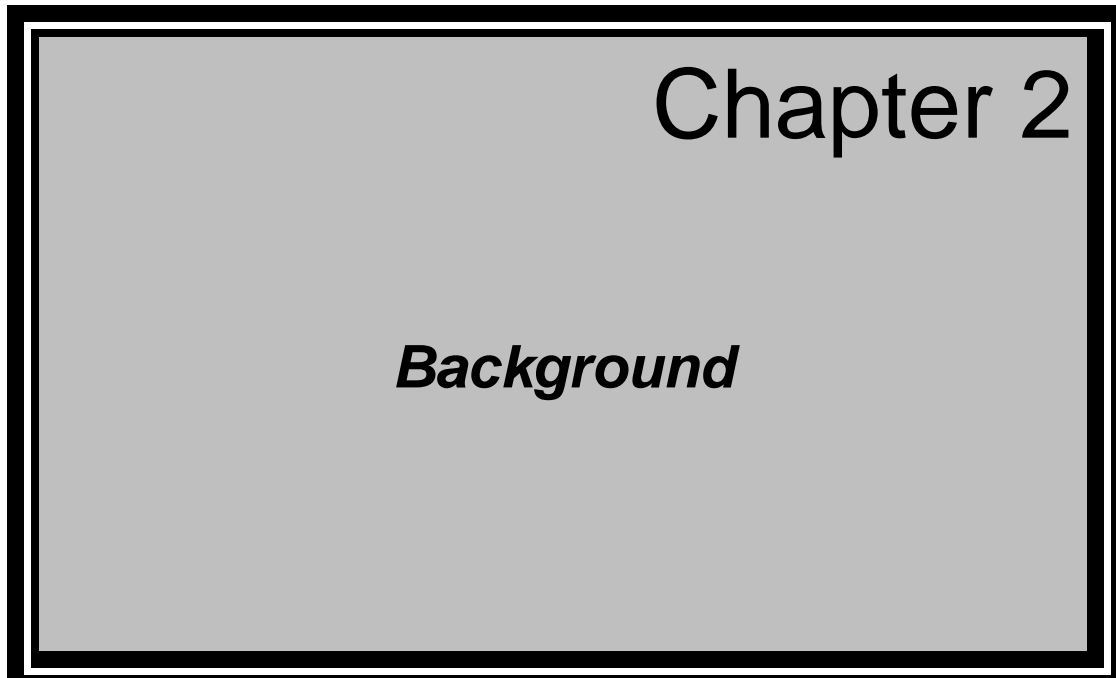
To achieve this aim, the following objectives were undertaken:

- to investigate the effect of radial clearance on the maximum contact stress and lubrication regime of PEEK based cervical TDRs.
- to assess the strength of PEEK (static and fatigue) after ageing and sterilisation.
- to assess the tribological performance of the NuNec[®] cervical disc under laboratory conditions, by determining the wear rate and lubrication regime.

To meet the objectives of this work, the studies that were performed are described in the chapters summarised below.

Chapter 2 provides the essential background for the research conducted in this thesis. Information regarding the cervical spine, TDRs and PEEK is given. In chapter 3, the general materials and methods used for the following chapters (4-6) are provided. Chapter 4 presents a theoretical analysis of PEEK based cervical TDRs. In this chapter, the peak contact stress and minimum lubrication film thickness between the bearing surfaces were determined, as the radial clearance or lubricant was varied. Chapter 5 investigates the effects of thermal ageing and gamma sterilisation on the flexural strength of PEEK 450G. In this chapter, the static and fatigue strength of PEEK 450G were obtained via three-point flexural bend tests. Chapter 6 presents an *in-vitro* tribological assessment of the NuNec[®] cervical disc replacement. 5 million

cycle wear simulations were performed using single station spine simulators, following the ISO 18192-1 (2011) standard. Friction tests were also conducted, before and after wear tests; the corresponding lubrication regimes were determined via Stribeck analysis. Finally, in chapter 7, an overall discussion and conclusion is provided regarding the applicability of PEEK for a cervical disc replacement design.



2.1 Chapter overview

This chapter provides the background for the research conducted in this thesis. The anatomy and biomechanics of the spine, intervertebral disc degeneration and general treatments for this condition are given in section 2.2. Total disc replacement is briefly introduced in section 2.3. The basic mechanical properties of PEEK and its biocompatibility are discussed in section 2.4. Since this thesis involves the study of friction, wear and lubrication, knowledge of tribology is required (section 2.5). The chapter closes with a summary of the background information in section 2.6.

2.2 Cervical spine

2.2.1 Anatomy of the spine

The human spine is divided into five regions as shown in Fig. 2.1. From cranial to caudal, the first seven (C1-C7) vertebrae constitute the cervical spine which provide neck flexibility and head movement (Kurtz & Edidin, 2006). The atlas (C1) and axis (C2) are very different to the rest of the cervical vertebrae; they form a synovial joint rather than being separated by an intervertebral disc (McMinn *et al.*, 1998). The first intervertebral disc locates between the C2 and C3 vertebral bodies, and is normally named according to its adjacent vertebrae.

Each individual cervical vertebra comprises several essential structures (Fig. 2.2). A flat slightly concaved vertebra body serves as the main load-bearing region, thus spinal load can transmit along the vertebra column. Foramen formed by the lamina and pedicles provides a central pathway for the spinal cord. The orthogonally located spinous process and transverse processes provide anchor points for muscle and soft tissue attachment. Articular processes lead to the formation of facet joints with adjacent vertebrae (McMinn *et al.*, 1998; Louis-Ugbo *et al.*, 2012). Facet joints are hinge-like synovial joints which control spinal motion and aid spinal column stability.

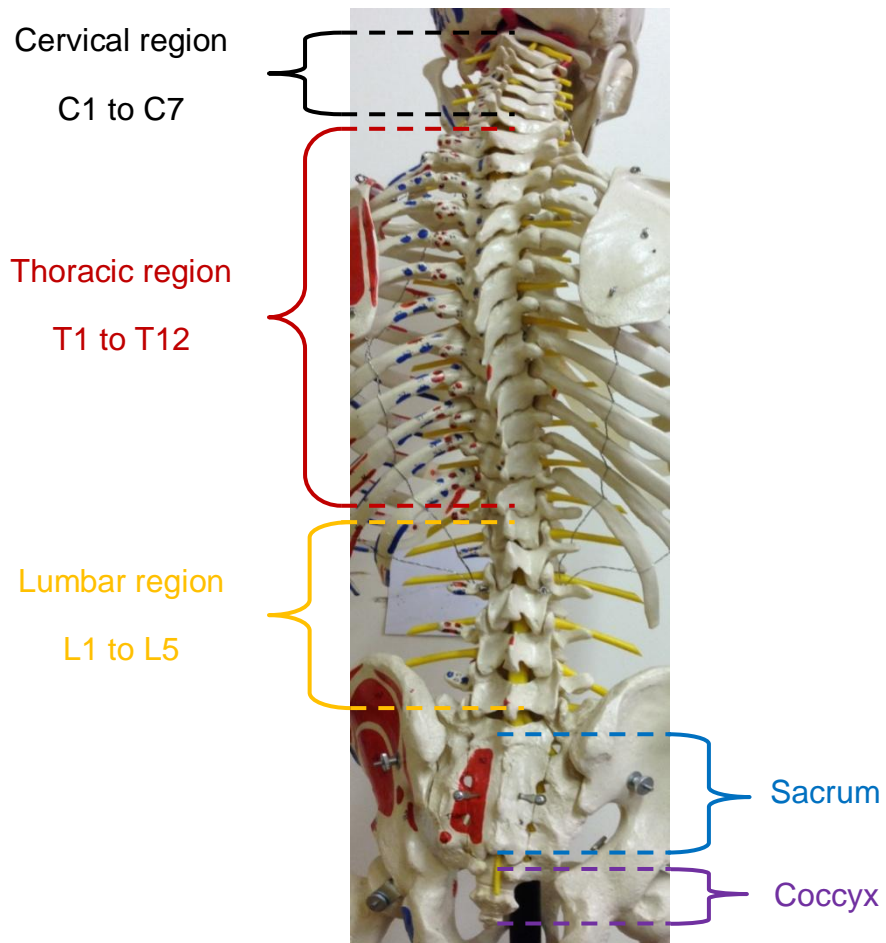


Fig. 2.1: Anatomy structure of the spine (author's own photograph, adapted from Kurtz & Eddin, 2006).

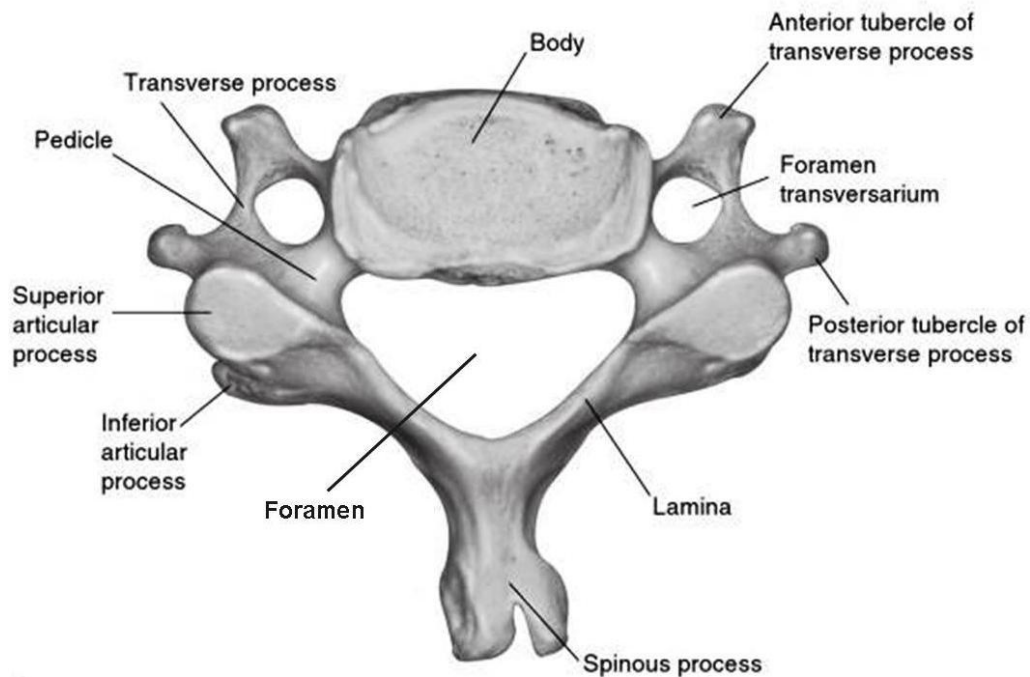


Fig. 2.2: The essential structure of a typical cervical vertebra (adapted from Louis-Ugbo *et al.*, 2012).

2.2.2 Intervertebral disc

The intervertebral disc is a fibrocartilagenous structure situated between each of the rigid vertebrae (Roberts *et al.*, 2006). It allows spinal motions and contributes to the overall stability of the spinal column (Guerin & Elliott, 2006). Each disc includes several essential components as shown in Fig. 2.3. An inner gelatinous nucleus pulposus is surrounded by an outer annulus fibrosus (*i.e.* fibrous ring). Two cartilaginous endplates are located at the superior and inferior of the intervertebral disc, and adjacent to the vertebrae. The shape and size of the intervertebral discs vary along the spinal column. The cervical disc

is relatively small, with a round cross-section, which facilitates maximum flexibility of the neck. In contrast, the lumbar disc is optimised for structural support, with a larger kidney-like cross-section (Kurtz & Edidin, 2006).

The nucleus pulposus is composed of randomly distributed collagen fibrils in a hydrated extrafibrillar matrix. The main constituent is water which accounts for 70-80% of its mass (Guerin & Elliott, 2006). Apart from water, collagens and proteoglycans contribute to most of its dry mass (Cassinelli *et al.*, 2001; Guerin & Elliott, 2006). The predominated proteoglycans in the intervertebral disc is aggrecan (*i.e.* chondroitin sulphate) which is composed of many glycosaminoglycan (GAG) molecules and a core protein (Cassinelli *et al.*, 2001). Since the GAG is negatively charged, it leads to the formation of an osmotic pressure within the nucleus pulposus. Water molecules are drawn into the nucleus pulposus, and this process is called pressurization. The ability of the nucleus pulposus to pressurize is essential for efficiently absorbing and transmitting axial loads through the spine (Guerin & Elliott, 2006; Pruitt & Chakravartula, 2011).

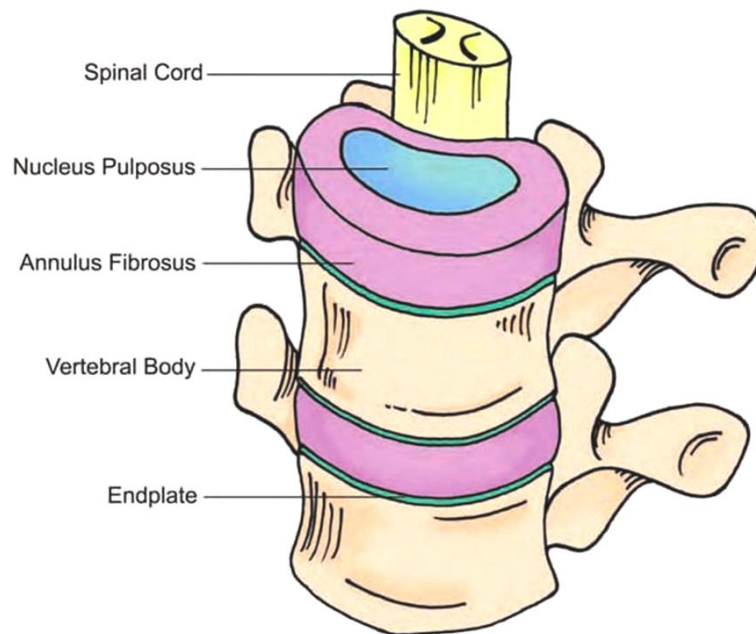


Fig. 2.3: The essential components of intervertebral disc (Guerin & Elliott, 2006).

Apart from intervertebral disc, other soft tissues of the spine include ligaments and the spinal cord which splits into the cauda equina at the lumbar vertebrae (Guerin & Elliott, 2006). Ligaments are connective tissues which tether the vertebrae together, aid stable spinal motion and prevent injury from overextension (Guerin & Elliott, 2006; Pruitt & Chakravartula, 2011). The spinal cord is a soft fragile neuron structure which conducts nerve impulse and actuates muscle contraction (Guerin & Elliott, 2006).

2.2.3 Biomechanics of the cervical spine

2.2.3.1 Anatomic coordinates

The kinematic motions of the spine are normally described according to an anatomic reference frame (*i.e.* anatomic coordinates). In the anatomic coordinates (Fig. 2.4), superior and inferior indicates the upward and downward vertical directions, respectively. The front of the body is called anterior, while the back of the body is termed posterior. The left and right side of the body are the lateral sides and the medial direction is defined as towards the middle of the body (McMinn *et al.*, 1998; Kurtz & Edidin, 2006).

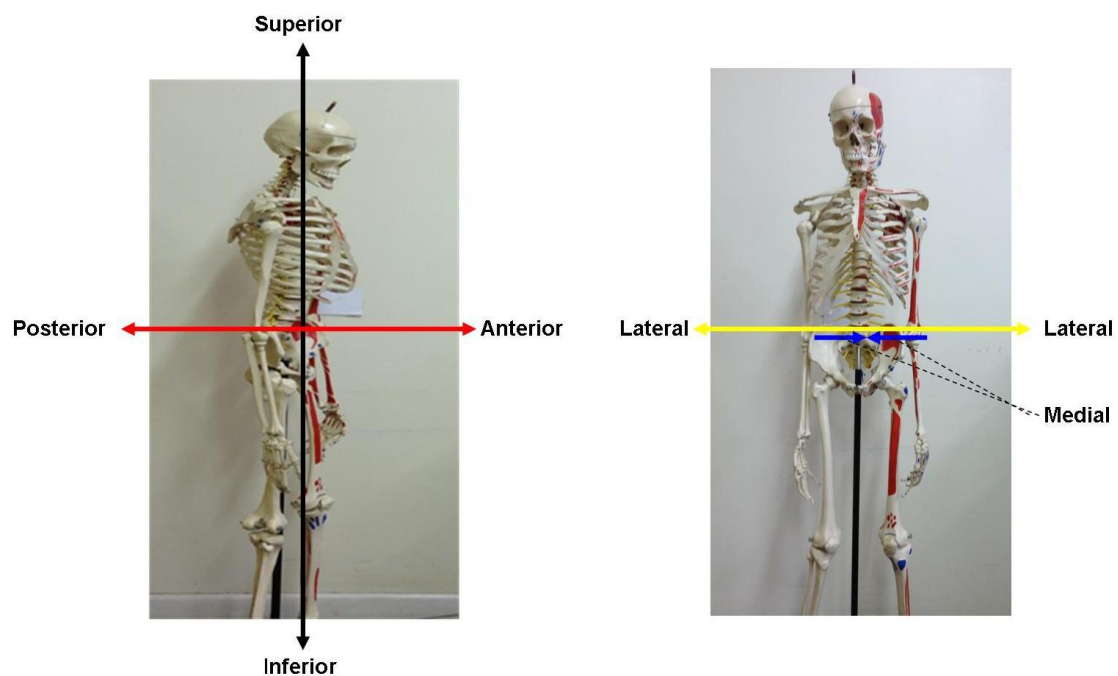


Fig. 2.4: Anatomic coordinate system (author's own photographs, adapted from Kurtz & Edidin, 2006).

2.2.3.2 Motion of the cervical spine

The human spine offers a range of motions as shown in Fig. 2.5. Flexion-extension motion means the body bending in the anterior-posterior directions, respectively. Sideways bending of the body is known as lateral bending and axial torsion refers to axial rotation (Kurtz & Edidin, 2006). In the C3-C7 region, the observed maximum ranges of angular motion are $\pm 10^\circ$, $\pm 11^\circ$ and $\pm 7^\circ$ for flexion-extension, lateral bending and axial rotation, respectively (Dvorak *et al.*, 1992). A detailed description of the ranges of motion for each cervical spine segment is shown in Table 2.1.



Fig. 2.5: The kinematic motions of the spine a) extension, b) flexion, c) lateral bend, and d) axial rotation.

Table 2.1: Range of motion (mean \pm standard deviation) for each cervical spine segment (Panjabi *et al.*, 2001).

Disc Segment	Flexion [°]	Extension [°]	Lateral bend [°]	Axial rotation [°]
C2-C3	3.5 \pm 1.3	2.7 \pm 1.0	9.6 \pm 1.8	3.3 \pm 0.8
C3-C4	4.3 \pm 2.9	3.4 \pm 2.1	9.0 \pm 1.9	5.1 \pm 1.2
C4-C5	5.3 \pm 3.0	4.8 \pm 1.9	9.3 \pm 1.7	6.8 \pm 1.3
C5-C6	5.5 \pm 2.6	4.4 \pm 2.8	6.5 \pm 1.5	5.0 \pm 1.0
C6-C7	3.7 \pm 2.1	3.4 \pm 1.9	5.4 \pm 1.5	2.9 \pm 0.8

2.2.3.3 Loading of the cervical spine

The loads acting on the cervical spine mainly arise from the weight of the head. Moreover, posture induced muscle contraction can result in additional compressive forces acting on the cervical spine (Cripton *et al.*, 2006). Spinal loading can be determined experimentally via the measurement of intradiscal pressures (*i.e.* the hydrostatic pressure of the nucleus pulposus). This technique is based on the fact that intradiscal pressure is linearly related to the applied load (Nachemson, 1981; Cripton *et al.*, 2001).

The intradiscal pressures of the cervical discs were found to be similar among different disc levels, by Hattori *et al.* (1981). In this study, the *in-vivo* intradiscal pressures were measured under a range of head postures. By using Hattori's

in-vivo intradiscal pressure results and applying the Nachemson's relationship (1981) (cited in Cripton *et al.*, 2006) between the intradiscal pressure and applied force, the cervical spine load can be predicted. It is estimated to be in the range of 53 to 155 N for each cervical disc, and the standard upright position imposes 75 N compressive load (Cripton *et al.*, 2006).

2.2.3.4 Standard test method for spinal implants

Apart from the above mentioned literature findings, the International Standard Organization (ISO) and the American Society for Testing and Materials (ASTM) published the ISO 18192-1 (2011) and ASTM F2423 (2005) protocols for *in-vitro* wear testing of disc replacement devices. The recommended load and motion parameters are shown in Tables 2.2 and 2.3, respectively.

ISO and ASTM methods are similar in testing approach; here an axial compressive load is applied to the disc replacement, combined with rotational motions (flexion/extension, lateral bending, and axial rotation). It is worth mentioning that different loading conditions are used in the two standards. A sinusoidal varying axial compressive load is used in the ISO method; in contrast, the ASTM method adopts a static axial load. Further, a smaller range of axial rotation is recommended by the ISO method. Up to now, it is unclear whether these differences would lead to different wear outcomes. Both ISO

and ASTM methods are still in the refining stage. It is unknown which standard will produce the more clinically relevant wear patterns or wear rates, due to a lack of retrieved implants in clinical studies (Graham, 2006).

Table: 2.2: Range of motion for cervical spine as defined by ASTM F2423 (2005) and ISO 18192-1 (2011).

Methods	Flexion (°)	Extension (°)	Lateral bend (°)	Axial rotation (°)	Frequency (Hz)
ASTM F2423	7.5	7.5	± 6	± 6	1
ISO 18192-1	7.5	7.5	± 6	± 4	< 2

Table: 2.3: Recommended axial loading for wear testing of cervical disc prosthesis as defined by ASTM F2423 (2005) and ISO 18192-1(2011).

	Load type	Load range
ASTM F2423	Constant	100 N
ISO 18192-1	Sinusoidal	50 N (Min) – 150 N (Max)

2.2.4 Spinal pain

2.2.4.1 Introduction

Spinal pain is a common public health problem and up to 80% of the population will experience some degree of back and neck pain in their lifetime (McCarberg *et al.*, 2012). In the UK, the annual prevalence rate of back pain is reported as 36% (Walsh *et al.*, 1992). There is no significant difference between genders, but prevalence does show a rise with age. Other factors shown to increase the risk of back and neck pain include poor physical fitness, smoking, and heavy manual work (McCarberg *et al.*, 2012).

The costs of back and neck pain treatments are substantial and can result in an economic burden to the individual, industry and government. As an example, the annual direct healthcare cost in the USA for treating back pain is estimated at \$193.9 billion (McCarberg *et al.*, 2012). In comparison, the direct cost of the treatment of back pain has reached up to £ 1.6 billion per year in the UK (Maniadakis & Gray, 1999). If including other indirect costs such as employment and holistic care costs, the annual overall cost of the UK rises up to £ 12 billion (Maniadakis & Gray, 1999; Urban & Roberts, 2003).

2.2.4.2 Nature of disc degeneration & ageing

Intervertebral disc degeneration is one of the most common causes of back and neck pain (Cassinelli *et al.*, 2001; Urban & Roberts, 2003; Guerin & Elliott, 2006). Sources of pain include nerve root impingement caused by disc herniation and osteophyte formation at the rim of the cartilaginous endplate.

Due to the avascular and low cellularity nature of the intervertebral disc, it is susceptible to nutritional deficiency, degenerative diseases and ageing (Guerin & Elliott, 2006). Ageing of the intervertebral disc is universal and inevitable (Cassinelli *et al.*, 2001; Guerin & Elliott, 2006). The structure, composition and function of the intervertebral disc undergo degenerative changes with time. Ageing and degeneration may initially occur at the cellular level such as alteration in cell type, proliferation and death (Roberts *et al.*, 2006; Zhao *et al.*, 2007). This may progress to morphological and functional changes in each component of the intervertebral disc.

As a result of ageing, the translucent nucleus pulposus becomes increasingly dehydrated and fibrotic, which behaves more like a solid rather than a gel. This structural change is due to the massive reduction of proteoglycan content within the nucleus pulposus. It affects the ability of the nucleus pulposus to rehydrate and pressurize (*i.e.* attract and retain water). In consequence, the

overall load-bearing behaviour of the intervertebral disc is altered (Urban & Roberts, 2003; Guerin & Elliott, 2006).

Without the pressurization of the nucleus pulposus, the annulus fibrosus is loaded in compression rather than in tension. The inner annulus fibrosus layers no longer bulge outwards. This can lead to inward collapse, delamination and cracking (Cassinelli *et al.*, 200; Guerin & Elliott, 2006). The layers of the annulus fibrosus become disorganized and less distinct with age (Cassinelli *et al.*, 2001; Urban & Roberts, 2003).

Degeneration of the cartilaginous end plates of the intervertebral disc includes thinning, calcification and reduction of blood supply (Guerin & Elliott, 2006). This structural deterioration has a significant impact on the biochemical environment of the intervertebral disc and affects the cell metabolism by interfering with the transport of nutrients (glucose and oxygen) and removal of metabolic waste (lactic acid) (Cassinelli *et al.*, 2001; Roberts *et al.*, 2006).

2.2.4.3 General treatments

For neck and back pain, both conservative treatments (*e.g.* rest, physical therapy, activity modification and medication) and surgical interventions are available. Patients with early stage disc degeneration are expected to recover

from the pain, following a few weeks of conservative treatment. For severe disc degeneration with intractable pain, fusion surgery (FS) and motion preserved implantation (e.g. total disc replacement) are normally used.

Fusion surgery is considered as the “gold standard” of care for degenerative disc disease, discogenic pain and spinal deformities. In this surgical procedure, the degenerated intervertebral disc is removed and two adjacent vertebrae are fused together using a fusion cage and bone graft; besides metal plates and rods may be used in some cases (Guerin & Elliott, 2006). After successful fusion a single rigid spinal segment is formed. This removes the pain, but the spinal motion is eliminated at the treated level. These changes can alter the overall kinematics of the spine and have a significant impact on the adjacent intervertebral discs. Biomechanical and kinematic studies have shown significant increase in intra-disc pressure and range of motion, at the adjacent disc level after fusion surgery (Anderson & Rouleau, 2004). These alterations may lead to accelerated degeneration at adjacent intervertebral discs.

Clinical follow up studies of patients undergoing anterior cervical discectomy and fusion suggest that on average there is a prevalence of adjacent segment disease ranging from 9% to 17%. Additionally, the annual incidence of adjacent segment disease requiring additional surgery appears to be between

1.5% and 4% (Hilibrand & Robbins, 2004). FS may also require bone graft material harvested from the iliac crest. It is well documented that 20% of patients encounter iliac bone harvest related complications such as infection, pelvic fracture, and chronic donor site pain (Auerbach *et al.*, 2008).

2.3 Total disc replacement

2.3.1 Introduction

Total disc replacement (TDR) is a promising surgical intervention for treating advanced degenerative disc diseases. The primary aims of TDR are to restore pain-free spinal joint motion, as well as spinal segment loading capacity (Kurtz, 2006). In this surgical procedure, the degenerated intervertebral discs are removed, and replaced with artificial disc devices. By comparison with FS, TDR can preserve normal spinal motion and avoid bone graft induced complications (Anderson & Rouleau, 2004). Currently, this technique is also facing other problems (*e.g.* subsidence, device failure, and poor implantation) (Van *et al.*, 2003; Kurtz, 2006). Moreover, TDR is a relatively new technique, still in the immature development stage, and there is a lack of long-term clinical studies.

It has been suggested that TDR restores normal spinal alignment and preserves physiological motion patterns, thus adjacent disc degeneration may be delayed or even eliminated (Zechmeister *et al.*, 2011). The long-term benefit will be a reduction of the incidence of adjacent segment disc diseases. Up to now, this long-term benefit of TDR has yet to be proven, due to the lack of long-term clinical comparative studies. Among the available short-term clinical studies (Robertson *et al.*, 2005; Nabhan *et al.*, 2007; Heller *et al.*, 2008; Delamarter *et al.*, 2010), different disc designs (either Prodisc-C or Bryan) were used and make it harder to draw a unified conclusion. Apart from faster recover from surgery and patient satisfaction, there is no evidence shows that TDR is superior to FS, in terms of safety and symptom relief.

2.3.2 Contemporary cervical disc designs

Cervical TDR can be readily applied in patients presenting with neurological deficit, radiculopathy or myelopathy (Auerbach *et al.*, 2008). A number of cervical total disc implants that have been approved for use in patients including (as shown in Fig. 2.6):



Fig. 2.6: Contemporary cervical disc designs a) Prodisc-C, b) PCM, c) Prestige[®] ST, and d) Bryan (adapted from Kurtz, 2006).

- Prodisc-C (Synthes, Paoli, PA, USA) is a metal-on-polymer based cervical disc design. A ball-on-socket bearing configuration is adopted. It consists of two metallic end plates made of CoCrMo alloy and an UHMWPE core. The UHMWPE core is firmly attached to the inferior metallic end plate by the manufacturer and the domed convex surface of the core articulates against the concaved surface of the superior metallic end plate (Kurtz, 2006).
- PCM (Cervitech, Rockaway, NJ, USA) includes two end plates (cranial and caudal) made of CoCrMo and an UHMWPE core. Just like the Prodisc-C,

the UHMWPE core is fixed to the caudal end plate and motion only occurs between the domed UHMWPE surface and the inferior surface of the cranial end plate.

- Prestige[®] ST (Medtronic Sofamor Danek, Memphis, TN, USA) is a metal-on-metal based cervical disc. It adopts a ball-in-trough based articulation design and is fabricated from 316-stainless steel with anterior screw fixation. Due to the magnetic resonance image incompatibility of stainless steel, an improved Prestige design (*i.e.* Prestige[®] LP) has been introduced. The essential articulation configuration remains the same. A titanium based composite is used instead of the stainless steel. Two parallel rails on each component are used to achieve primary fixation rather than using anterior screw fixation (Kurtz, 2006).
- Bryan (Medtronic Sofamor Danek, Memphis, TN, USA) is an elastomeric ball-on-socket based cervical disc. It incorporates a mobile bi-convex polyurethane (high-durometer) core that articulates against clamshell-shaped titanium alloy end plates (Hallab, 2008). The essential components include two metal end plates, a polymer core, a polymer sheath and metallic centralizing pins. In this design, a unique soft polyurethane (low-durometer) flexible membrane or sheath is used to provide a controlled fluid lubrication environment and the articulation surfaces are protected from soft-tissue encroachment (Kurtz, 2006; Hallab,

2008). After implantation, the polymer core is expected to remain hydrated and articulate against the metal shells in an aqueous saline environment.

Among these current cervical disc designs, the essential design principles are based on either replicating the natural structure (e.g. Bryan) or the kinematics (e.g. Prodisc-C) of a healthy intervertebral disc (Kurtz, 2006). Cervical disc prostheses can be further classified as unconstrained, semi-constrained and constrained designs. However, that there is lack of unified classification rules in the current literature among different authors (Kurtz, 2006; Sears *et al.*, 2006; Galbusera *et al.*, 2008). For each particular design, different constraints may occur in the two-dimensional planes (coronal, sagittal and transverse). This can be easily understood by considering the degrees of freedom of each implant allowed. For example, the constrained design of the Prodisc-C, allows only three degrees of freedom (*i.e.* rotational motion in each 2D plane). An unconstrained disc prosthesis (e.g. Bryan) is capable of both translation and rotation, with six degrees of freedom. A semi-constrained design such as the Prestige[®] ST only offers four degrees of freedom (translation in the anterior-posterior direction plus rotation in each 2D plane).

Biomechanical studies of the functional spine unit shows that the constrained disc design has a fixed centre of rotation (COR) and will guide spinal unit

motion (Sears *et al.*, 2006; Galbusera *et al.*, 2008). In contrast, a mobile COR is found in unconstrained designs and has the ability to adopt the COR of the functional spine unit. Thus, the posterior facet joints and surrounding soft tissue are protected from abnormal loading during axial rotation. However, the shear stress encountered during flexion-extension or lateral bending motion is directly transmitted to the facet joints. For the constrained design, these circumstances are completely reversed.

2.3.3 Wears debris induced issues (bearing material combinations)

A metal-on-metal combination or metal-on-polyethylene combination is normally used as the articulation surfaces in current cervical disc designs. Wear debris generated as a result of relative motion may induce an adverse tissue response (*e.g.* inflammation and osteolysis) and eventually lead to implant loosening (Howling *et al.*, 2003; Ingham & Fisher, 2005). The actual tissue response depends on the nature of the particulate debris; the severity of the response is affected by the size, quantity and shape of the wear particles (Goodman, 2007; Utzschneider *et al.*, 2010).

The immune system of the human body modulates the biological response to foreign particles (*i.e.* wear debris). A foreign body granulomatous response is proposed for polymer based wear debris (*e.g.* UHMWPE). It is a non-specific

and macrophage mediated innate immune response, via the production of inflammatory cytokines (Goodman, 2007). On the other hand, metal wear debris (in-soluble form) is found to induce an adaptive type IV immune response (*i.e.* hypersensitivity reaction). This immune response is 'antigen specific which involves a specific antigen, co-stimulatory molecules, an antigen presenting cell and T lymphocytes' (Goodman, 2007).

Metal alloys used in orthopaedic implants rely on the formation of a passive layer to prevent *in-vivo* corrosion (Oskouian *et al.*, 2004; Hallab, 2008). Relative articulation may destroy this protective layer and expose the underlying material for corrosion. The release of corrosion by-products into surrounding tissue is a clinical concern. For example, a significant increase of blood serum metal ion (cobalt and chromium) concentration was observed after implantation of the Maverick lumbar disc (Zeh *et al.*, 2007). Despite that cobalt and chromium are the essential trace elements for human metabolism and excessive ion accumulation in peri-prosthetic tissue will lead to potential complications (Brown, 2006). For example, cobalt has been reported to cause cardiomyopathy and thyroid dysfunction (Oskouian *et al.*, 2004) and chromium can lead to both cardiac and renal dysfunction (Hallab, 2008). The detailed description of metal ion induced complications can be found elsewhere (Hallab, 2008).

2.4 PEEK as a biomaterial

2.4.1 Introduction

With the intention of overcoming the wear debris induced issues associated with current cervical disc designs, new bearing materials have been introduced. PEEK is one such material with great potential, due to a combination of good mechanical performance (Jones *et al.*, 1985) and proven biocompatibility (Jeffery, 2012).

PEEK is a semi-crystal high performance thermoplastic of the poly-aryl family (Béland, 1990; Kurtz & Devine, 2007). It was first introduced into the market by ICI (Imperial Chemical Industries) in 1981, under the trade name of Victrex[®] PEEK for industry application. A straightforward nucleophilic synthesis route is adopted; the general degree of crystallinity ranges from 30-35% (Kurtz & Devine, 2007), and the maximum achievable crystallinity is about 40% (Béland, 1990).

The medical grade PEEK arrived in 1998 and is marketed as PEEK-OPTIMA[™] by Invibio Ltd. (Thornton-Cleveleys, Lancashire, UK) which is a subsidiary of Victrex plc. (Kurtz & Devine, 2007). In comparison, the two grades of PEEK are virtually identical in properties; the only difference is the level of cleanness required during synthesis and fabrication. PEEK-OPTIMA[™] is synthesised in a

clean room production environment, under a higher quality control system. Thus, the quality and purity of the material is ensured for long-term implantation (Kurtz, 2012a). The detailed nomenclature and product description of the historical PEEK products can be found elsewhere (Kurtz & Devine, 2007).

2.4.2 Chemical structure

The linear homogenous aromatic backbone of PEEK conforms to a resonance stable arrangement, where the ether and ketone functional groups located at the opposite end of the benzene rings, as show in Fig. 2.7 (Béland, 1990, Kurtz & Devine, 2007). A planar zigzag conformation is adopted for PEEK molecular chains, with a bond angle of 125° . Moreover, the faces of the aromatic rings are slightly twisted and the actual torsional angle depends on the crystallisation temperature (Reitman *et al.*, 2012). During crystallisation, the aromatic linear chains are packed into orthorhombic crystal unit cell. These unit cells are further aligned and fold into lamellae and disperse in the amorphous phase. Under certain conditions, these lamellae can further organise into larger spherulites (Kurtz & Devine, 2007; Reitman *et al.*, 2012). The size of the crystal and its perfection are dependent on the thermal history and the nature of fillers (Reitman *et al.*, 2012).

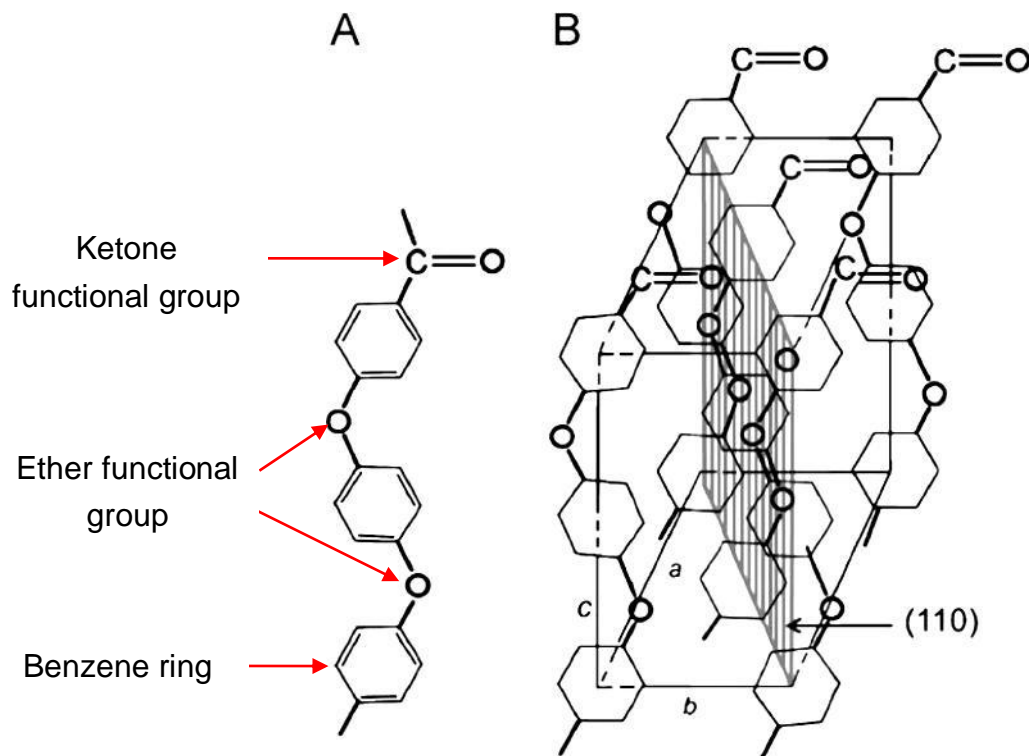


Fig. 2.7: a) PEEK chemical structure unit and b) Orthorhombic crystal unit cell for PEEK (adapted from Kurtz & Devine, 2007).

Due to the inherent compatibility with carbon fibre (*i.e.* good interfacial bonding stress), PEEK is normally reinforced with either discrete short or long continuous carbon fibre, in order to enhance its mechanical performance. There are two sorts of carbon fibre which are PAN (Poly-acryl-nitrile) based and pitch-based. PAN based carbon fibre is converted from an acryl-nitrile copolymer and pitch based carbon fibre is synthesised from mesophase pitch. In practice, PAN based carbon fibre tends to have higher tensile strength and higher compressive strength than pitch based carbon fibre, due to its

turbostratic character (inter-crystalline and intra-crystalline disorder caused by fibrils cross-linkage) (Stuart, 2012).

2.4.3 Fabrication of PEEK based devices

Despite PEEK being a high-performance thermoplastic, it can be readily fabricated using conventional techniques, such as injection moulding, extrusion, *etc.*. Extrusion followed by machining is the main method for fabrication of PEEK based implants (Kurtz, 2012a). This may also include an annealing treatment with the intention of releasing internal residual stresses formed during production. This residual stress can reduce the physical performance of the finished implant.

2.4.4 Mechanical properties of PEEK

For the inherent resonance stable chemical structure of PEEK, it generally shows high thermal stability and high mechanical performance. PEEK exhibits a high glass transition temperature (T_g) of 143°C and a high melting temperature (T_m) of 343°C (Béland, 1990).

The mechanical properties of PEEK are normally associated with its microstructure (*i.e.* crystallinity, size of the crystals and their perfection). The

microstructure development is controlled by the different thermal history (Reitman *et al.*, 2012). The general mechanical properties of neat PEEK (*i.e.* unreinforced) products are shown in Table 2.4. In practice, the neat PEEK shows virtually no anisotropy behaviour with a tan colour appearance. The fibre reinforced PEEK shows a significant anisotropy character and has a black colour appearance (Jones *et al.*, 1985).

The mechanical behaviour of PEEK can be described based on three terms: stiffness, strength and toughness (Jones *et al.*, 1985). PEEK is a visco-elastic material, hence its stiffness is sensitive to time under load (*i.e.* creep) and temperature. However, under *in-vivo* conditions (37°C body temperature), the elastic behaviour of PEEK is found to be relatively insensitive to temperature (Rae *et al.*, 2007). At small strain (< 0.03), at room temperature, PEEK 450G displays a linear relationship between stress and strain in both tension and compression. After reaching the yield point, PEEK undergoes varying post-yield hardening or softening characteristics, depending on the temperature and strain rate (Kurtz & Devine, 2007; Rae *et al.*, 2007). The complete investigation of the strain rate and temperature effects on the mechanical properties of PEEK was described by Rae *et al.* (2007).

Table 2.4: Typical material properties of PEEK 450G and PEEK Optima-LT1, compared with ASTM PEEK biomaterial specification and UHMWPE (Kurtz & Devine, 2007; ASTM F2026, 2010; PEEK™ 450G datasheet, 2012; PEEK Optima-LT1 product specification, 2102).

Property	Victrex® PEEK 450G	PEEK Optima® LT1	ASTM F2026	UHMWPE
Density, kg/m ³	1300	1300	1280-1320	932-945
Flexural modulus (GPa)	4.1	4.1	3	0.8-1.6
Flexural strength (MPa)	165	165	110	N/A
Tensile strength (MPa), at yield	100	100	90	39-48
Tensile elongation (%), at break	45	40	5	350-525
Impact strength, notched Izod (kJ/m ²)	7.5	7.5	4	N/A

Toughness covers a broader range of fracture properties under either static, impact or fatigue loading conditions (Jones *et al.*, 1985). The toughness of a material is normally measured via a IFI (instrumental falling weight impact) comparative approach (Rae *et al.*, 2007; Sobieraj & Rimnac, 2012). For example, the Izod test is a high strain test which relies on a pendulum being

dropped from a specific height, to impact and fracture a notched or cracked specimen, in order to measure the energy absorbed by the material (Jones *et al.*, 1985; Sobieraj & Rimnac, 2012). The total absorbing energy composes of crack initiation energy and crack propagation energy. In the case of neat PEEK, the crack initiation energy is the main energy absorbing stage (Jones *et al.*, 1985).

For measuring the intrinsic toughness property of PEEK, stress life approach and fatigue crack propagation methods can be used (Sobieraj & Rimnac, 2012). Moreover, an artificial stress concentration (*i.e.* notch) can be adopted with the intention to mimic the *in-vivo* wear fatigue. Under normal functioning, the articulating counter face may be scratched or ploughed, leading to the formation of local stress concentrations. In addition, defects on the surface can also lead to generation of local stress concentrations (Rae *et al.*, 2007).

2.4.5 Biocompatibility of PEEK

2.4.5.1 Introduction

Biocompatibility has been defined as ‘the ability of a material to perform with an appropriate host response in a specific application’ (Brown, 2006). The biocompatibility evaluations of PEEK biomaterial can be classified into two

categories (implant form and particulate form), via different methods (using cell cultures or animal model).

2.4.5.2 *Implant form*

In general, the cellular response for an artificial implant is encapsulation (Brown, 2006). A fibrous layer is formed around the implant and separates it from the rest of the body. This phenomenon can be avoided by a porous coating or texture on the implant surface.

In a peri-prosthetic tissue retrieved study (Toth *et al.*, 2006), a PEEK-Optima based threaded interbody fusion device (14 mm diameter x 20 mm length) packed with autograft or rhBMP-2 (Bone morphogenetic protein-2) was evaluated using sheep lumbar spine for a period of 6 months. Based on the observed cytological response, only mild chronic inflammation consisting of a few macrophages was observed in tissues adjacent to the PEEK devices. It demonstrated that PEEK based implants were well tolerated by the spinal tissues.

2.4.5.3 Particulate form

There are several studies (Rivard *et al.*, 2001; Howling *et al.*, 2003; Utzschneider *et al.*, 2010) that report on the biocompatibility of PEEK wear particles, however none focus on wear particles generated in cervical TDR.

For example, spherical shaped PEEK particles (with a mean diameter of 40 μm) were used by Rivard *et al.* (2001) in an animal model biocompatibility study. The obtained histopathologic evidence suggests that PEEK (Victrex[®] PEEK 150G) based particles are harmless to the spinal cord and nerve roots. It is worth mentioning that the PEEK particles they utilized were completely different in size and shape than the wear particles generated from cervical TDR. A recent *in-vitro* wear study showed that PEEK-on-PEEK self-mating articulation for cervical disc results in submicron (from 0.23 to 0.51 μm) particle size distribution with a mean roundness of 0.5 (Grupp *et al.*, 2010).

An *in-vitro* monocyte comparative study showed that PEEK based particles were non-cytotoxic and less inflammatory than UHMWPE particles of similar size and shape (Hallab *et al.*, 2012). In this study, submicron sized (0.7 μm) PEEK Optima-LT1 particles were evaluated, at a dose of 20 particles-per-cell for a maximum of 48 hours. A granular flake-like particle shape with average aspect ratios from 1.1-1.5 (round to oval) was observed for the PEEK particles.

2.5 Basic tribology

2.5.1 Introduction

In this thesis, the tribological performance of a new bearing material was examined (for cervical disc replacement designs); an understanding of the basic tribology is necessary. It includes the study of friction, wear and lubrication (Jin & Fisher, 2008; Ludema, 2012).

Tribology mainly concerns surfaces in relative motion, thus the surface layer properties and the surface textures are important considerations. Generally speaking, the surface texture is composed of two essential elements (roughness and waviness) (ISO 4287, 1998). Roughness is defined as the fine irregularities with short wavelength (hill and valley based fluctuation), due to the intrinsic features of the machining or polishing process. Waviness is the widely spaced surface macro-irregularities with longer wavelengths, and it may be caused by the vibration in the machining process or the deflection of the work piece (Jin & Fisher, 2008).

Surface roughness can be quantified using either a contacting stylus method or a non-contacting interferometry method. The most commonly used surface roughness parameters are the arithmetical mean roughness (S_a) and root mean square roughness (S_q). However, these parameters only show the

surface variation in the vertical direction (*i.e.* height); they do not provide spacing information of the surface asperities (Bhushan, 1998; Jin & Fisher, 2008).

2.5.2 Friction

Friction is the interaction forces between molecular fields when two solids approach one another (Myshkin & Kovalev, 2009; Ludema, 2012); the resistive force which is parallel to the direction of motion, is called the friction force (Bhushan, 1998). In the context of polymers, the study of friction mainly involves two major components (adhesion and deformation). Where, adhesion component originates from the adhesive junctions formed between the asperities of the mated solid surfaces (Myshkin & Kovalev, 2009). On the other hand, the deformation component of friction (*i.e.* hysteresis friction) is due to the resistance of the polymer being ploughed away by the asperities of the mated counter-face (Myshkin & Kovalev, 2009).

Theoretically, the friction force is not affected by the sliding velocity. Actually, for polymer based joint replacement, a high sliding velocity can lead to significant change in friction coefficient (*i.e.* the ratio between friction force and the applied normal force) due to local temperature rises. This is because polymers are visco-elastic materials and very sensitive to frictional heating.

Moreover, it has been known that the friction fatigue (*i.e.* fatigue wear) is initiated at the points where the maximum tangential stress takes place and the position of the maximum tangential stress is dependent on the friction coefficient (Myshkin & Kovalev, 2009).

2.5.3 Wear

Wear is defined as 'progressive loss of substance from the operating surface of a body occurring as a result of relative motion at the surface' (Jin & Fisher, 2008). In the context of polymer wear, there are three main wear mechanisms involved which are listed at below:

- *Abrasive wear*

Abrasive wear is caused by 'hard asperities on the counterface and/or hard particles that move over the polymer surface' (Myshkin & Kovalev, 2009). The polymer surface is ploughed to form plastic ridges with/without removal of material. According to the shape and contact angles of the abrasive points (*i.e.* surface asperities or hard abrasive particles), material can either be plastically ploughed to form ridges adjacent to the developing groove or removed as fine chips (*i.e.* wear debris) (Bhushan, 1998; Myshkin & Kovalev, 2009). The newly developed plastic ridges further increase the surface roughness; the generated wear debris may get trapped in the contact zone and contribute to additional

third-body abrasion.

- *Adhesive wear*

Adhesive wear is normally associated when a soft surface is in rubbing contact with a hard counterface. Adhesive junctions are formed at the asperity contacts (*i.e.* discrete contact spot) by either chemical or physical interactions. During relative motion, if the strength of these junctions exceeds the cohesive strength of the weaker material, the weaker material will tear off and fragments are formed (Myshkin & Kovalev, 2009). Some part of this fragment is transferred onto the hard counterface and forms a thin film; the rest of the fragment is removed from the contact zone as wear debris (Bhushan, 1998). In this kind of wear mechanism the formation, growth and rupture of the adhesive junction are crucial.

- *Fatigue wear*

Fatigue wear is different to the bulk material fatigue and only spans the surface and sub-surface regions (Myshkin & Kovalev, 2009). Under repeated rolling or sliding, the maximum shear stress induces irreversible change which leads to the formation of surface or subsurface cracks (Bhushan, 1998). These cracks are often initially from stress concentrations, such as a surface scratch and sub-surface void. Wear debris (in the form of fragments) are produced, due to breakup of the polymer surface; pitting and delamination based wear

phenomena can be observed (Myshkin & Kovalev, 2009).

2.5.4 Lubrication

The main lubrication regimes are shown in Fig. 2.8. They are briefly described as follows (Bhushan, 1998; Jin & Fisher, 2008):

- *Fluid-film lubrication*

Load is fully sustained by the viscous pressure of the lubricant and complete separation of the bearing surface is achieved (*i.e.* no asperity contact occurs).

The behaviour of lubrication is governed by the viscosity of the lubricant; the friction is optimally minimised.

- *Boundary lubrication*

In this lubrication mode, extensive surface asperity contact occurs, in order to increase the contact area and reduce the contact pressure. The physical and chemical properties of the lubricant are essential. The transition to boundary lubrication can be caused by increased load, decreased speed or reduced lubricant viscosity.

- *Mixed lubrication*

This lubrication regime is the transition zone between the fluid film and boundary lubrication regions. The viscous pressure generated between the bearing surfaces is not sufficient to support the whole loading, thus the load is partially carried by the contact between the deformed surface asperities.

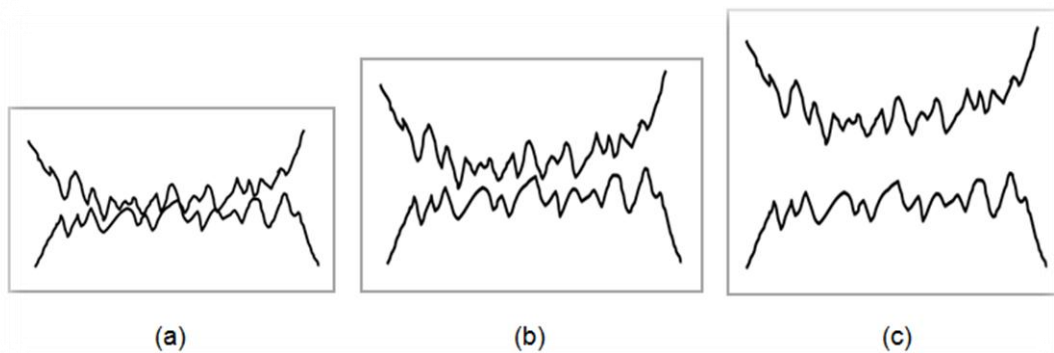
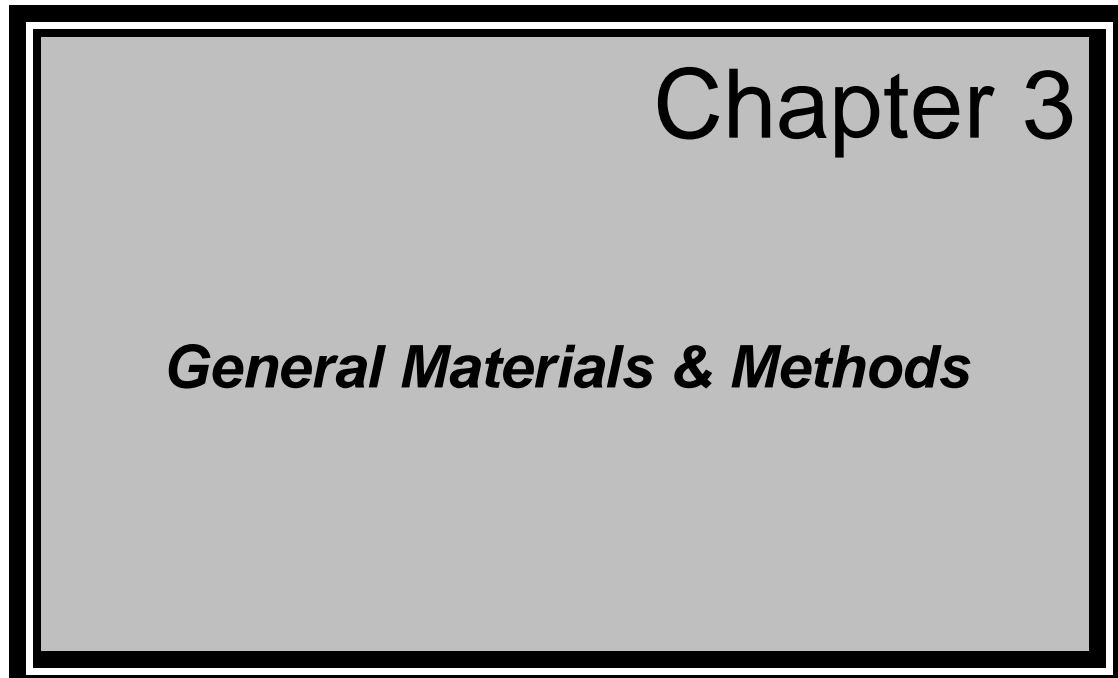


Fig. 2.8: Schematic diagram of a) boundary lubrication, b) mixed lubrication, and c) fluid-film lubrication (author's own drawing, adapted from Jin & Fisher, 2008).

2.6 Chapter conclusion

This chapter has provided the necessary background information about the spine, cervical disc replacement devices and current bearing materials related issues. The rest of the thesis will go on to describe the research undertaken to evaluate PEEK as a potential bearing material for cervical disc replacements. In the next chapter, the general materials and methods used are introduced.

A large rectangular box with a thick black border and a light gray background. The text "Chapter 3" is in the top right corner, and "General Materials & Methods" is centered in the middle.

Chapter 3

General Materials & Methods

3.1 Chapter overview

In this chapter, the general materials and methods used for the research are presented. In section 3.2, a detailed review of the materials is provided. The equipment used is introduced in section 3.3, in chapter order. The methods for preparing samples for examination and the preparation method used for the lubricant are presented in section 3.4. Finally, a concise chapter summary is given in section 3.5. It should be noted that subsequent chapters will include additional materials and methods specific to certain experiments.

3.2 Materials

3.2.1 PEEK 450G

Fifteen PEEK 450G square sheets (Fig. 3.1) were obtained from Victrex plc. (Lancashire, UK) for the flexural bending tests detailed in chapter 5. These sheets were fabricated via extrusion with a density of 1300 kg/m^3 , and had a beige colour appearance. The nominal dimensions of the sheets were $150 \times 150 \times 6 \text{ mm}$, with a tolerance on the thickness of between $+0.2 \text{ mm}$ to $+0.7 \text{ mm}$.

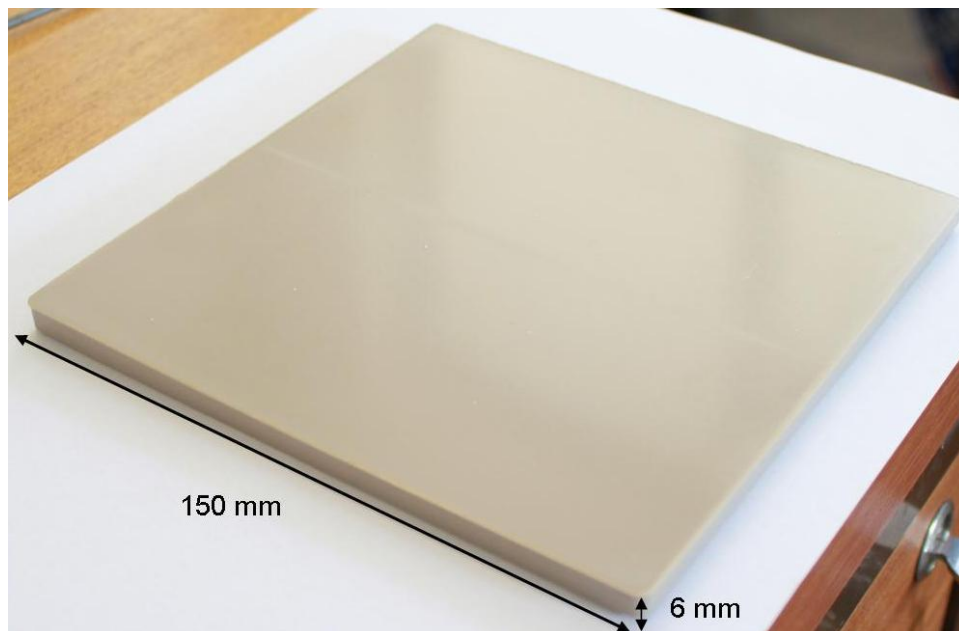


Fig. 3.1: PEEK 450G sheet.

3.2.2 NuNec[®] cervical discs

Five NuNec[®] cervical discs (Pioneer Surgical Technology Inc., Driebergen, Netherlands) were used in this study, one for theoretical analysis (chapter 4) and four for wear and frictional torque tests (chapter 6). The smallest available footprint (Anterior/Posterior 12 mm and Lateral 14 mm, with a nominal total disc height of 5 mm) was chosen with intention of replicating the worst case operational scenario. This cervical disc replacement is a two-piece ball-on-socket, PEEK-on-PEEK articulating device and is shown in Fig. 3.2. A novel feature of the device is the cam fixation mechanism that is used for short-term fixation. Metal blades extend from the device to grip the bone. These golden metal cams (as shown in Fig. 3.2b) are made of titanium alloy (Ti-4Al-6V) and coated with a thin layer of titanium nitride. Long-term fixation of the device is achieved via the hydroxyapatite coated endplates. Finally, tantalum based radiopaque markers are embedded to facilitate postoperative diagnostic visualization.

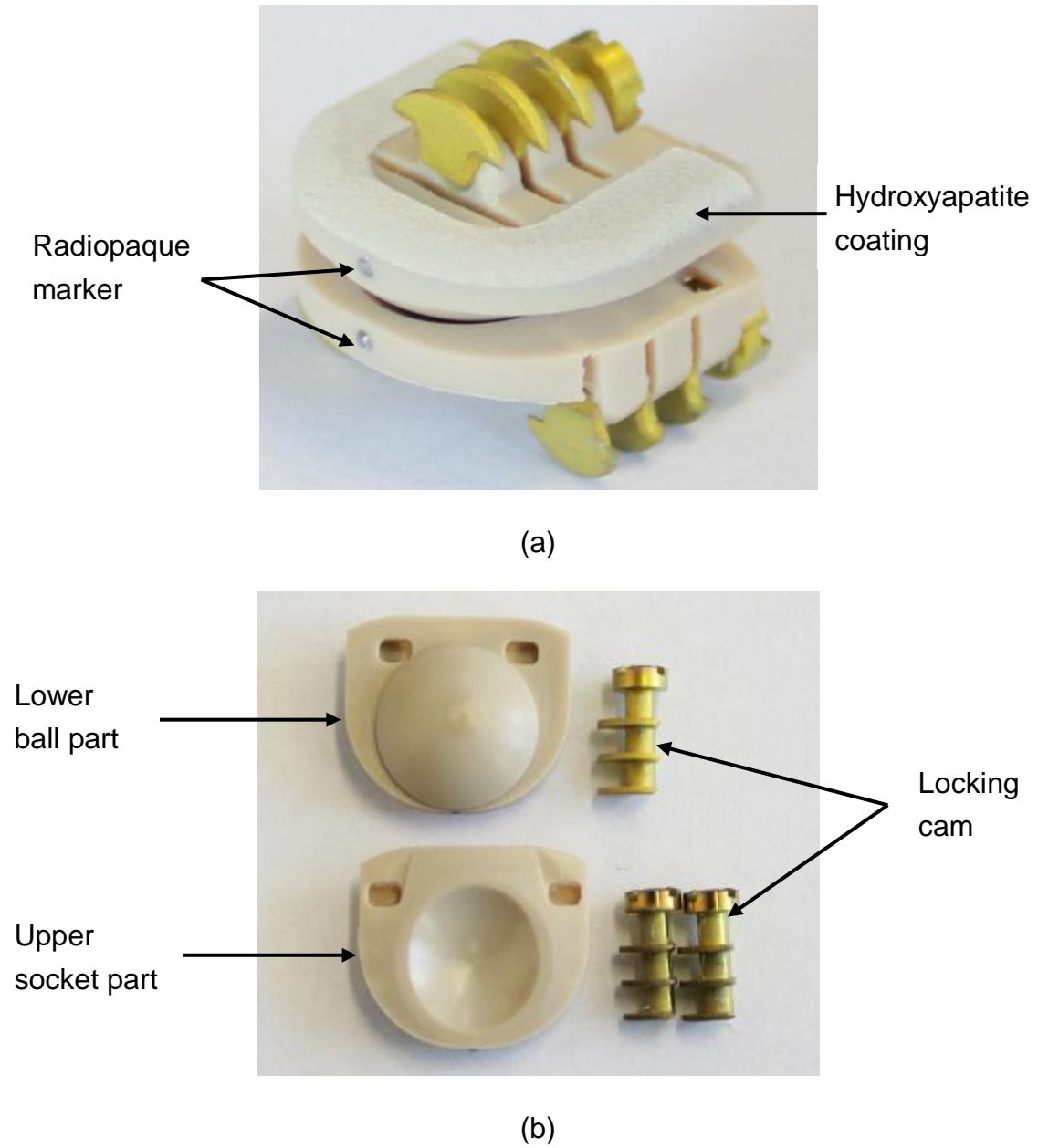


Fig. 3.2: The NuNec[®] cervical disc arthroplasty system a) assembled and b) disassembled.

3.3 Equipment

3.3.1 Coordinate Measuring Machine (CMM)

A DEA-swift manual CMM (Hexagon Metrology Ltd., Telford, UK) equipped with a 2 mm diameter TP8 mechanical touch-trigger probe (Renishaw plc., Kingswood, UK) was used to determine the radii of the ball and socket components of the NuNec[®] cervical disc, in section 4.3.4.1.

This CMM machine composes of three axes (as shown in Fig 3.3). These axes are orthogonal to each other in a three dimensional coordinate system. During profile measuring, 15 randomly selected points were taken across the whole bearing surface of the specimen. The positions of these points in the 3D coordinate system were recorded and sent to a computer for further analysis. PowerINSPECT 4315 data manipulation software (Delcam Ltd., Small Heath, Birmingham) was used to reconstruct the profile of the articulation surfaces and to obtain the corresponding radii. The volumetric accuracy of this CMM is stated as $4 + 5L/1000 \mu\text{m}$. It means that the error for zero measured length is 4 μm , and for every additional meter of length measured it becomes 5 μm larger.

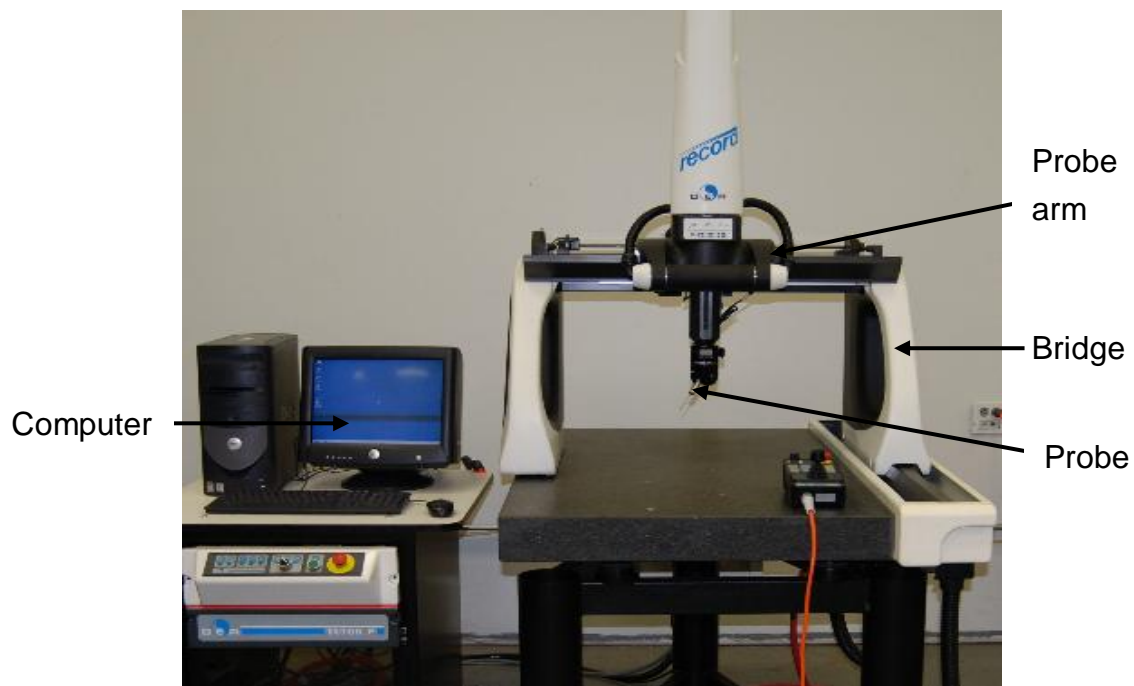


Fig. 3.3: DEA-Swift CMM. The measuring ranges are 510 mm (X-axis: lateral direction), 410 mm (Y-axis: anterior-posterior direction) and 330 mm (Z-axis: inferior-superior direction).

3.3.2 Talysurf 120L

A Talysurf-120L (Taylor Hobson Ltd., Leicester, UK) profilometer (as shown in Fig. 3.4) was used to quantify the surface roughness of the NuNec[®] cervical disc, in section 4.3.4.2. The basic working principle of the machine is that a contact stylus moves across the surface to be measured under 1 mN vertical load; the variation in depth is recorded by a transducer.

In this study, a chisel-edge diamond stylus with a 2 μm radius was adopted and Talysurf series 4.00 (Taylor Hobson Ltd., Leicester, UK) was used as the operation software. Surface examination was performed with an examining area of 5 x 5 mm, around the centre of the samples. To perform the surface measurements, the samples were fixed to the base of the profiler. The stylus was then manually moved down until there was roughly a 2 mm gap between the stylus and the examining surface. The stylus automatically examined the surface in equally spaced rows with a sampling spacing of 0.5 μm . The obtained data was manipulated using Talymap universal 3.1.8 software (Taylor Hobson Ltd., Leicester, UK) to analyze the obtained surface topography data. In doing this, the first step was to choose an appropriate profile filter, such that the measured noise and unwanted vibrations were removed. According to the radius of the stylus and the ISO 3274 (1996) recommendations, a filter with 0.8 mm cut-off length was used. A filter is defined as the intersection between the roughness and waviness component (ISO 4287, 1998). After separation of roughness and waviness was performed, a 3D topography image of the surface roughness was obtained (Fig. 3.5). Moreover, the surface roughness parameters such as S_a (arithmetical mean surface roughness) and S_q (root mean square roughness) can also be given.

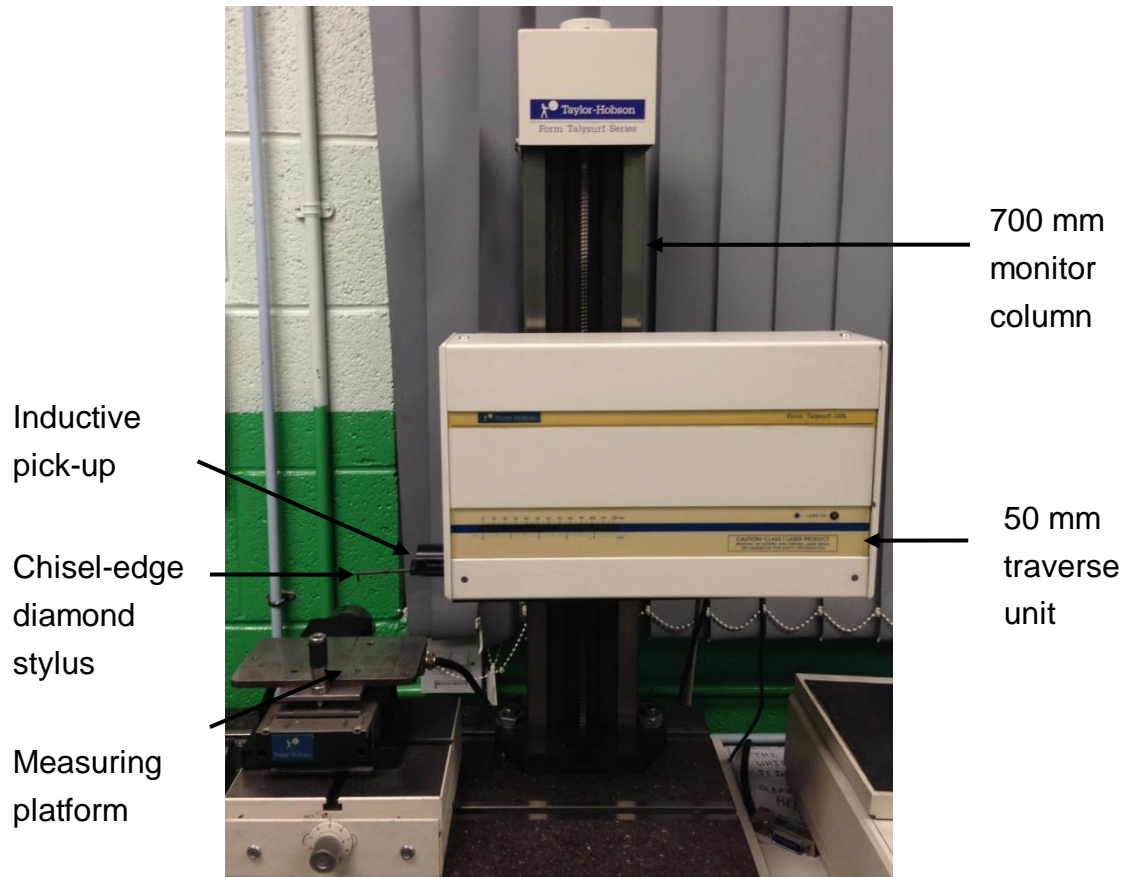


Fig. 3.4: Talysurf-120L. The measuring range is 10 mm and the measuring speed is 0.5 mm/s.

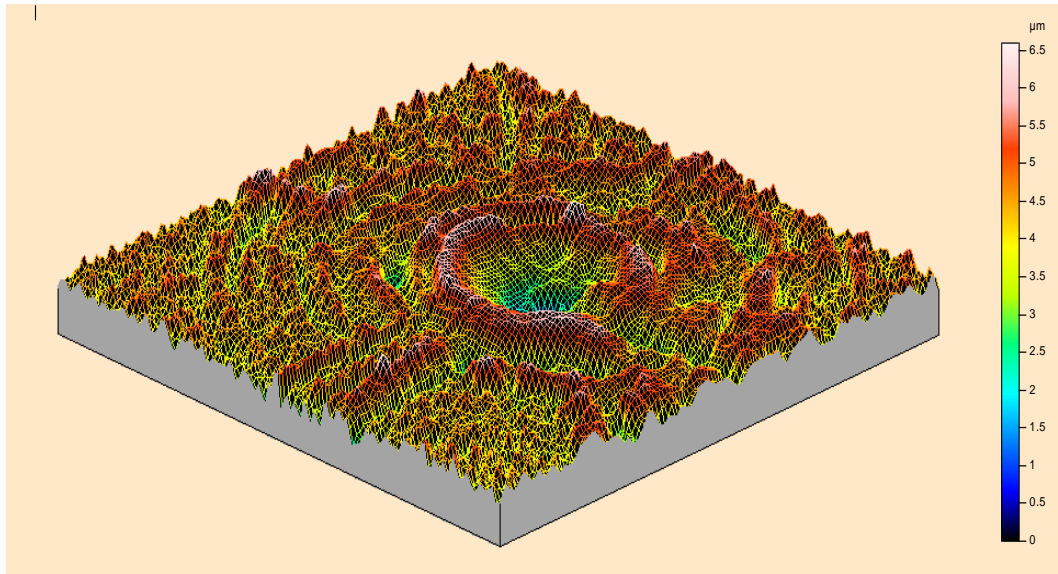


Fig. 3.5: The 3D surface roughness for convex surface (ball component) after separation of waviness, using a cut-off length 0.8 mm.

3.3.3 Lloyd 6000R

A Lloyd 6000R materials testing machine (Lloyd Instruments Ltd., West Sussex, UK) equipped with a 5 kN load cell (Fig. 3.6) was used to conduct the static flexural bending tests in section 5.3.4. It is operated by Windap V1.6 software (Lloyd Instruments Ltd., West Sussex, UK). The crosshead was driven by twin lead screws and a high precision servo motor to achieve a wide range of speeds (0.01 to 1020 mm/min) throughout the full load range (0 to 5 kN). Before testing, the required displacement range and cross-head speed was pre-set in the operator interface. The load and displacement readings were recorded throughout the test, which were then exported into an Excel compatible file for further analysis.

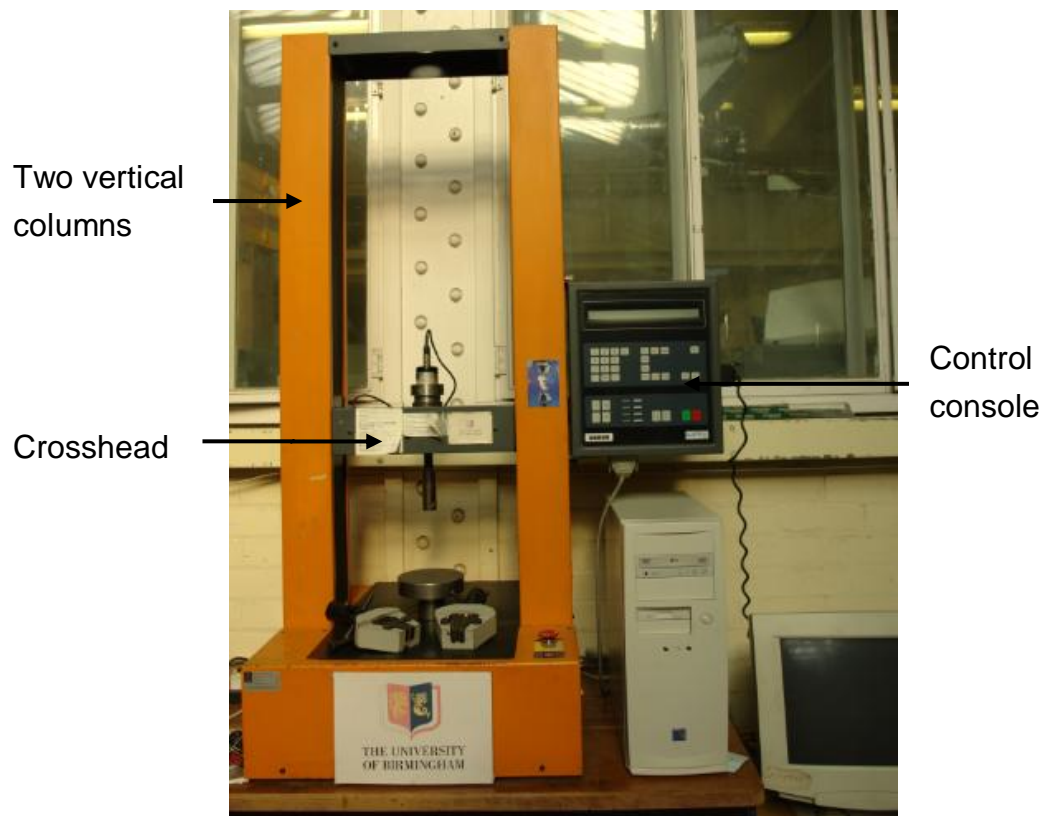


Fig. 3.6: Lloyd 6000R materials testing machine. The vertical travel length of the crosshead is roughly equal to 1000 mm.

3.3.4 Bose ELF-3300 test machine

A Bose ELF-3300 materials testing machine (Bose Corporation, ElectroForce Systems Group, Minnesota, USA) equipped with a 3 kN 1010CCH-1K-B load cell (Bose Corporation, ElectroForce Systems Group, Minnesota, USA) (Fig. 3.7) was used to perform the dynamic flexural bending tests (*i.e.* the fatigue tests) in section 5.3.5. It is fitted with two actuators which are capable of performing either axial load, or torsional load, or both. The loading capacity are ± 3 kN for dynamic motion, ± 2.1 kN for static motion and ± 24 N·m for axial

rotation motion. The initial working space of this equipment is 40.6 cm wide by 50.0 cm high. The vertical working distance can be easily adjusted using an integrated lift. The position of the axial actuator can be manually moved up and down to any desired position along the vertical column, and fixed in place using locking screws.

WinTest[®] 4.1 (Bose Corporation, ElectroForce Systems Group, Minnesota, USA) operation software was used to operate the testing machine. It provides a user interface for data acquisition, waveform generation and instrument control. During the fatigue tests, the three-point bending test rig (as described in section 5.3.3) was attached to both the top and bottom plate. The top plate is attached to the machine actuator and is controlled by the software and capable of travelling ± 12 mm in the vertical direction; the bottom plate is fixed in position.

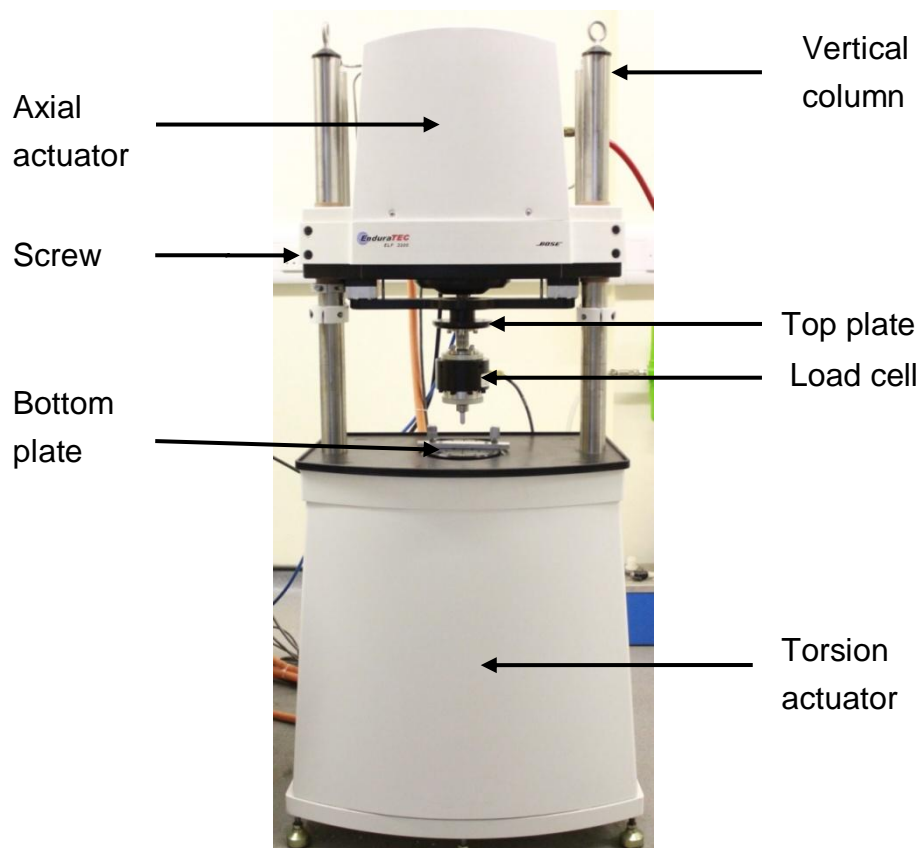


Fig. 3.7: Bose ELF 3300 material test machine

3.3.5 Bose spine simulator

The wear and frictional torque tests (in chapter 6) were performed using three single station Bose SDWS-1 Spine Simulators (Bose Corporation, ElectroForce Systems Group, Minnesota, USA) (as shown in Fig. 3.8). These customized simulators are capable of performing $\pm 12^\circ$ flexion/extension, $\pm 10^\circ$ lateral bend, $\pm 8^\circ$ axial rotation, under a maximum 3 kN axial load, at 0 to 2 Hz frequency. Moreover, it allows ± 12 mm translation in vertical direction.

Two of the simulators are equipped with a uni-axial 3 kN Bose 1010CCH-1K-B load cell (Fig. 3.9a). The third simulator is fitted with a multi-axial AMTI MC3-6-1000 load cell (Berkshire, England) which can measure the bending moments (M_x , M_y , and M_z) and enable frictional torque measurement (Fig. 3.9b). The measuring range is ± 15 N·m for each motion, and the measuring accuracy is ± 0.01 N·m.

All three spine simulators are controlled by WinTest[®] 4.1 control software. Each simulator is composed of several essential elements (one dedicated power tower, four actuators, one personal computer, temperature control modules, and the main test chamber) as shown in Fig. 3.10. An enlarged view of the main test chamber is shown in Fig. 3.11. The top adaptor is connected to the top plate using split clamps and screws. The lower adaptor is mounted on the bottom surface of the Perspex thermal chamber via screw fixation (Fig. 3.11b). This assembly was then slid onto the heating block (Fig. 3.11c), and fixed in place using split clamps and screws. A thermal probe was then inserted through the compression fitting located in the side of the Perspex chamber, which provided real-time temperature monitoring of the lubricant. Based on this reading, the heating block was controlled by the software either to provide a maximum heating rate of 0.2°C/min or to be switched off.

During testing, the temperature of the thermal chamber was maintained at 37°C (*i.e.* body temperature). The top plate was driven by the actuators to provide the flexion-extension and lateral bending motions; the lower plate (*i.e.* the bottom surface of the thermal chamber) was moved axially to provide axial rotation and axial compression. Moreover, the lower plate is free to move ± 5 mm in the horizontal plane or it can be locked in position, via four screws located beneath the heating block (see Fig. 3.11c). Before testing, these locks were hand tightened and the lower plate was completely locked.

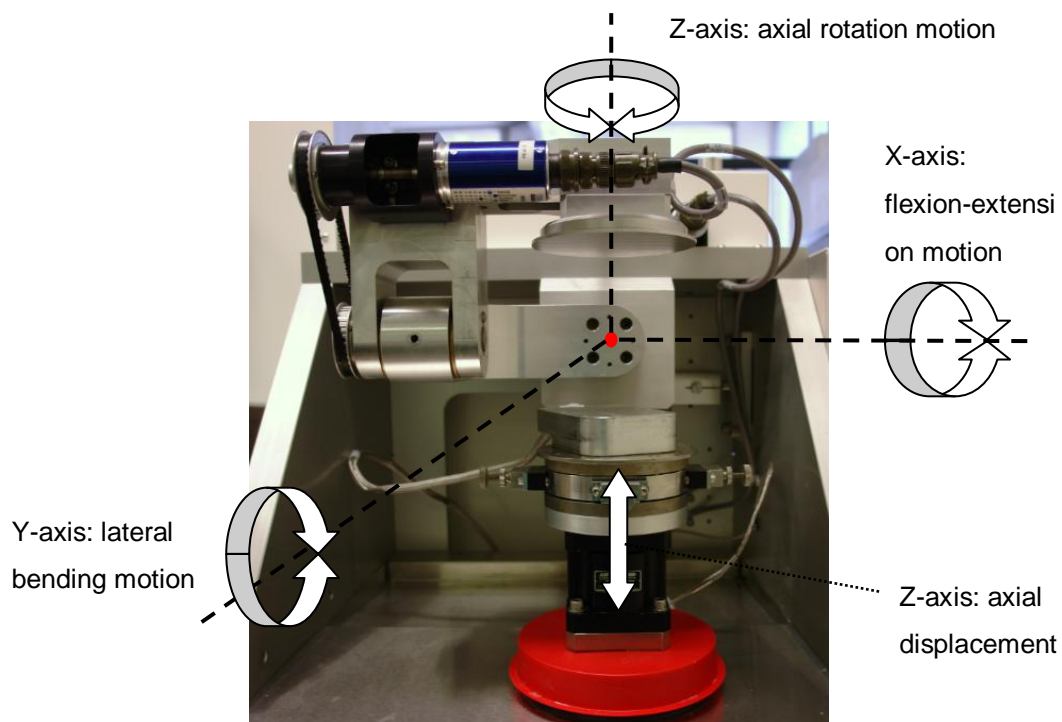


Fig. 3.8: Bose SDWS-1 single station spine simulator equipped with a multi-axial load cell. Black dashed lines represent the x, y, and z axes. The red dot is the location of the centre of rotation of this spine simulator.

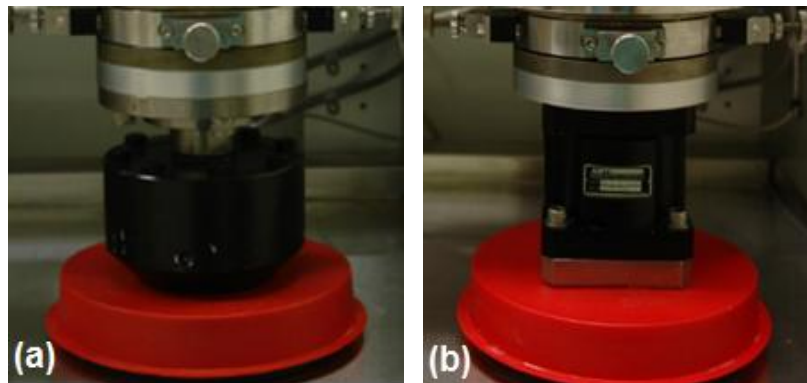


Fig. 3.9: a) uni-axial load cell and b) multi-axial load cell.

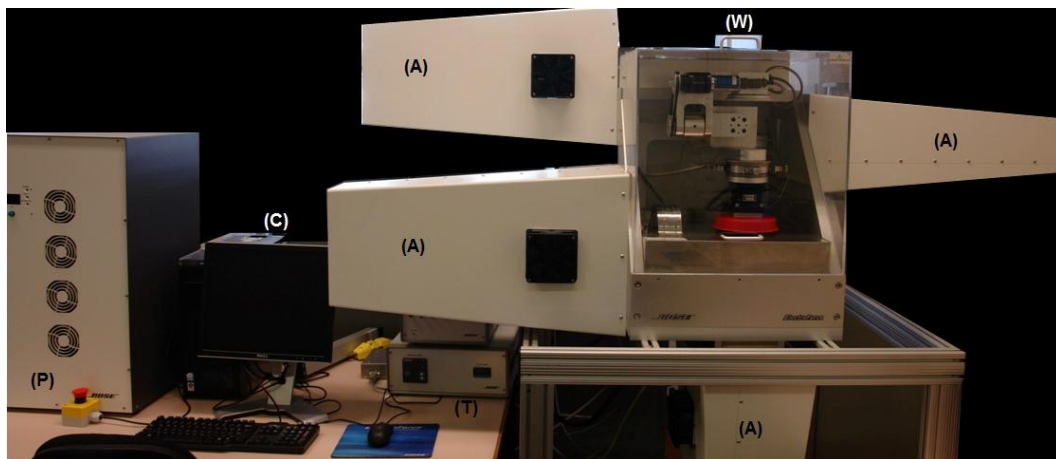


Fig. 3.10: Essential components of the Bose Spine Simulator. A) actuator, C) computer, T) temperature module, P) power tower, and W) main test chamber.

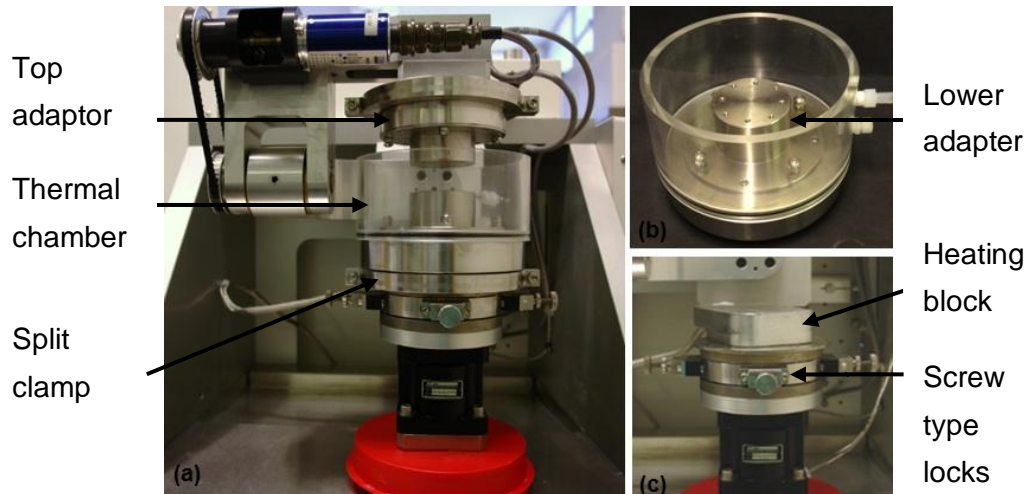


Fig. 3.11: a) Enlarged view of the main test chamber, b) thermal chamber with lower adaptor and c) heating block.

3.3.6 Bose ELF-3330 test machine

The dynamic load soak control (section 6.3.3) was performed using a Bose 3330 II materials testing machine (Bose Corporation, ElectroForce Systems Group, Minnesota, USA) (Fig. 3.12) which was also controlled by Wintest[®] 4.1. This machine is a combination of the Bose ELF-3300 test instrument and the Bose SDWS-1 spine simulator. It has one actuator that only provides axial compression. This machine is equipped with a Bose 1010CCH-1K-B load cell, and capable to carry out ± 3 kN dynamic load, at 0 to 100 Hz frequency. Like the Bose ELF-3300 test machine, the vertical working space of this machine can be manually adjusted along the vertical column. The top plate is controlled by the software and is capable of travelling ± 12 mm in vertical direction; the bottom plate (*i.e.* bottom surface of the thermal chamber) is fixed in position.

This machine is modified from the standard configuration; a Perspex thermal chamber is included for load soak control. Like the Bose spine simulator, the basic fixation, temperature control and heating mechanisms are the same.

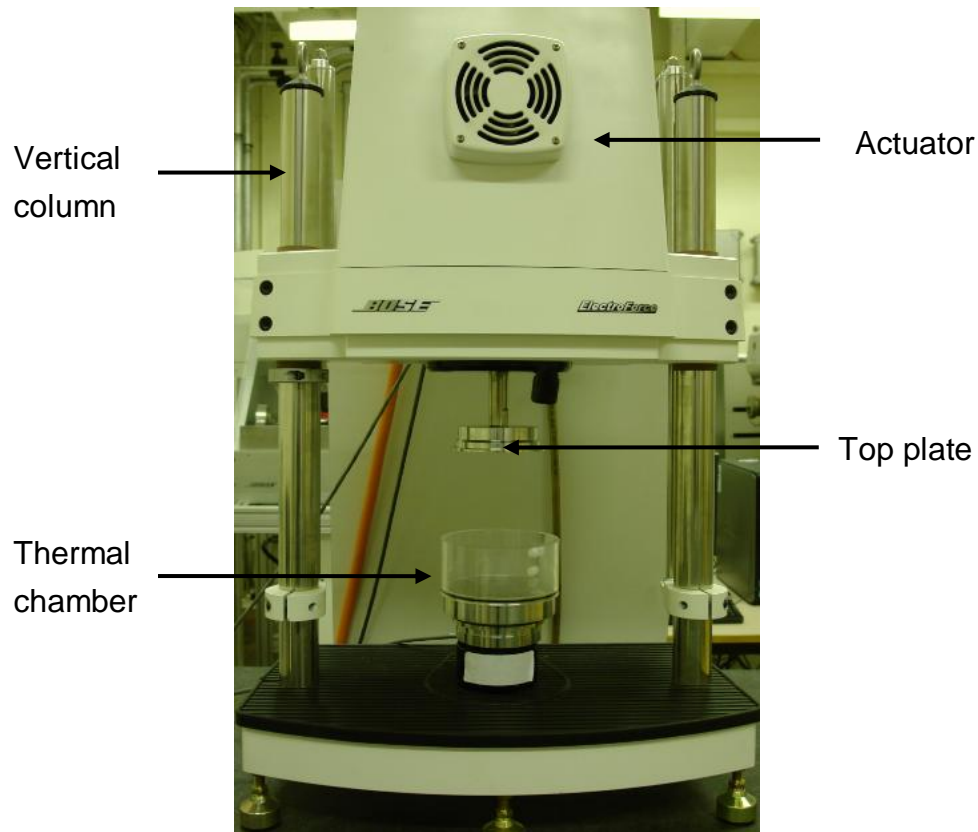


Fig. 3.12: Bose ELF-3330 II material test machine

3.3.7 Interferometer

A Non-contact surface roughness method was used in section 6.3.3.5, with the intention of preventing surface damage to the NuNec[®] cervical discs, before wear simulation. A KLA-Tencor MicroXAM2 interferometer (Omniscan Ltd., Wrexham, UK) was utilized (Fig. 3.13). This equipment is an optical

interferometer which uses the interference patterns of light to achieve a 3D surface map, without physically touching the examined surface. Sufficient light reflection is required for effective surface mapping.

In this research, the scanning area was 639 x 859 μm at the pole of the sample. A 10 \times objective lens was used in the surface mapping process. Scanning Probe Image Processor software (Image Metrology A/S, Copenhagen, Denmark) was employed for the analysis of the acquired topology data. By selecting the desired output surface roughness parameters, a 3D surface roughness image was obtained (Fig. 3.14). The requested surface roughness parameters are on top of this 3D image.

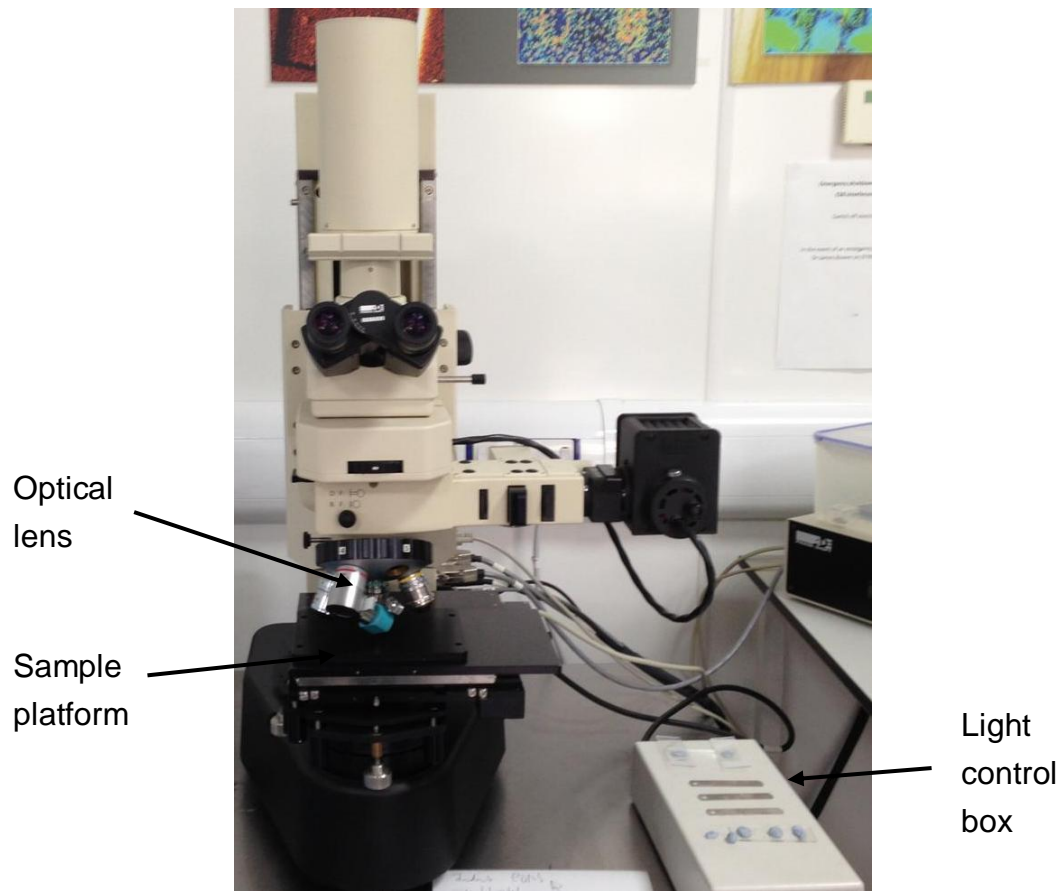


Fig. 3.13: The KLA-Tencor MicroXAM2 interferometer

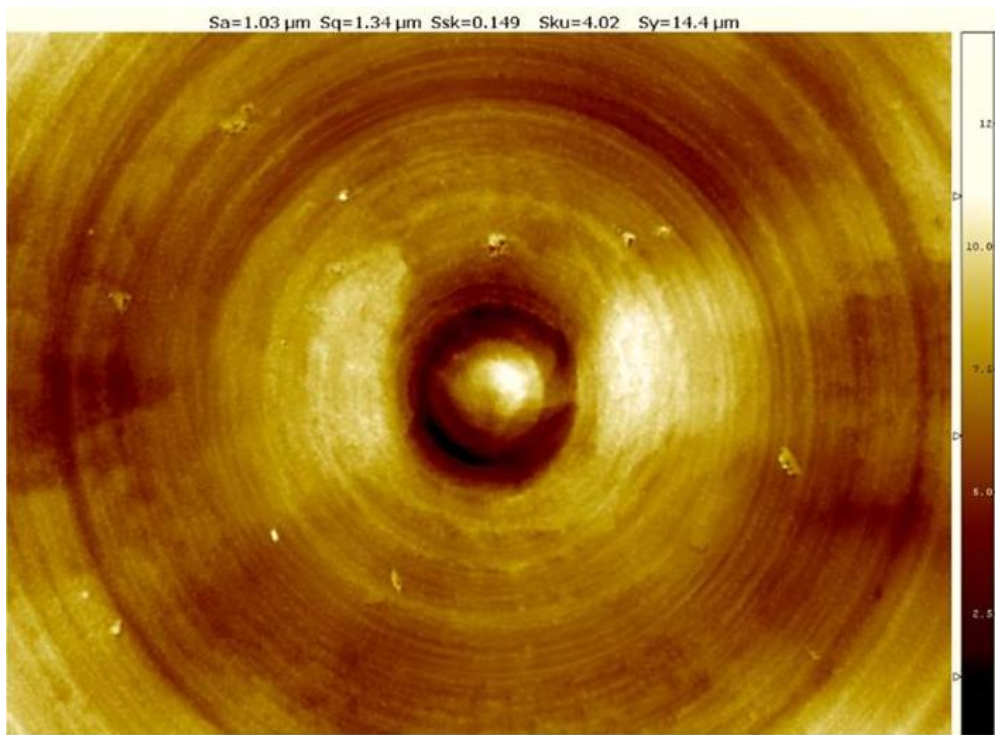


Fig. 3.14: An example of the 3D surface roughness image.

3.3.8 Rheometer

The viscosity of the lubricant (used in chapter 6) was measured using an AR-G2 cone-on-plate rheometer (TA Instruments Ltd., West Sussex, UK) (Fig. 3.15). A standard steel cone (60 mm diameter and a 2° angle) was used and controlled by the AR Instrument Control software (TA Instruments Ltd., West Sussex, UK).

To perform the viscosity measurement, about 5 mL of the lubricant was first placed on the stationary plate of the rheometer using a plastic pipette. Then, the rotation cone was automatically brought down, until it touched the surface

of the lubricant. Viscosity measurements were then performed under steady state flow from 0.01 /s to 100 /s shear rate, at 37°C (body temperature). After data acquisition, Rheology Advantage V5.7.0 (TA Instruments Ltd., West Sussex, UK) was used to process the obtained data. A graph of viscosity against shear rate was obtained. Different lubricant models can be applied to give a constant viscosity value. In this study, a Newtonian model was chosen.

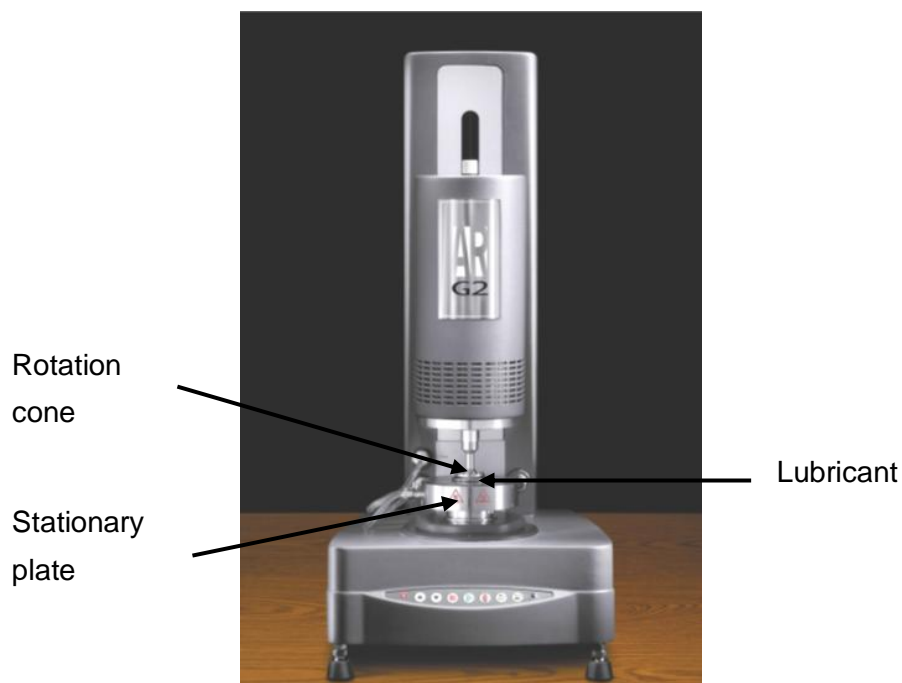


Fig. 3.15: Picture of AR-G2 rheometer.

3.4 Methods

3.4.1 Preparation of the samples

Fluid up-take (*i.e.* absorption) is a critical concern for polymer based disc prosthesis, particularly when wear is measured via the mass of samples. During wear simulation, the absorbed fluid could mask the actual wear results; a load soak control is necessary. The maximum fluid up-take ratio of PEEK is reported to roughly account for 5 % of its weight (Kurtz & Devine, 2007). In this study, the NuNec[®] cervical discs were soaked in de-ionised water for more than four weeks to stabilize the mass, before wear testing (Grupps *et al.*, 2010). Two days prior to test start date, disc samples were removed from the soak; a standard cleaning and weighing procedure (detailed in the following section) was performed.

3.4.2 Clean, dry and weighing protocol

A simplified clean, dry and weighing protocol was designed according the ISO 14242-2 (2000) standard. The disc specimens were initially cleaned using a liquid detergent (Fairy washing liquid, Procter & Gamble, Surrey, UK) and then rinsed twice with tap water. Specimens were then soaked in Virkon disinfectant solution with a concentration of 10 mg/L (Antec International Ltd., Sudbury, UK) for 20 minutes, to destroy bacterial contamination. After that, the specimens

were washed once with tap water and twice with distilled water. Specimens were then ultrasonically cleaned in a propan-2-ol bath (Scientific Laboratory Supplies, Hessle C, East Yorkshire, UK) for at least 5 minutes. The specimens were then wiped with acetone (Sigma-Aldrich, MO, USA) to remove any trace of grease or dirt. Finally, the specimens were dried and wiped over with low lint clean-room wipes (Cleanroom shop, Cumbria, UK) and placed in a dust free plastic container. After being left at room temperature for 48 hours, each specimen was gravimetrically measured using an OHAUS GA200D digital balance (OHAUS Europe GmbH, Switzerland) with 0.1 mg precision. Each disc was weighed six times with different orientations, and the average mass was calculated for each disc component (*i.e.* ball and socket parts). Skin contact was avoided with the disc specimens by using glove and plastic tweezers throughout weighing procedure.

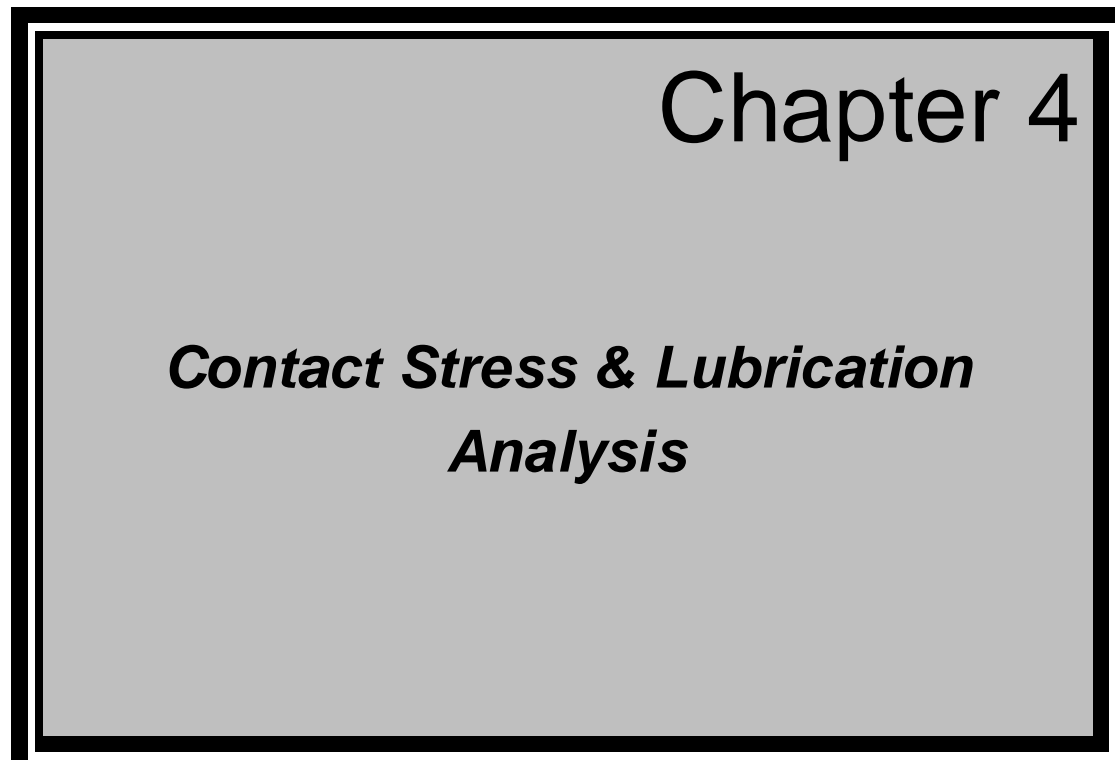
3.4.3 Lubricant preparation

A calf serum based lubricant was prepared for the wear and friction simulations (chapter 6). Raw bovine serum S101 was obtained from Sera-lab (West Sussex, UK) with batch No. W504111. The original protein concentration was 75 g/L and the albumin/globulin ratio was 4.1/3.6. In order to achieve a protein concentration of 20 ± 2 g/L (ISO 18192-1, 2011), the raw bovine serum must be diluted with the appropriate amount of de-ionized water.

A bottle of 500 mL serum was defrosted in a refrigerator at 5°C for 24 hours before dilution. Once the serum was thoroughly defrosted, it was diluted with 1.375 L of de-ionized water. Subsequently, 0.5625 g of sodium azide powder (Sigma-Aldrich, MO, USA) was added to this diluted serum solution to give a concentrate of 0.3 g/L. This final serum solution can only be used for one week before protein denature occurs, thus regular changing of the lubricant was required. The remaining serum solution was stored in a refrigerator and was used within two weeks from the date it was made.

3.5 Chapter summary

In this chapter, the materials and equipment used by the following chapters (4 - 6) are introduced. Victrex[®] PEEK 450G and NuNec[®] cervical discs were chosen as the test materials. Bose instruments were used as the main test equipments. Three-point flexural bending fatigue test was conducted using Bose ELF-3300 material test machine; wear and frictional torque tests were performed using Bose SDWS-1 spine simulators. The corresponding methods used in the wear and frictional torque tests were also described. Specimens were prepared according to a previous wear study (Grupp *et al.*, 2010); wear measurement and lubricant preparation are based on ISO standards.

A large rectangular box with a double black border. The background is light gray. The text is centered and reads: "Chapter 4" in a large, black, sans-serif font at the top right. Below it, "Contact Stress & Lubrication Analysis" is written in a bold, italicized, black, sans-serif font.

Chapter 4

Contact Stress & Lubrication Analysis

4.1 Chapter overview

This chapter presents a theoretical analysis of the maximum contact stress and the lubrication regimes for a PEEK based self-mating cervical total disc replacement. It begins with an introduction section 4.2 which describes the motivation for the analysis. The relevant materials and the specific methods are described in section 4.3. Section 4.4 states the major findings and is followed by a discussion section 4.5. The chapter concludes with a brief summary in section 4.6. The work described in this chapter has already been published (Xin *et al.*, 2012).

4.2 Introduction

This theoretical analysis chapter offers a rationale for the design of PEEK based cervical discs. The likely operating conditions (contact stress and lubrication regime) were determined; the effect of radial clearance (which is an important design parameter for TDR) was also investigated. Moreover, it provides context for the subsequent fatigue (chapter 5) and wear (chapter 6) experiments.

Contact mechanics is used to investigate the stress-strain state near the contact region of solid bodies as a function of their shape, material properties and loading conditions (Goryacheva, 1998). In the case of polymer based ball-on-socket design, both Hertzian (Hertz) and Johnson-Kendall-Roberts (JKR) contact models are applicable (Nikolai & Alexander, 2009). The Hertz model is a fully elastic sphere-sphere contact model which analyzed the stress distribution by considering the contact geometry and the elastic deformation properties of materials. The main assumptions are listed below (Dintwa *et al.*, 2008; Adams, 2012):

- The contacting bodies are made of isotropic and homogeneous materials.
- The contact radius is much less than the radii of curvature of the contacting bodies
- The strains are sufficiently small and linear elasticity applies.

- Each solid body can be considered as an elastic half-space, with a smooth and frictionless contact surface.

The main limitation of the Hertz theory is that it neglects the surface adhesion force in the contact of two surfaces (Faghihnejad & Zeng, 2013). On the other hand, the JKR model is an improved elastic contact model which considers adhesive forces in the contact zone (Nikolai & Alexander, 2009). This model is based on the assumption that surface interactions only occur within an infinitely small contact area, other adhesive forces beyond this area are negligible.

In this chapter, the theoretical lubrication regime predication is based on the determination of the lambda ratio. According to experimental observation, if the lambda ratio is greater than 3, then a fluid film lubrication regime occurs. In this situation, the bearing surfaces are completely separated, thus wear and friction are optimally minimized. A lambda ratio of less than unity indicates boundary lubrication and substantial contact between surface asperities will occur. A lambda ratio of between 1 and 3 indicates a mixed-lubrication regime (Hutchings, 1992).

4.3 Materials & Methods

4.3.1 Disc Model

NuNec[®] cervical disc replacement (as detailed in section 3.2.2) is a semi-constrained design which attempts to replicate the natural kinematics of the spinal disc by adopting a ball-on-socket articulation (Kurtz, 2006). It is equivalent to a ball-and-socket joint, with the ball having a radius R_1 and socket having a radius of R_2 (as shown in Fig. 4.1). The Young's modulus and Poisson's ratio for both the ball and socket were E and ν , respectively. The radial clearance c between the ball and socket was defined as:

$$c = R_2 - R_1 \quad (1)$$

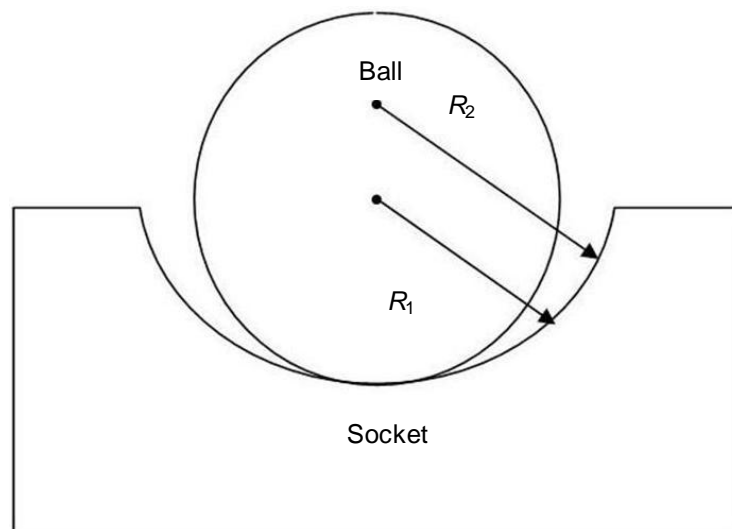


Fig. 4.1: Schematic diagram showing the geometry of the ball-and-socket joint
(adapted from Wenzel & Shepherd, 2007)

4.3.2 Contact Stress

4.3.2.1 Hertzian contact model

For comparison, both Hertz and JKR elastic contact models were employed to analyze the surface contact stresses between the bearing surfaces. In the case of Hertz contact model, the maximum contact stress (P_{\max}) was determined from (Goryacheva, 1998; Wenzel & Shepherd, 2007; Johnson, 2008):

$$P_{\max} = \left[\frac{6FE'^2}{\pi^3 R^2} \right]^{\frac{1}{3}} \quad (2)$$

where F is the applied force, E' is the equivalent elastic modulus for the two bearing materials and R is the equivalent radius for ball and socket. These two parameters were calculated from:

$$E' = \frac{E}{2(1-\nu^2)} \quad (3)$$

and

$$R = \frac{R_1(R_1 + c)}{c} \quad (4)$$

4.3.2.2 Johnson-Kendall-Roberts contact model

In JKR elastic contact model, an extra term (P') is used to take account of the interaction force within the elastic contact zone (Nikolai & Alexander, 2009; Faghihnejad & Zeng, 2013). The maximum contact stress can be calculated using Eq. 5.

$$P_{\max} = P + P' \quad (5)$$

where P is the loading stress, and P' is the adhesion stress. These two terms were calculated from:

$$P = \frac{2aE'}{\pi R} \quad (6)$$

and

$$P' = -\left(\frac{4\gamma E'}{\pi a}\right)^{\frac{1}{2}} \quad (7)$$

where γ is the work of adhesion per unit area, and a is the real contact radius which can be derived from the following:

$$a^3 = \frac{3R}{4E'} \left(F + 3\gamma\pi R + \sqrt{6\gamma\pi R F + (3\gamma\pi R)^2} \right) \quad (8)$$

4.3.3 Lubrication regimes

4.3.3.1 Lambda ratio

The lubrication regime was predicted by calculating the corresponding lambda ratio (λ) and given as:

$$\lambda = \frac{h_{\min}}{\sigma} \quad (9)$$

where h_{\min} is the minimum effective film thickness and σ is the compound surface roughness given by:

$$\sigma = \sqrt{S_{a1}^2 + S_{a2}^2} \quad (10)$$

where S_{a1} and S_{a2} are the mean surface roughness of the bearing surfaces for the ball and socket, respectively.

4.3.3.2 Minimum effective film thickness

The minimum film thickness between the bearing surfaces was calculated using the formula (Eq. 11) proposed by Hamrock & Dowson (1997). This equation has been used by in many studies of joint replacement, such as hip joint (Mattei *et al.*, 2011) and lumbar TDR (Shaheen & Shepherd, 2007).

$$h_{\min} = 2.8R \left(\frac{\eta u}{E^* R} \right)^{0.65} \left(\frac{F}{E^* R^2} \right)^{-0.21} \quad (11)$$

where, η is the lubricant viscosity, E^* is the equivalent modulus of elasticity and u is the entraining velocity. The later two parameters were calculated from:

$$E^* = \frac{E}{(1-\nu^2)} \quad (12)$$

and

$$u = \frac{\omega R_1}{2} \quad (13)$$

where ω is the angular velocity in radians.

4.3.4 Parameters

4.3.4.1 Radii of the socket & ball

The radii of the ball and socket of the NuNec[®] cervical disc replacement were measured using a DEA-Swift manual coordinate measuring machine (Hexagon Metrology Ltd., Telford, UK), following the procedure described in section 3.3.1. Five repeated measurements were taken for the ball part and the socket part, respectively. The socket was found to have a mean (\pm standard deviation) radius of 7.019 ± 0.026 mm and the ball had a radius of 6.308 ± 0.005 mm. For the analysis in this chapter, the ball radius was chosen as 6.3 mm and the socket radius was chosen as 7 mm, thus giving a radial clearance of 0.7 mm. Since the aim of this chapter was to understand the effect of

different radial clearances on stresses and lubrication regimes, in addition to a radial clearance of 0.7 mm, radial clearances of 0.05, 0.1 and 0.15 mm, which have been used by other investigators (Shaheen & Shepherd, 2007; Wenzel & Shepherd, 2007; Clewlow *et al.*, 2008) were also used for comparative analysis.

4.3.4.2 Contact surface roughness measurement

Surface roughness of the bearing surfaces was measured using a Taylsurf-120L profilometer (Taylor Hobson Ltd., Leicester, UK) and following the procedure described in section 3.3.2. The obtained arithmetic mean surface roughness (S_a), for all of the respective bearing surfaces, were found to be 0.585 μm for the ball and 0.525 μm for the socket. The corresponding compound surface roughness value σ (Eq. 10) was calculated to be 0.786 μm .

4.3.4.3 Other parameters

The surface energy of PEEK 450G has been reported as 0.044 J/m^2 (Zhang *et al.*, 2011); the work of adhesion (γ) between PEEK self-mating surfaces is equal to twice of its surface energy (Faghihnejad & Zeng, 2013). The angular velocity (ω) for the human cervical spine has been reported to be in the range of 0 rad/s (at rest) to 4.5 rad/s (during motion) (Salvia *et al.*, 2006). This can be

converted into an entraining velocity using Eq. 13. Interstitial fluid was proposed as the natural lubricant for the intervertebral disc (Graham, 2006). However, bovine serum which is normally used for *in-vitro* wear testing of disc replacements (ISO18192-1, 2011) was also considered. An interstitial fluid with a viscosity of 1.24 mPa·s was considered as the primary lubricant based on the work of (Zurovsky *et al.*, 1994; Windberger *et al.*, 2003); 25% bovine serum (diluted with deionised water) with a viscosity of 0.9 mPa·s was used as a comparison (as used by Jin *et al.*, 2003; Mattei *et al.*, 2011). The maximum compressive loading for the cervical disc was assumed to be 150 N, selected according to the recommended value from ISO 18192-1 (2011). The Young's modulus (E) and Poisson's ratio (ν) of PEEK were taken to be 3.7 GPa and 0.36, respectively (Kurtz & Devine, 2007; PEEK™ 450G datasheet, 2012).

In this chapter, the radial clearance or lubricant was varied between the bearing surfaces of the disc replacement and the theoretical contact stress and minimum film thickness were calculated. A summary of the parameters and variables used are shown in Table 4.1.

Table 4.1: Summary of constant parameters and variables used.

Parameter	Constant	Variable
Load, F (N)	-	0-150
Radius of ball, R_1 (mm)	6.3	-
Angular velocity, ω (rad/s)	-	0-4.5
Radial clearance, c (mm)	-	0.05, 0.1, 0.15, 0.7
Young's modulus, E (GPa)	3.7	-
Poisson's ratio, ν	0.36	-
Work of adhesion, γ (J/m ²)	0.088	
Viscosity, η (mP·S)	-	0.9, 1.24
Compound surface roughness, σ (μm)	0.786	-

4.4 Results

4.4.1 Contact stress

Fig. 4.2 shows the variation of maximum contact stress with force for TDR with different radial clearances. For a PEEK cervical disc under 150 N loading, the maximum contact stress is in the range 5.9 to 32.1 MPa (for a range of radial clearances from 0.05 to 0.7 mm). The effect of adopting different contact models is shown in Fig. 4.3. Where, the maximum contact stresses calculated using the Hertz and JKR contact model were plotted against the applied force,

for a radial clearance value of 0.7 mm. The obtained trend lines are almost identical and overlap each other.

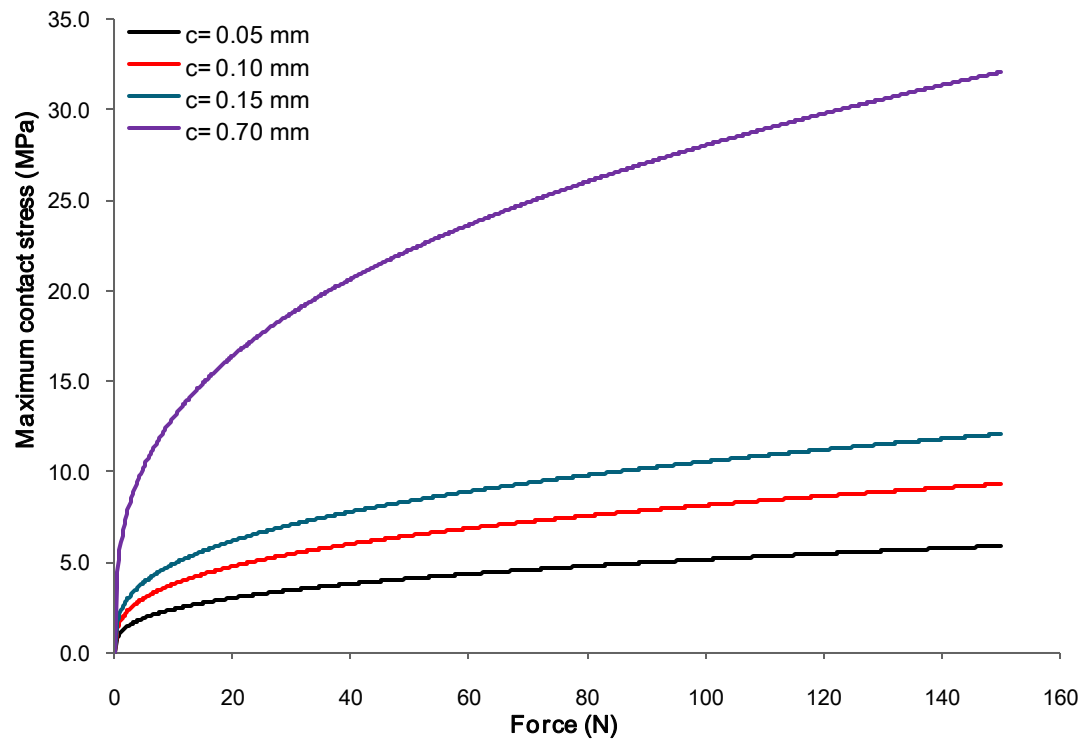


Fig. 4.2: Variation of maximum contact stress with force, for radial clearance values of 0.05, 0.10, 0.15 and 0.7 mm.

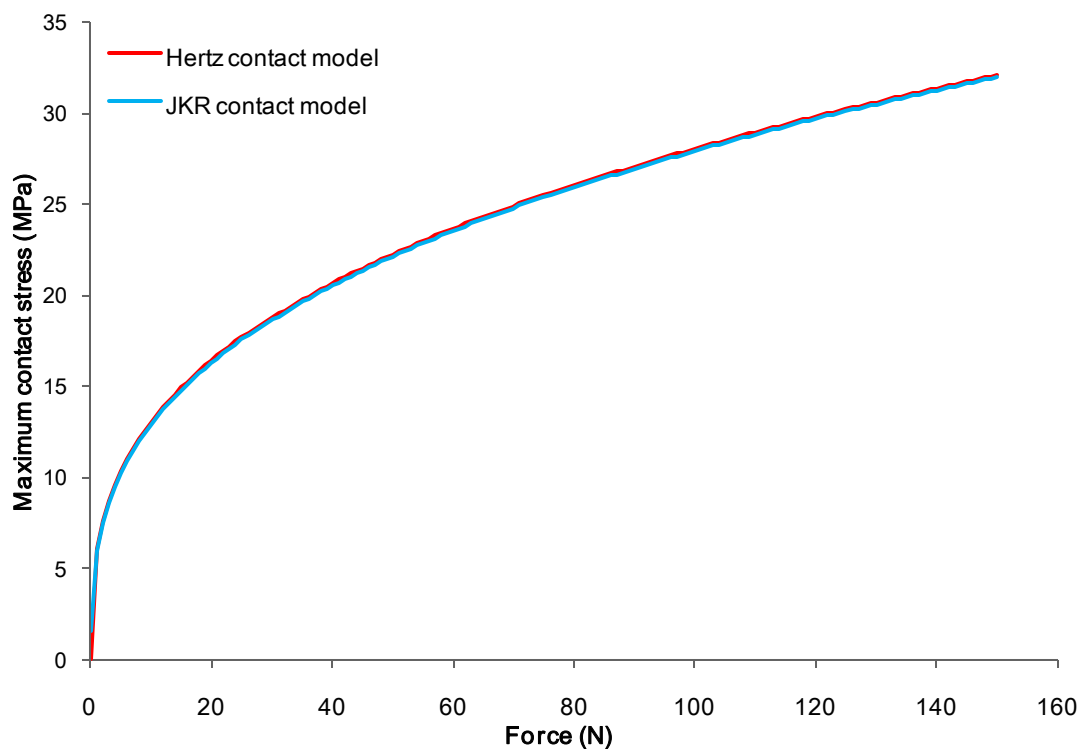


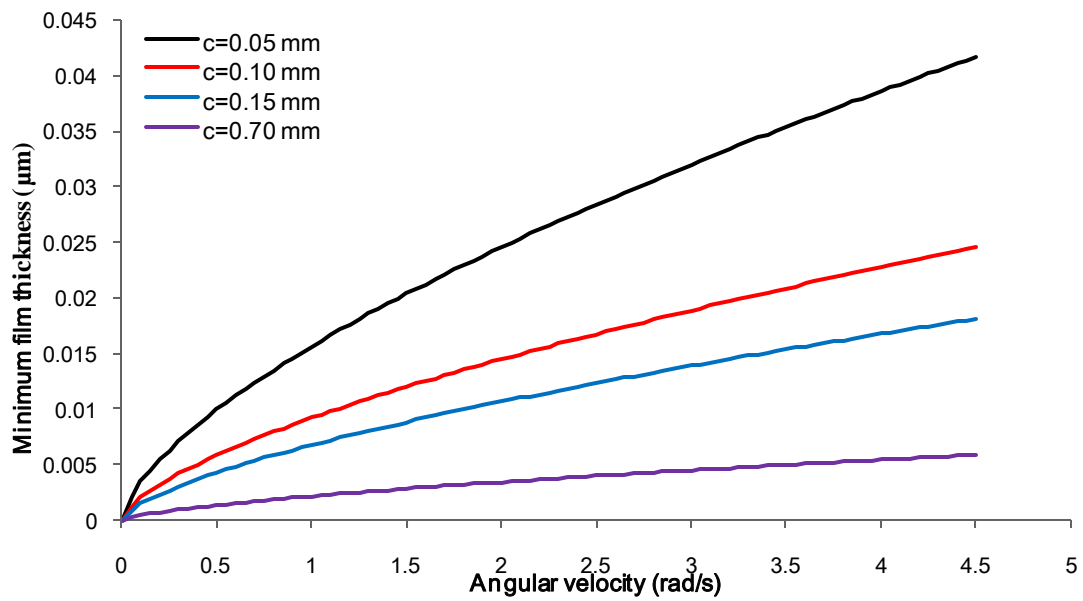
Fig. 4.3: Variation of maximum contact stress with force for a radial clearance value of 0.7 mm, calculated using the Hertz and JKR contact model.

4.4.2 Lubrication

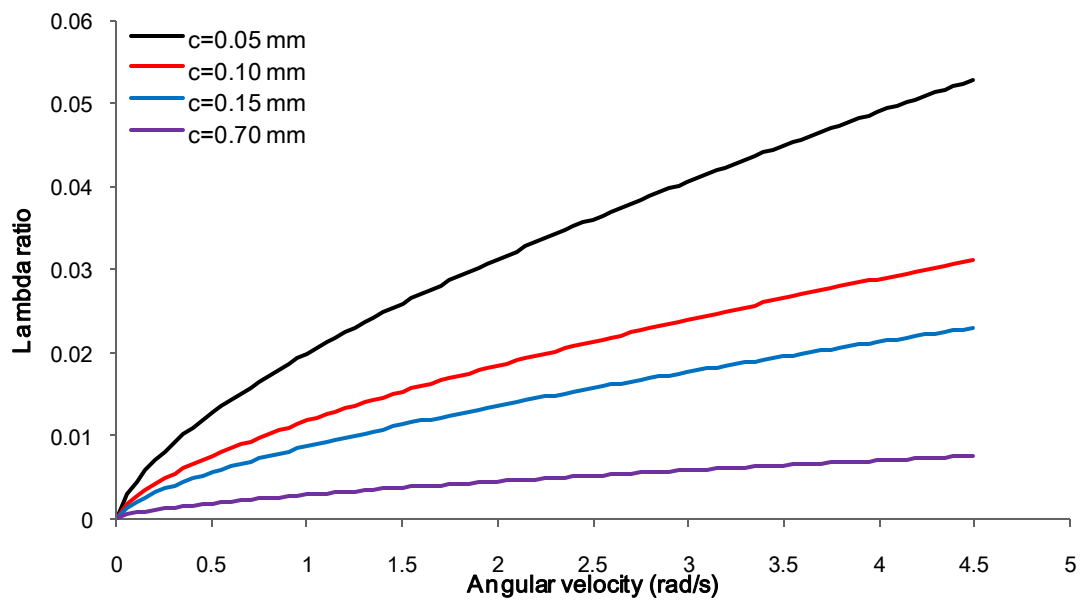
The variation of minimum film thickness by adopting different radial clearances is shown in Fig. 4.4a; the corresponding lambda ratio variation is given in Fig. 4.4b. The predicted minimum film thickness was in the range 0 to 0.042 μm with a lambda ratio range from 0 to 0.052. This finding indicates that the PEEK based cervical discs are likely to operate within a boundary lubrication regime across the whole range of angular velocities and under 150 N loading.

The effects of load on the minimum film thickness and lambda ratio are shown in Fig. 4.5a and 4.5b, respectively. They show that the applied load has a detrimental effect on both the minimum film thickness and the lambda ratio. Moreover, the calculated lambda ratio is always below unity and indicates boundary lubrication.

Fig. 4.6a&b show the variation of minimum film thickness and lambda ratio, respectively, when different lubricants are employed. The minimum film thickness can be enhanced by incorporating a more viscous lubricant; the lambda ratio can be increased in a similar manner. In spite of this, the lubrication regime is still boundary lubrication, regardless of the lubricant used.

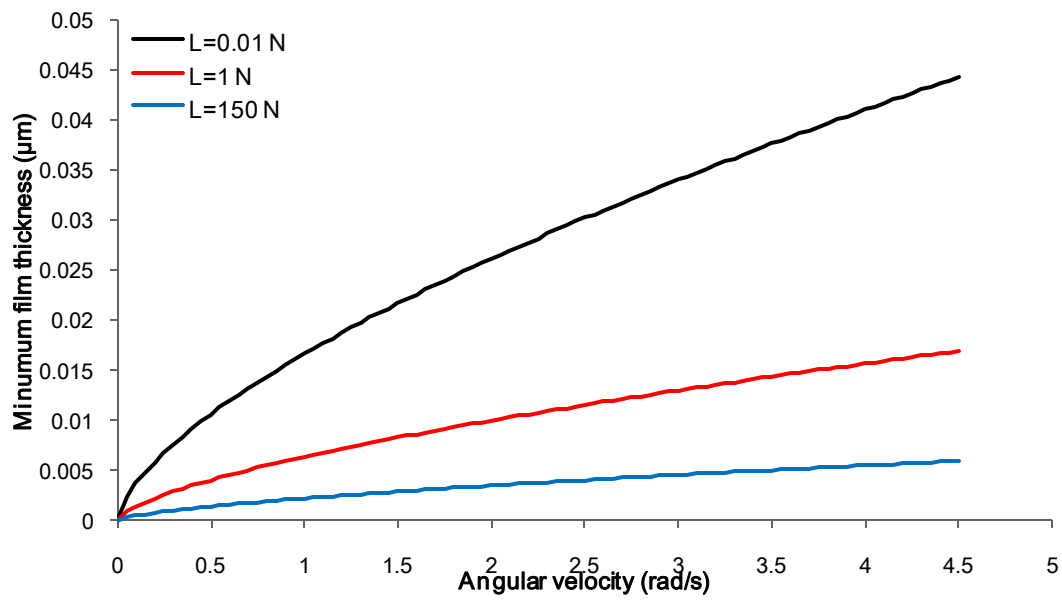


a)

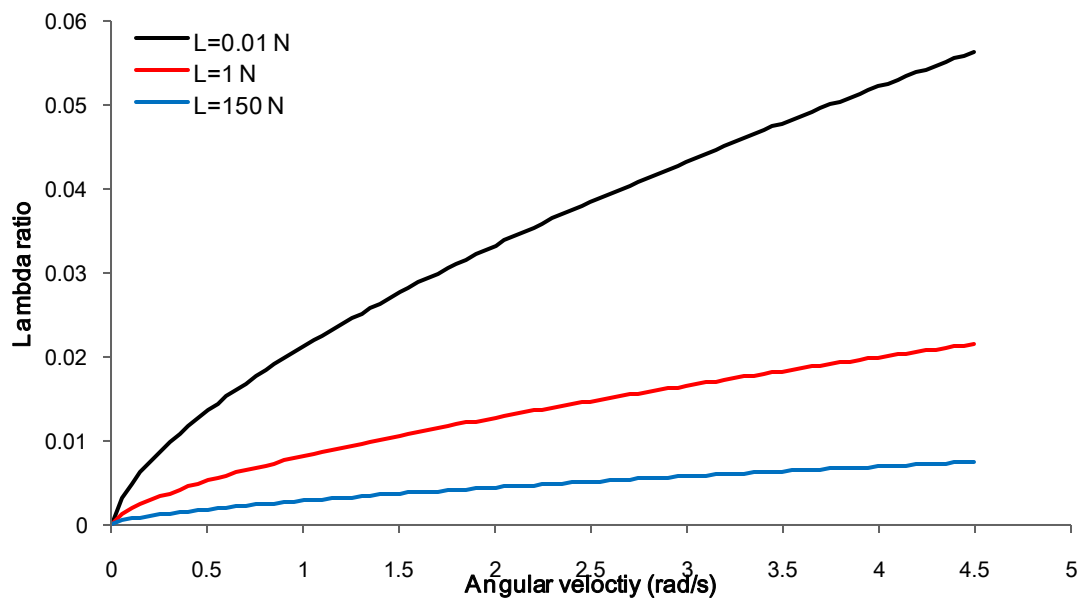


b)

Fig. 4.4: a) Variation of minimum film thickness with angular velocity; b) Variation of Lambda ratio with angular velocity. Each figure is plotted for a cervical disc replacement under 150 N load, using interstitial fluid as the lubricant.

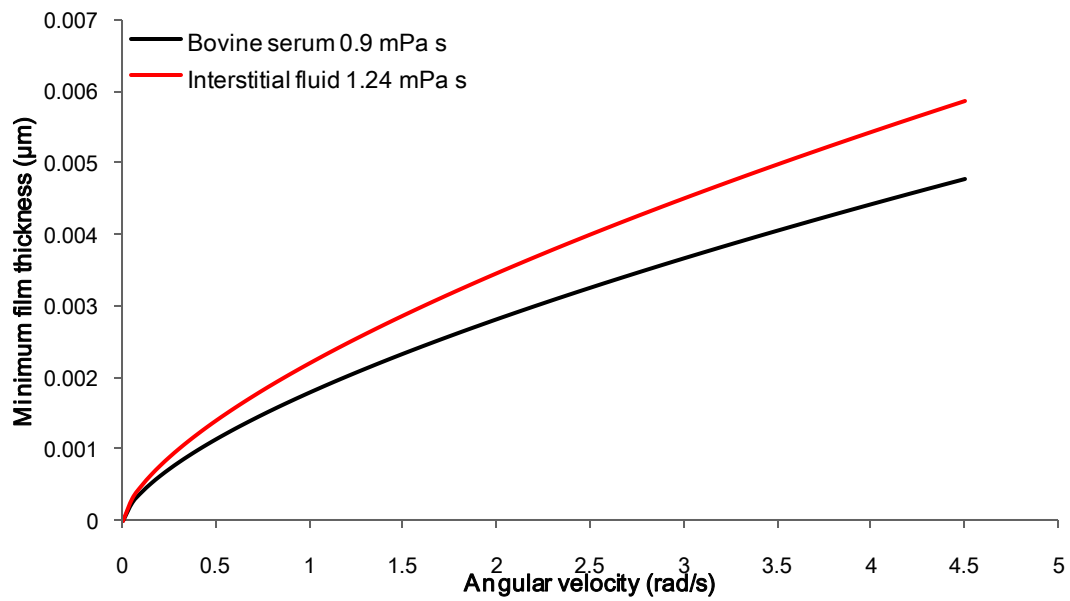


a)

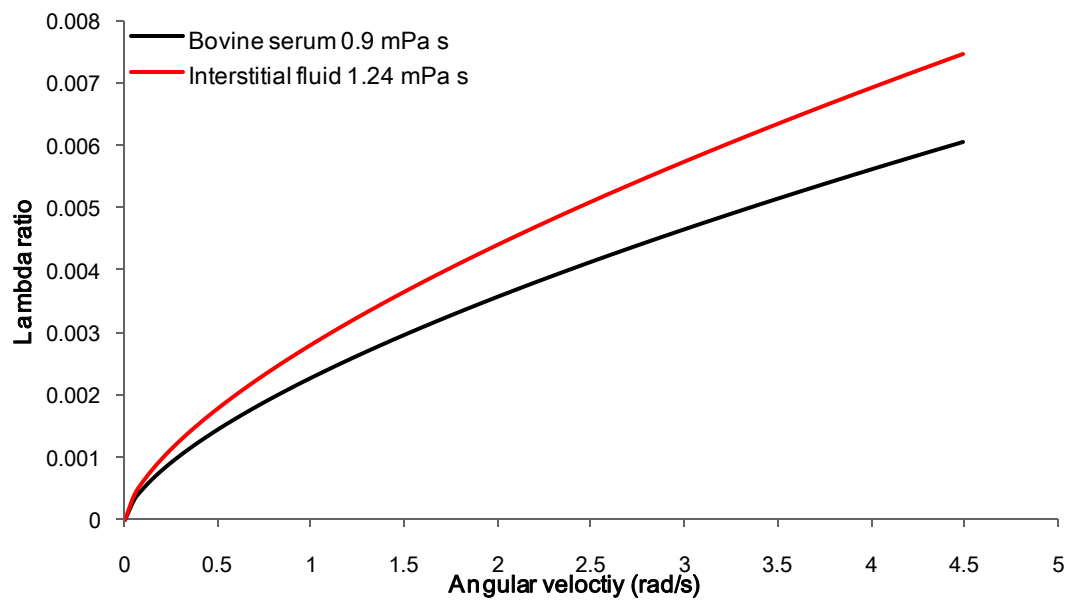


b)

Fig. 4.5: a) Variation of minimum film thickness with angular velocity; b) Variation of Lambda ratio with angular velocity. Each figure is plotted for a cervical disc replacement at a radial clearance value of 0.7 mm, using interstitial fluid as the lubricant.



a)



b)

Fig. 4.6: a) Variation of minimum film thickness with angular velocity; b) Variation of Lambda ratio with angular velocity. Each figure is plotted for a cervical disc replacement at a radial clearance value of 0.7 mm, under 150 N load.

4.5 Discussion

For the NuNec[®] cervical disc the maximum contact stress it was subjected to was 32.1 MPa. It is well below the yield strength of PEEK 450G under compression which is documented as 120 MPa (PEEK[™] 450G datasheet, 2012). Furthermore, the fatigue strength of PEEK 450G with a crystallinity value of 22.5 % was reported as 58.72 MPa at one million cycles (Abu Bakar *et al.*, 2003; Tang *et al.*, 2004). It is predicted that the stress experienced by the contact surface of this disc is insufficient to result in material fatigue. Nevertheless, high cycle fatigue tests of at least 10 million cycles are still required to ensure the structural safety of cervical disc replacement during long-term application (ASTM F2346, 2005).

In theory, the JKR contact model is superior to the Hertz contact model, because it can take the surface interaction force (*i.e.* adhesion force) into account. In this study, these two contact models make no difference (as shown in Fig. 4.3). This is because the actual real contact radius is very small (roughly about 1.51 mm under 150 N load) (refer to Appendix A for detail) and surface energy of PEEK is negligibly small at 0.044 J/m² (Zhang *et al.*, 2011).

According to the calculated lambda ratios, the NuNec[®] cervical disc will operate under a boundary lubrication regime. This means that there will be

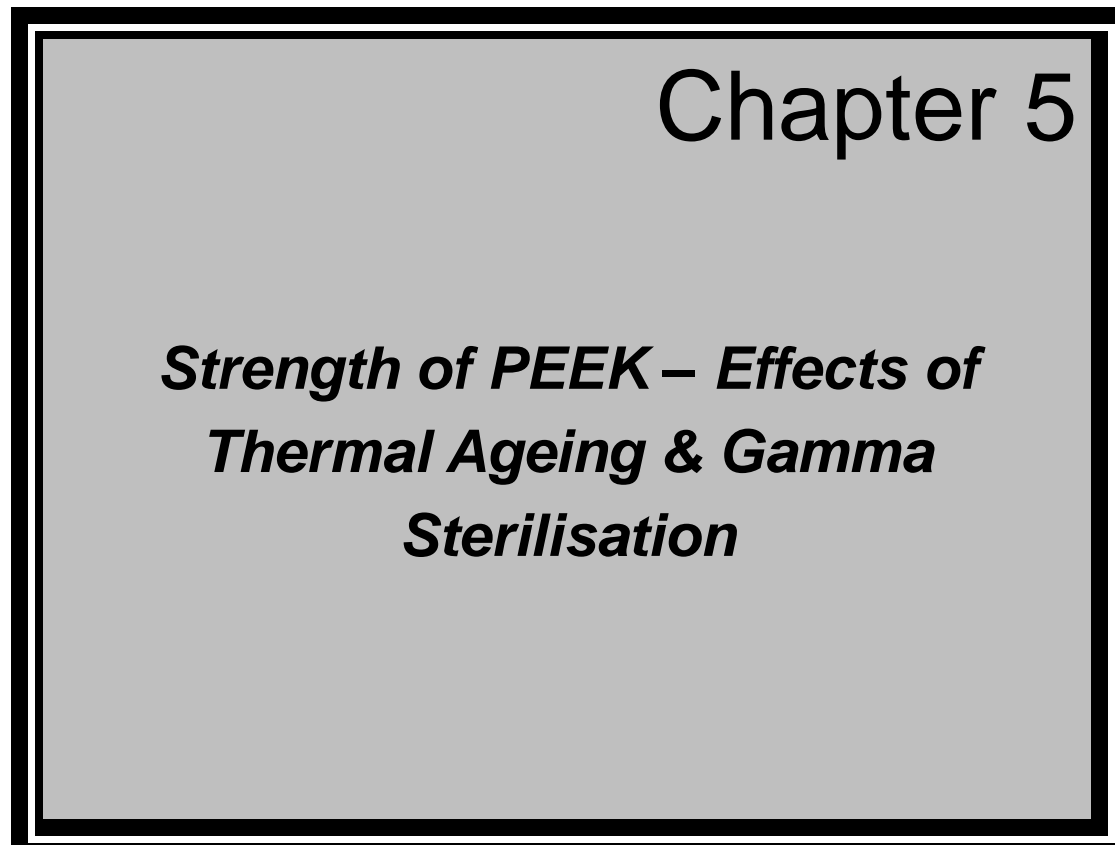
significant surface asperities in contact and wear will occur. To the author's knowledge, there is no other published cervical disc lubrication analysis. A previous study has shown that for lumbar disc arthroplasty most devices will also operate with a boundary lubrication regime (Shaheen & Shepherd, 2007), but a direct comparison with cervical discs is unwise due to the different motions and loads. However, hip joints have been studied in more detail; insights can be gained from these studies (Scholes & Unsworth, 2000; Jin *et al.*, 2003).

There are two significant limitations to the lubrication analysis conducted in this chapter. The first relates to the basic assumption of the Hamrock-Dowson formula that the lubricants (bovine serum and interstitial fluid) utilized are Newtonian, iso-viscous fluids (Hamrock & Dowson, 1997). Actually, bovine serum is a Non-Newtonian fluid and shows a reduction of viscosity as the shear rate increased (detailed in section 6.3.4). This fact may further reduce the actual minimum lubrication film thickness. Secondly, the lubrication analysis is limited to steady-state motion. This is a simplified model to represent the motion of the neck, and is highly unlikely to reflect reality. The intention of adopting this simplified motion is to ascertain the potential of this cervical disc to be operated under a fluid lubrication regime by altering its radial clearance, lubricant or load. A more realistic examination of lubrication

regime can be achieved through experimental measurements of the frictional torque and plotting of the Stribeck curve.

4.6 Chapter summary

This chapter has predicted the likely contact stress and lubrication regime of a PEEK self-mating cervical disc. It indicates that the NuNec[®] cervical disc will operate under a boundary lubrication regime, with the generation of wear debris likely. The maximum contact stress was found to be 32.1 MPa, but this is less than either the compressive yield strength or fatigue strength of PEEK 450G. In the next chapter, the fatigue performance of PEEK was assessed in bulk material form, and the effects of thermal ageing and sterilisation were also investigated.

A large rectangular box with a thick black border. The background is light gray. The text is centered and reads: "Chapter 5" in a large font at the top right, and "Strength of PEEK – Effects of Thermal Ageing & Gamma Sterilisation" in a bold, italicized font in the center.

Chapter 5

Strength of PEEK – Effects of Thermal Ageing & Gamma Sterilisation

5.1 Chapter overview

This chapter investigates the effects of thermal ageing and gamma sterilisation on the flexural strengths of PEEK 450G. It starts with a brief background section 5.2, where the essential information is given. Section 5.3 presents the materials and methods. This is followed by the results section 5.4 and a discussion section 5.5. At the end of this chapter, a concise chapter summary is given in section 5.6. The work described in this chapter has already been published (Xin *et al.*, 2013a).

5.2 Background

5.2.1 Introduction

PEEK and its composite have been extensively used in a range of medical implants, such as the Brantigan lumbar intervertebral body fusion cage (Depuy Spine, Rayaham, MA), total joint replacement (Epoch hip stem by Zimmer Inc., Warsaw, IN) and disc replacement bearing surfaces (NuBac[®] Lumbar intra-disc and NuNec[®] cervical disc by Pioneer Surgical Technology Inc., Driebergen, Netherlands) (Kurtz&Devine, 2007). The fatigue property of this biomaterial is of particular interest for the biomaterials community. In addition to this, polymers are susceptible to the effect of radiation sterilisation and ageing. The general outcomes include the formation of an oxidation layer, discolouration and embrittlement (Massey, 2005). Understanding these characteristics is crucial for determining the operational longevity and structural safety of polymer based medical implants (Baker *et al.*, 2000).

Several studies (Curtis *et al.*, 1988; Buggy & Dillon, 1991; Brillhart & Gregory, 1991; Brillhart & Botsis, 1992; Nisitani *et al.*, 1992; Brillhart & Botsis, 1994; Abu Bakar *et al.*, 2003; Tang *et al.*, 2004; Sobieraj *et al.*, 2010; Schamobron *et al.*, 2010; Sobieraj & Rimnac, 2012) have presented fatigue data on PEEK and its composites; however, none of them have considered the effects caused by sterilisation and ageing. Whether there is any significant deterioration in the

fatigue performance of PEEK is still unknown, thus the main aim of the research described in this chapter is to answer this question.

5.2.2 Polymer fatigue

Fatigue of a polymer is a process in which damage accumulates due to the repetitive application of loads (Ritchie, 2003). To assess the fatigue characteristic of a polymer, different approaches can be adopted; the polymer can be tested either in its bulk material form or in its actual product form. For the intrinsic low thermal conductivity of a polymer (compared to other materials), the localized temperature rise due to high frequency fatigue experiments can lead to a significant concern about deterioration of the mechanical properties (Curtis *et al.*, 1998). On the other hand, conducting low frequency fatigue experiments is normally costly and time consuming, especially when using an actual product and in a simulated physiological environment (Teoh, 2000).

5.2.3 Fatigue assessment approach

The classic methods of quantifying the intrinsic fatigue behaviour of a polymer material can take two forms: the total-life (stress/life) fatigue approach and the fracture-mechanics approach (crack propagation method) (Teoh, 2000; Ritchie, 2003). Both methods are classified as stress-control experiments by BS

3518-1 (1993), where a constant cyclic stress is applied to the bulk material, under a certain waveform and frequency, until failure occurs. The total-life fatigue approach uses an un-notched specimen to generate the required stress-life (S-N) plot; the stress amplitude is generally plotted against the number of cycles to failure on a linear-log scale (Ritchie, 2003). The main methodology assumes that the specimen is initially defect-free without a stress concentration; the fatigue failure is then a consequence of void nucleation and subsequent crack growth to a critical size (Sobieraj & Rimnac, 2012). In comparison, fracture-mechanics is a defect-tolerant fatigue approach which incorporates a notched specimen with pre-defined notch geometry (Ritchie, 2003). By assuming that linear elastic fracture mechanics conditions are applied, the crack growth kinematics can be investigated (Sobieraj & Rimnac, 2012). For the fatigue research conducted in this chapter, total-fatigue life approach is preferred, due to its simplicity and feasibility.

5.2.4 Historical studies of PEEK fatigue

To understand the fatigue performance and possible failure mechanisms of PEEK and its composites, many tests have been conducted under different testing conditions, as shown in Table 5.1. Most of the fatigue studies used either a tensile-tensile or a flexural bending mode, with an R ratio (minimum stress divided by the maximum stress) of 0.1 in a sinusoidal wave-form for 10^6

cycles, under either 0.5 or 5 Hz frequency, at 23°C room temperature. Because the limitation of funding and equipment, flexural bending mode is chosen for the fatigue research conducted in this chapter. As unreinforced PEEK is a homogenous thermoplastic and based on the ISO 178 (2003) recommendation, a 3-point flexural bending configuration is used rather than 4-point flexural bending.

Table 5.1: Test conditions of historical PEEK fatigue studies.

Materials	Testing mode	R ratio	Force format	Testing condition	Max cycle
Victrex PEEK 450G , (Abu Bakar <i>et al.</i> , 2003)	Tension-tension	0.1	Sinusoidal	25°C, 5Hz	10 ⁶
Victrex PEEK ,(Jones <i>et al.</i> , 1985)	Zero-tension	N/A	Square wave	23°C, 0.5Hz	10 ⁶
Continuous carbon fibre reinforced PEEK ,(Schambron <i>et al.</i> , 2010)	Flexural bending	0.1	Sinusoidal	60°C, 1Hz	10 ⁶
APC-2 ,(Curtis <i>et al.</i> , 1998)	Compression /tension	N/A	Sinusoidal /square	23°C, 0.5Hz	10 ⁷
APC-2 ,(Buggy & Dillon, 1991)	Flexural bending	0.1	Sinusoidal	23°C, 5Hz	10 ⁷
<ul style="list-style-type: none"> • APC-2 is a continuous carbon fibre reinforced PEEK • Not all information is given for each study. 					

5.2.5 Accelerated ageing of PEEK

Ageing of polymers may occur during shelf-storage or after implantation (*i.e.* biodegradation). The properties of a polymer degrade over time and lead to a potential safety risk (White, 2006). The durability of medical polymers can be evaluated using accelerated ageing method, in order to simulate long-term natural ageing in a relative short period of time.

Biodegradation is the chemical breakdown of materials by the action of living organisms that leads to changes in physical properties. It mainly involves two major aspects, hydrolysis and oxidation (Ratner, 2012). Up to now, there is no standard procedure for simulating long-term *in-vivo* ageing of PEEK biomaterials. This is in part due to the difficulty in simulating all the variables exposed under *in-vivo* conditions (*e.g.* chemical interaction with biological substance or cells) using an *in-vitro* ageing method.

ASTM has published the F2003-02 (2008) practice which is specified for accelerated ageing of UHMWPE. It uses the combined effect of elevated temperature and oxygen pressure to simulate long-term ageing. Samples are placed in an oxygen environment at 70°C and 5 bar atmosphere pressure, for 15 days. Several authors (Cartwright & Devine, 2005; Bao *et al.*, 2007) adopt this ASTM practice in their experiments, in order to investigate the ageing effect

on either the mechanical properties or tribological performance of PEEK. However, the applicability of this standard is still unknown. In addition, this practice is very rigorous and sensitive to the testing condition such as temperature and heating rate (Lu *et al.*, 2002), thus leading to large variations and need for precisely controlled apparatus (*e.g.* Parr pressure vessel 4760 series, Parr Instrument Ltd., USA). Oven thermal ageing is another common practice for accelerated ageing of PEEK (Buggy & Carew, 1994; Sınmazçelik & Yılmaz, 2007; Schambron *et al.*, 2010). It only uses the effect of elevated temperature to simulate the long-term ageing outcome. By comparison, it is a relatively simple method and easy to perform. Due to this fact, oven thermal ageing is preferred. The next question is then how to select the appropriate ageing temperature.

Hemmerlinch (1980) suggests that the maximum ageing temperature should be less than the glass transition temperature of the material and should not lead to any unnatural physical or chemical change. Normally the ageing temperature used for thermal ageing of polymers is around 60°C (Lambert *et al.*, 2001). Because PEEK is a high performance thermoplastic with a high glass transition temperature of 143°C (section 2.4.4). A high ageing temperature of 90°C is selected for the thermal ageing pre-treatment conducted in this chapter. This ageing temperature has been previously used by Schambron *et al.* (2010)

for investigating the effects of environmental ageing on the static and cyclic bending properties of braided carbon fibre/PEEK bone plates.

5.2.6 Sterilisation

For medical devices, sterilisation is a mandatory process before implantation. Gamma irradiation is normally used due to its convenience, low cost and good penetration ability (Massey, 2005). This ionized irradiation can effectively kill pathogens, bacterial and micro-organisms, due to its ability to break the chemical bonds of organic compounds. The standard sterilisation dose for medical devices is 25-40 kGy of gamma irradiation, from a cobalt 60 isotope (^{60}Co) source (Kurtz, 2012b).

5.3 Materials & Methods

5.3.1 PEEK specimen preparation

The PEEK specimens were prepared from unreinforced PEEK 450G (Victrex plc., Lancashire, UK) sheets (refer to section 3.2.1). These sheets were cut using a band saw (1 mm blade thickness) into rectangular specimens with 140 mm length x 15 mm width (as shown in Fig. 5.1), according to ISO 178 (2003). Prior to testing, the exact dimensions of each specimen were measured using a digital calliper (Fisher Scientific Ltd., UK) with 0.01 mm precision, at three

different locations along each specimen's length. In addition, a visual inspection was also performed; specimens with obvious surface scratches or twists were withdrawn and replaced with new specimens.

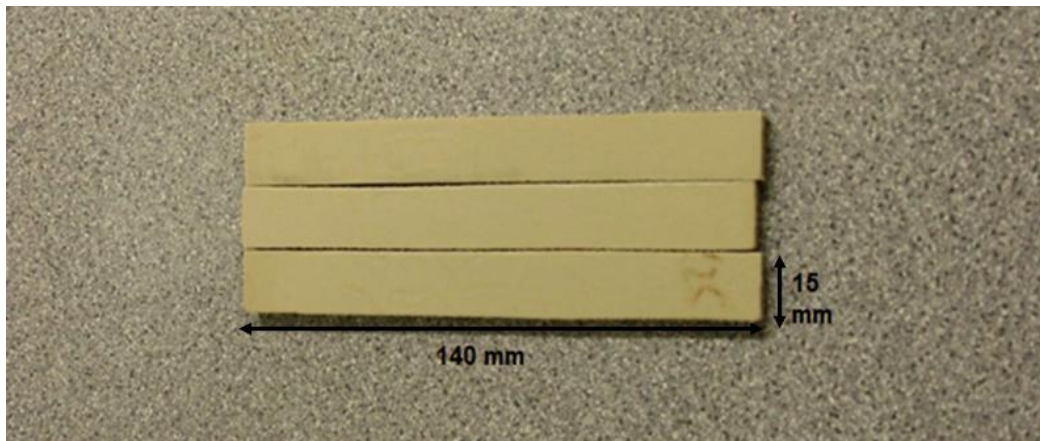


Fig. 5.1: PEEK 450G rectangular specimens (nominal thickness is 6 mm).

5.3.2 Annealing, sterilisation & ageing

The PEEK specimens were divided into five groups, according to whether the specimens had been annealed, sterilised or aged (Table 5.2). A standard annealing procedure was conducted according to the manufacturer's recommendations (PEEK processing guide, 2012) and using a Cabolite PN30 oven (Scientific Laboratory Supplies Ltd., Orchard house, Hessle, East Riding of Yorkshire, UK). PEEK specimens were initially placed in the oven and dried for three hours at 150°C. The oven temperature was then gradually increased with a heating rate of 10°C per hour. Once 250°C was reached, it was held at

this temperature for a minimum of 4 hours. After the holding stage, the oven temperature was steadily decreased at 10°C per hour, until the temperature was below 140°C. Finally, the oven was switch off and the PEEK specimen was allowed to cool down to room temperature. Sterilisation pre-treatment was achieved using gamma-irradiation, in a dosage range of 25-40 kGy by Isotron Ltd. (Moray Road, Elgin Industrial Estate, Swindon, UK). Specimens that were aged were placed in the Cabolite PN30 oven, at 90°C for either 96 days or 192 days (Schambron, 2010).

Table 5.2: Pre-treatments and subsequent static and dynamic test methods for all PEEK 450G specimens.

Group No.	Annealing	Sterilisation	Thermal ageing	No. of specimens	Test method
1	No	No	No	7	Static
2	Yes	No	No	7	Static
3	Yes	Yes	No	7	Static
				10	Dynamic
4	Yes	Yes	90°C, 96 days	7	Static
				11	Dynamic
5	Yes	Yes	90°C, 192 days	7	Static
				10	Dynamic

5.3.3 Testing rig (three-point bending)

An aluminium test rig (as shown in Fig. 5.2) was designed and manufactured, according to ISO178 (2003). The lower test rig consisted of two supports (112 mm apart) that was attached to the base of the testing machine. The upper test rig was attached to the actuator of the testing machine and consisted of a bar with a 5 mm radius at the end. A detailed engineering drawing of the testing rig can be found in Appendix B.

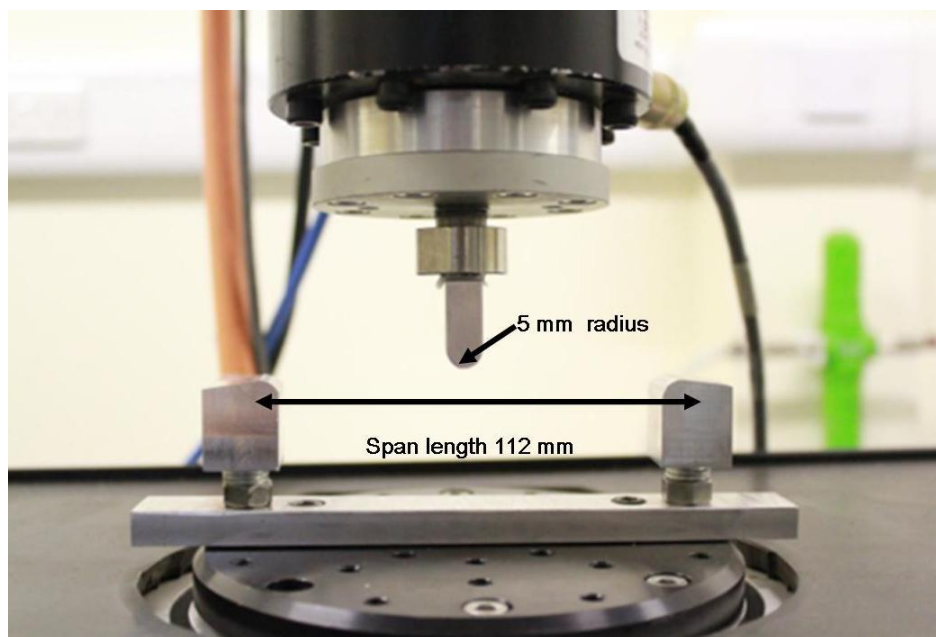


Fig. 5.2: Three-point bend test rig.

5.3.4 Static tests

Static three-point bend tests were performed according to ISO 178 (2003), using a Lloyd 6000R materials testing machine (Lloyd Instruments Ltd., West

Sussex, UK) which was operated by Windap V1.6 software (detailed in section 3.3.3). The PEEK specimen was symmetrically placed on the two upright supports. The actuator of the materials testing machine was set to lower, at a rate of 2 mm/min (ISO 178, 2003). Load and displacement were recorded throughout the tests. Testing continued until a maximum displacement of 40 mm had been applied. Graphs of load against displacement were plotted. Seven specimens from each of the five groups in Table 5.2 were tested.

In the load-displacement graph, the peak load (*i.e.* maximum sustained load) was considered as the yielding load (F) and its corresponding displacement was defined as the yielding displacement (δ). The flexural strength (σ) was then calculated according to Eq. 1 (ISO 178, 2003).

$$\sigma = \frac{3Fl}{2bd^2} \quad (1)$$

where l is the span length, b is the width and d is the thickness.

5.3.5 Dynamic tests

All dynamic tests were performed with the same three-point bending test rig, as described in section 5.3.3. For the dynamic tests a Bose 3300 materials testing machine (Bose Corporation, ElectroForce Systems Group, Minnesota,

USA) was used, controlled by Win test software (detailed in section 3.3.4). Testing involved applying a sinusoidally varying force at a frequency of 5 Hz, at room temperature. The ratio of minimum to maximum force was 0.1. The maximum force applied to a specimen was based on a percentage (85-62.5%, 2.5% decrements) of the static yield strength of group 3 specimens, determined in section 5.4.1. Ten PEEK specimens from group 3 and group 5, and 11 from group 4 (Table 5.2) were subjected to the dynamic tests. For each fatigue group, one of the PEEK specimens served as a tuning sample. Testing continued until fracture of a specimen or 10 million cycles. Graphs of stress against number of cycles to failure (*i.e.* stress-life) were plotted on a log scale, and the corresponding gradients and intercepts were determined via linear regression fitting.

5.3.6 Scanning electron microscopy

Scanning electron microscopy (SEM) fractography images can provide essential insights regarding the fracture mechanisms of PEEK due to fatigue. Therefore, the fractured PEEK surfaces (fatigue group 3 only) were analysed using a Philips XL-30 FEG environmental scanning electron microscope (SEM) with Oxford Inca EDS system (FEI Company, Hillsboro, USA). The specimens were initially prepared by cutting the fractured sample into a rectangular block (5 × 15 × 7 mm) and then sputter coating with a thin layer of gold using a

Polaron E5000 sputter-coating unit (Polaron Ltd., London, UK). SEM scans were then taken at 5 kV acceleration voltages. The obtained fractography images were then interpreted according to the literature studies (Sobieraj *et al.*, 2010; Sobieraj & Rimnac, 2012).

5.3.7 Statistical analysis

Statistical analysis was performed using Sigmaplot Version 11.0 (Systat Software Inc., London, UK). One way ANOVA plus Tukey pair-wise multiple comparisons were adopted to compare the static strength results amongst the five groups.

For the dynamic fatigue results, analysis of the regression coefficients of the stress-life graph was performed according to the method proposed by Cohen (1983). For a linear regression line with one dependent variable (y_i) and one independent variable (x_i), the estimated standard errors of gradient () and intercept () can be obtained from Eqns. 2 and 3, respectively.

$$\hat{\sigma}_{\beta_0} = \hat{\sigma}_{\varepsilon} \sqrt{\frac{1}{n} + \frac{\bar{x}^2}{\sum_{i=1}^n (x_i - \bar{x})^2}} \quad (2)$$

and

$$\hat{\sigma}_{\beta_1} = \hat{\sigma}_{\varepsilon} \sqrt{\frac{1}{\sum_{i=1}^n (x_i - \bar{x})^2}} \quad (3)$$

Where n is the number of observation (*i.e.* the number specimens used for each fatigue group) and \bar{x} is the mean value of x (*i.e.* the average number of cycle achieved within each fatigue group); the subscript i represents the n th of observation. $\hat{\sigma}_{\varepsilon}$ is the unbiased mean error and defined as follow:

$$\hat{\sigma}_{\varepsilon} = \sqrt{\frac{\sum_{i=1}^n (y_i - \hat{y}_i)^2}{n-2}} \quad (4)$$

where y_i is the actual stress value and \hat{y}_i is the predicted stress value from the linear regression line. Once the standard errors of the gradient and intercept are obtained, comparing between sub-groups can be performed using the Student-t test. The significance level was set at $p < 0.05$ for all statistical analysis.

5.4 Results

5.4.1 Static tests

A typical load-displacement graph of a PEEK specimen is shown in Fig. 5.3. It initially displays a linear trend. After reaching the yielding point, the PEEK specimen begins to deform plastically with a declining load, until the displacement limit (40 mm) is

reached. The obtained yielding loads and yielding displacements are shown in Table 5.3. One way ANOVA analysis shows that the yield strength among the annealed groups (group 2 to 5) were not significantly different ($p \geq 0.44$, for each two groups), while, the strength of group 1 was significantly smaller than group 2 ($p < 0.001$).

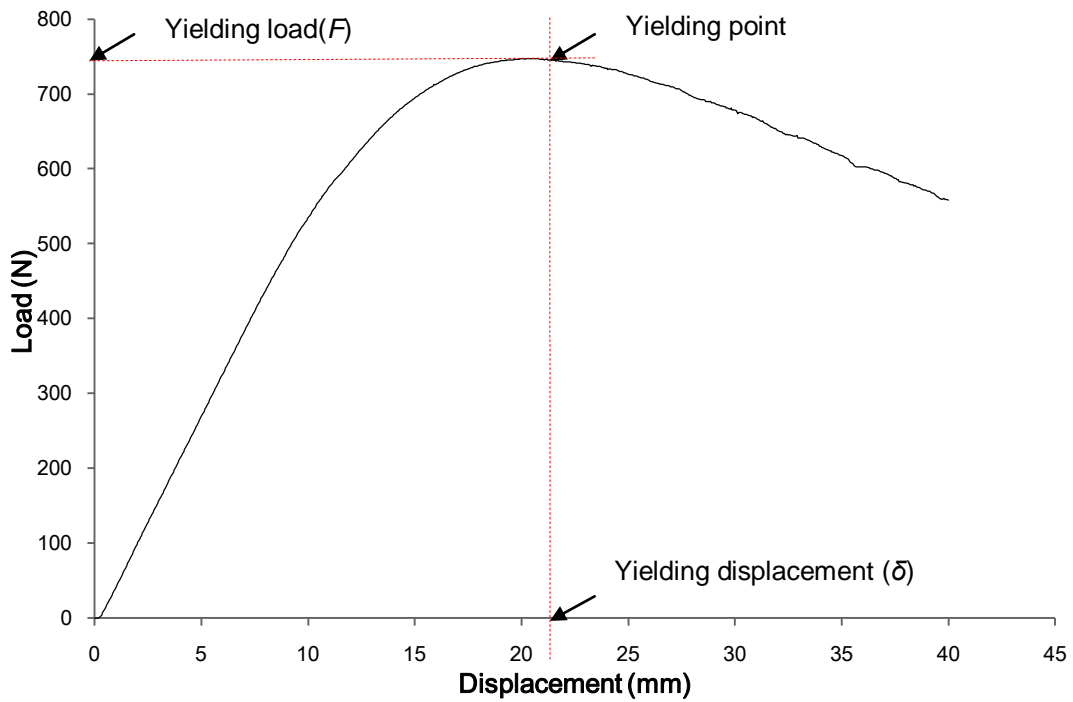


Fig. 5.3 Load-displacement curve for Group 3, specimen 2.

Table 5.3: Load at yield, deflection at yield and flexural strength for the static tests on the five groups of specimens. (All values mean \pm standard deviation)

Group No.	1	2	3	4	5
Load at yield (N)	611.5 \pm 28.4	731.3 \pm 33.7	721.3 \pm 34.8	749.7 \pm 25.0	741.8 \pm 31.6
Deflection at yield (mm)	20.2 \pm 1.0	22.5 \pm 1.6	21.1 \pm 1.0	21.00 \pm 0.6	21.0 \pm 1.1
Flexural strength (MPa)	139.8 \pm 6.5	167.2 \pm 7.7	164.88 \pm 7.9	171.36 \pm 5.7	169.6 \pm 7.2

5.4.2 Dynamic tests

The annealed and sterilised specimens were considered as the standard PEEK material for medical devices, thus flexural fatigue tests were only conducted for groups 3 to 5. The plotted stress-life curves from the dynamic tests are shown in Fig. 5.4. It can be seen that the number of cycles to failure increases with decreasing stress for each of the groups. The recorded flexural fatigue strengths (*i.e.* the stress corresponding to 10 million cycle survival) were 97.4 MPa (for group 4) and 107.4 MPa (for group 3 and group 5). The average fatigue strength of these three groups is 104.1 ± 5.8 MPa. After fitting the data points with linear regression lines, the corresponding gradients and intercepts are shown in Table 5.4. Student-t test of the regression coefficients shows that there is no significant difference between the regression lines.

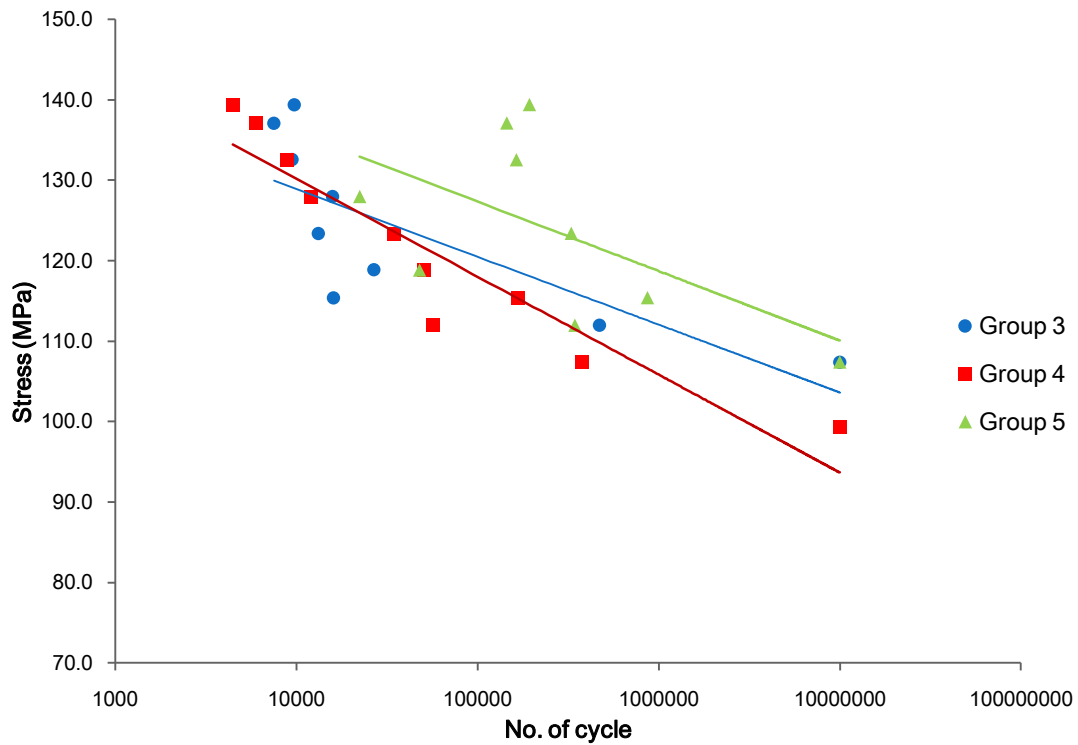


Figure 5.4: Stress against number of cycles to failure (or run out); x-axis is on a logarithmic scale, base 10.

Table 5.4: Coefficients of linear regression lines.

Group No.	Gradient	Intercept	Goodness of fit (R^2)
3	-8.4	162.7	0.78
4	-12.2	178.9	0.94
5	-8.6	170.56	0.58

5.4.3 Scanning electron microscopy

The SEM fractography images from the fatigue tests were used to determine the general fracture mechanisms. The main fracture pattern includes crack

initiation site, large parabolic propagation region and fast fracture zone (as shown in Fig. 5.5). The crack initiates at the void nucleation sites (Fig. 5.6b) and leads to the formation of large parabolic features (*i.e.* beachmarks). These beachmarks propagate along the fracture direction (Fig. 5.6a) until they reach the fast fracture zone. In this region, the sample undergoes brittle failure due to the remaining cross section no longer able to sustain the applied load. Moreover, fine striations (Fig. 5.6c) were observed in front of the beachmarks, which correspond to the crack opening and closing as the load is reversed.

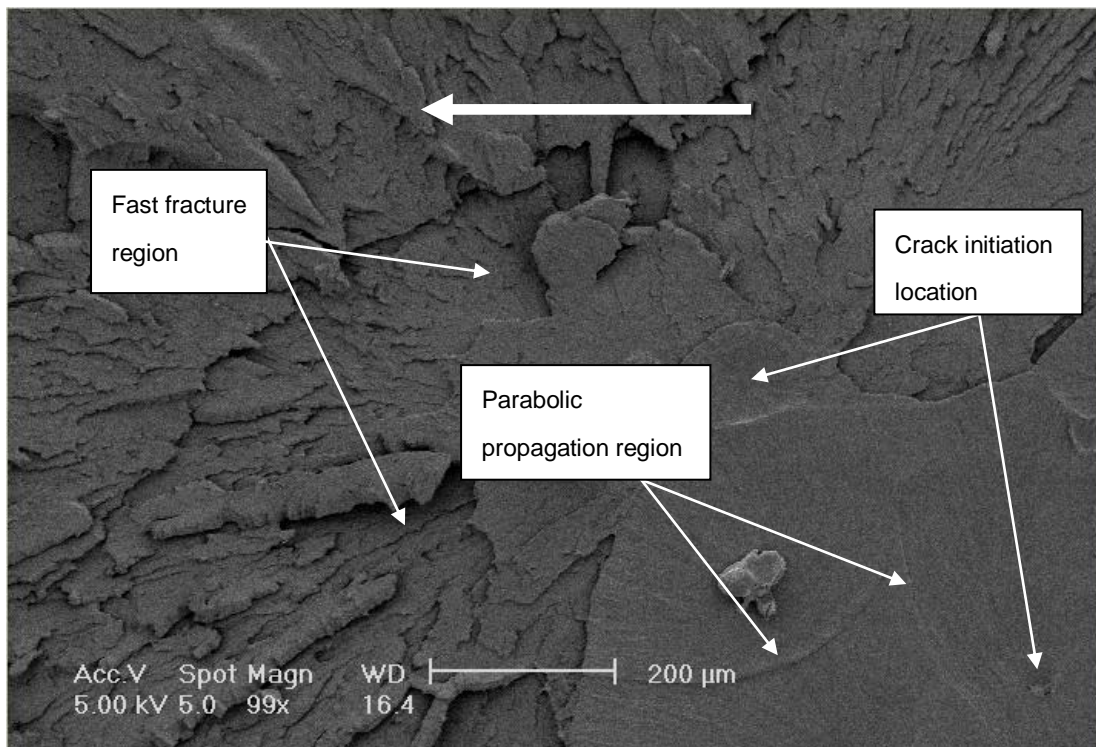


Fig. 5.5: SEM image for Group 3 dynamic, specimen 10 (the large white arrow indicates the fracture direction from right to left).

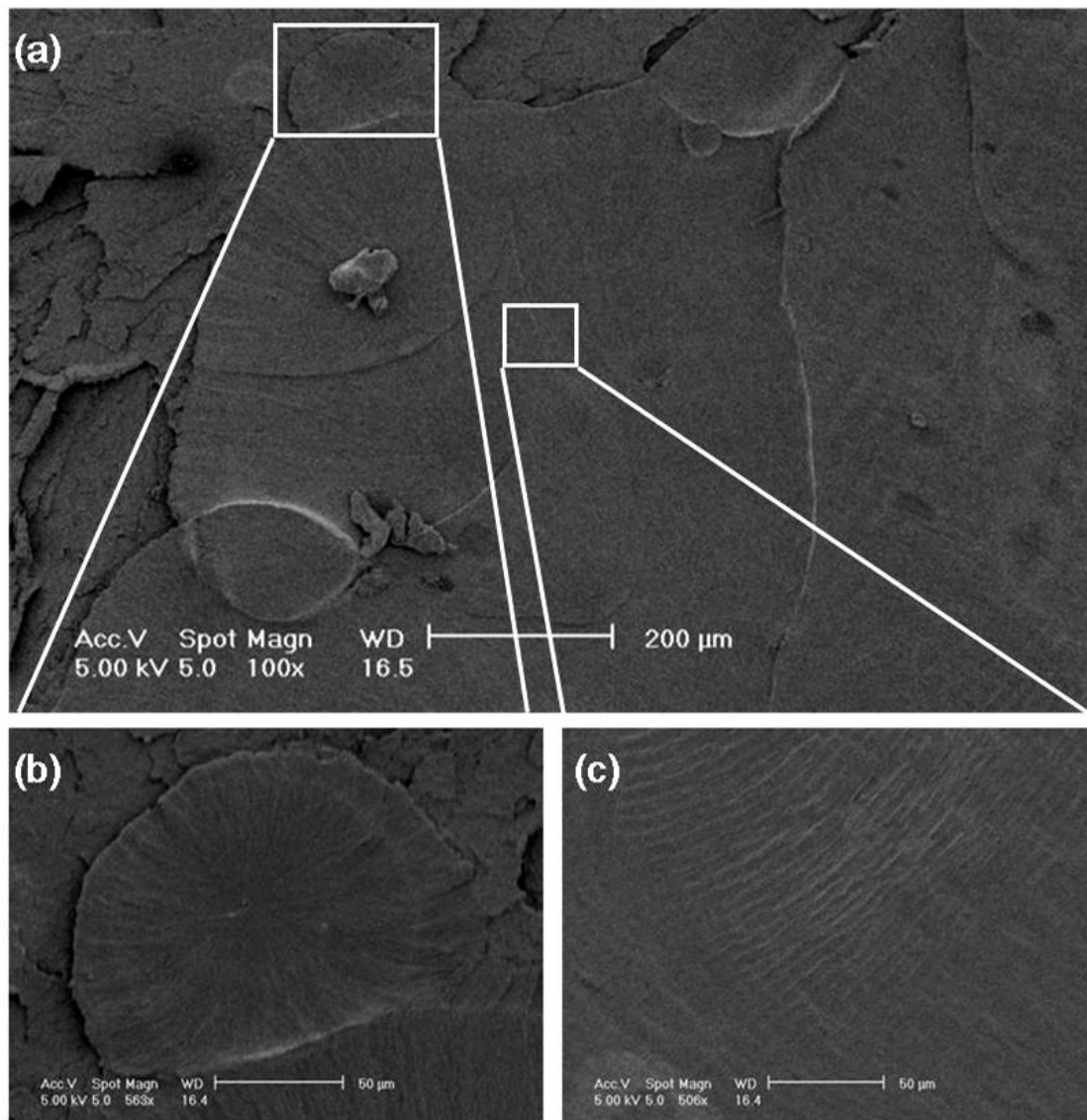


Fig. 5.6: a) Enlarged beech mark region, b) Void nucleation site and c) Fine fatigue striation.

5.5 Discussion

5.5.1 Static results

The flexural yield strengths of the annealed groups are comparable to the manufacturer's reported value of 165 MPa (PEEK™ 450G datasheet, 2012). Among groups 2 to 5, the statistical analysis shows that there are no significant changes in flexural yielding strength after either gamma sterilisation or thermal aging, or both ($p \geq 0.44$). This finding is consistent with other studies. Cartwright and Devine (2005) reported that 200 kGy gamma irradiation followed by extended ASTM F2003-02 (2008) accelerated ageing (70°C and in 5bar Oxygen pressure, for 40 days) did not lead to any significant flexural yielding strength deterioration of PEEK 450G extruded rod.

In this chapter, annealing treatment was used to release the internal residual stress caused during PEEK specimen fabrication. An obvious enhancement of flexural yield strength (groups 1 vs. 2, $p < 0.001$) was observed. This phenomenon can be explained as a gain in material crystallinity, which has been reported previously (Jaekel *et al.*, 2009). As mentioned previously (section 2.4.4), PEEK is a two-phase material and its mechanical strength is dominated by its crystal phase. Therefore, a higher crystallinity will lead to a higher mechanical strength (Zhang & Schlarb, 2009). Due to limitation of equipment, the actual crystallinity of PEEK specimens after different

treatments was not measured. Possible measuring methods include wide angle X-ray diffraction (WAXD) (Saib *et al.*, 1992; Jaekel *et al.*, 2009) or Fourier transform infrared spectroscopy (FTIR) (ASTM F2778, 2009). WAXD is a direct measuring method which provides bulk material crystallinity. In contrast, FTIR is an indirect measuring method which only provides surface layer crystallinity. Other method, such as differential scanning calorimetry (DSC) is not recommended, due to the reordering and recrystallisation issues occurred during measurement (Reitman *et al.*, 2012).

5.5.2 Fatigue results

The recorded flexural fatigue strengths were found to be in the range of 97.4 MPa to 107.4 MPa. Regression coefficients analysis shows that the stress-life curves (Fig. 5.4) were not statistically different to each other. This means that sterilisation, thermal ageing, or both do not induce any obvious change in fatigue performance; the fatigue strengths of the subgroups can be considered as from a single population. Mean fatigue strength of 104.1 ± 5.8 MPa was obtained for all the fatigue specimens. It roughly accounts for 63% of the reported flexural yielding strength of PEEK 450G (PEEKTM450G datasheet, 2012).

For the inherently stable aromatic structure of PEEK (refer to section 2.4.2), it is expected to withstand high levels of gamma irradiation (Massey, 2005). This remarkable irradiation resistance can be explained by considering the short-life free radicals (*i.e.* high energy contained unstable species) that were generated during the sterilisation process (Kurtz & Devine, 2007; Kurtz, 2012b). The irradiation dosage used for medical product sterilisation (25-40 KG of gamma irradiation) is too small to result in any significant change in properties of PEEK. The detailed chemical steps for PEEK irradiation degradation are described by Richaud *et al.* (2010).

It has been proposed that the fatigue strength of PEEK is dependent on both the intrinsic material attributes and extrinsic testing conditions (Sobieraj, 2012). Caution should be taken when adopting these fatigue data in actual implant design with different operation or testing conditions. However, the trends observed give an indication of material data. For example, fatigue testing of PEEK based spinal discs should be conducted in a 0.9% saline environmental bath at 37°C, under a testing rate of 2 Hz or less (ASTM F2346, 2005). In addition, it is worth noting that PEEK is a notch weakening material (Sobieraj *et al.*, 2010), thus design related weaknesses or material defects may lead to fatigue failure under low loads.

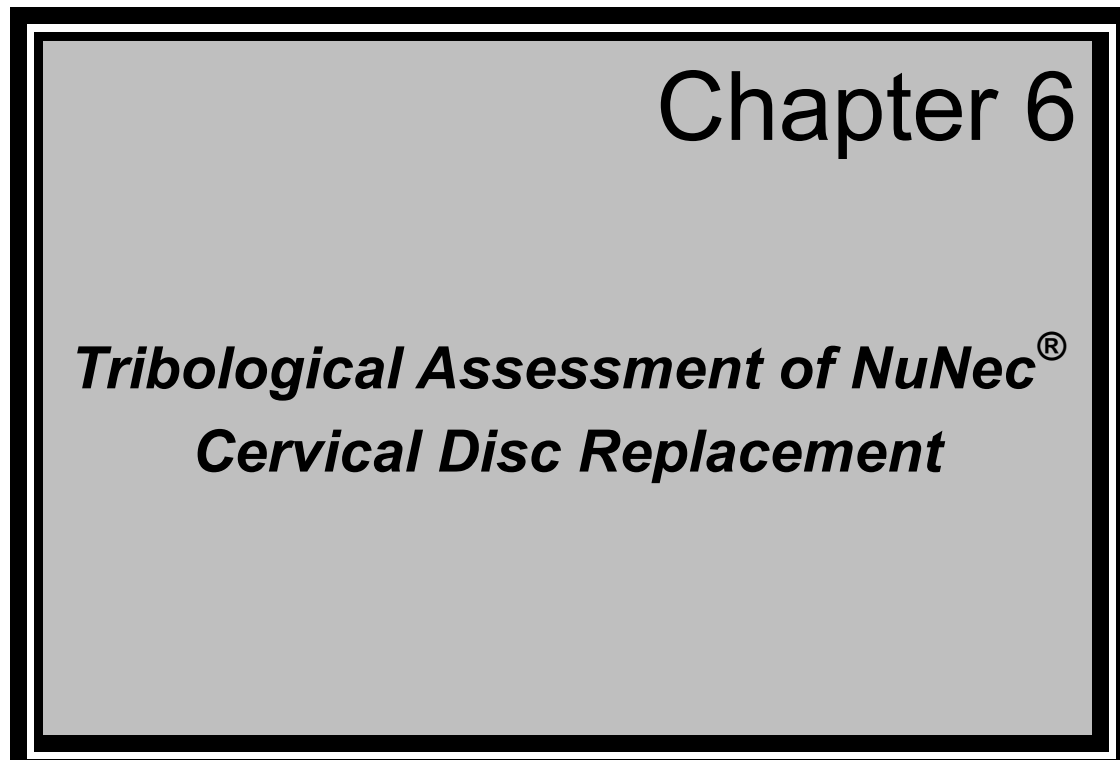
The observed fracture patterns are consistent with other studies (Rae *et al.*, 2007) where, fracture initiates as void nucleation at an inclusion/ flaw (as shown in Fig. 5.6b), leads to the formation of large parabolic features or beachmarks. During cyclic load, the crack propagates through the material and coalesces with other newly formed cracks, until they reach a critical length and result in fast brittle fracture. The fine fatigue striations (Fig. 5.6c) have also been seen in other PEEK fatigue studies (Sobieraj *et al.*, 2010; Sobieraj & Rimnac, 2012) and are an indication of individual cycles of fatigue crack growth.

5.5.3 Thermal ageing

In this chapter, thermal ageing is adopted to simulate the long-term *in-vitro* degradation of PEEK. According to the 10-degree empirical rule proposed by Lambert *et al.* (2001), 192 days and 90°C simulated ageing roughly corresponds to 60 years of real-time shelf ageing. This empirical rule is developed based on Arrhenius equation, and defined as elevating the temperature by 10 degrees roughly increases the rate of chemical reaction by two times (Hermmerlinch, 1998). Moreover, its applicable temperature range is from 0 to 100°C (Hukins *et al.*, 2008).

5.6 Chapter summary

In this chapter, the effects of sterilisation and thermal ageing on the static and fatigue flexural strengths of PEEK 450G were investigated. For static flexural strength, the effects of sterilisation combined with thermal ageing are negligible. In contrast, annealed samples demonstrated a significant enhancement in flexural strength, due to a release of residual stresses. The obtained flexural fatigue strength is in the range of 99.4 to 107.4 MPa. Sterilisation and thermal ageing did not lead to any obvious change in fatigue performance. In the following chapter, the tribological performance of the NuNec[®] cervical disc replacement was evaluated comprehensively.

A large rectangular box with a thick black border and a light gray background. Inside the box, the text is centered. At the top right, 'Chapter 6' is written in a large, black, sans-serif font. Below it, the title 'Tribological Assessment of NuNec[®] Cervical Disc Replacement' is written in a bold, italicized, black, sans-serif font.

Chapter 6

Tribological Assessment of NuNec[®] Cervical Disc Replacement

6.1 Chapter overview

This chapter presents an *in-vitro* tribological assessment of the NuNec[®] cervical disc replacement (Pioneer Surgical Technology Inc., Driebergen, Netherlands). It starts with a short introduction in section 6.2, where the essential background is given. The cervical disc test specimens and experimental methods are listed in section 6.3. The results, in terms of wear and frictional torque are presented in section 6.4. This is followed by a discussion of these results in section 6.5, and the chapter ends with a brief chapter summary in section 6.6. The work described in this chapter has already been published (Xin *et al.*, 2013b).

6.2 Introduction

6.2.1 Historical review of PEEK tribological studies

PEEK based self-mating articulation is a newly introduced bearing combination for cervical disc replacement designs, with great potential to overcome current wear debris induced complications (e.g. osteolysis and hypersensitivity) (detailed in section 2.3.3). A thorough tribological investigation is necessary for assessing its applicability.

In-vitro wear studies of PEEK self-mating bearing combinations are few (as shown in Tables 6.1 and 6.2). Among these studies, the pin-on-plate tribometer is the simplest and most widely accepted test which is normally used for screening potential biomaterials for bearing applications (Scholes & Unsworth, 2007; 2009; 2010). During a pin-on-plate test, a flat-ended pin slides against a plate, under reciprocation and rotational motion. At the end of a test, the obtained volumetric mass loss is converted into a wear factor to facilitate the comparison between different tests with different testing conditions and apparatus. It is worth mentioning that due to the oversimplification of the loading conditions and motion profiles, direct interpretation of the results of pin-on-plate experiments to the more complex loads and the stress states of actual spinal devices is unwise (Kurtz & Nevelos, 2012), however useful trends can be derived.

Table 6.1: PEEK self-mating wear performance (Historical control bearing combination of UHMWPE against CoCrMo is also included for comparison purpose).

Material combinations	Steady state wear factor, (10^{-6} mm³/N m)	Steady state gravimetric wear rate, \pmSD (mg/Mc)	Testing equipment
PEEK Optima™ self-mating (Scholes & Unsworth, 2010)	4.5		Pin-on-plate tribometer
PEEK Optima™ self-mating (Grupp <i>et al.</i> , 2010)		1.4 \pm 0.4	Endolab Multi-station Spine simulator
PEEK Optima™ self-mating (Kraft <i>et al.</i> , 2011)		1.44	Endolab Multi-station Spine simulator
UHMWPE against CoCrMo (Scholes & Unsworth, 2010)	1.1		Pin-on-plate tribometer
UHMWPE against CoCrMo (Grupp <i>et al.</i> , 2010)		1.0 \pm 0.1	Endolab Multi-station Spine simulator
UHMWPE against CoCrMo (Kraft <i>et al.</i> , 2011)		2.8	Endolab Multi-station Spine simulator

Table 6.2: Essential testing conditions for studies shown in Table 6.1.

Authors	Load & motion	Lubricate, temperature & test length
Scholes & Unsworth (2010)	40 N (2 MPa) static compression; 25 mm stroke distance, reciprocation and rotation pin (1 Hz).	Dilute bovine serum (15 g/l protein), at 37°C, for 2-5 million cycles (Mc).
Grupp <i>et al.</i> (2010)	50-150 N sinusoidal compression loading, $\pm 7.5^\circ$ flexion / extension (F/E), $\pm 6^\circ$ lateral bending (LB), $\pm 4^\circ$ axial rotation (AR), all motions at 1Hz and out of phase.	Dilute bovine serum (30 g/l protein), at 37°C, for 10 Mc.
Kraft <i>et al.</i> (2011)	50-150 N sinusoidal compression loading, $\pm 7.5^\circ$ F/E, $\pm 6^\circ$ LB, $\pm 4^\circ$ AR, all motion at 2 Hz.	Dilute bovine serum (30 g/l protein), at 37°C, for 10 Mc.

The assessments of PEEK in the form of an implant have been mainly undertaken using spine simulators (Grupp *et al.*, 2010; Kraft *et al.*, 2012). These simulators are capable of more closely matching both the magnitude of *in-vivo* loading and the natural kinematic profile of the intact joint. Due to the complex contact geometry of test samples, the majority of the wear results of simulator testing are presented as a gravimetric wear rate rather than as a wear factor.

For the *in-vitro* tribological studies of disc replacement, there are a lack of studies regarding the frictional torque and lubrication regime analysis. A recent frictional torque investigation of lumbar disc replacement using a functional spine simulator, under the 2008 version ISO 18192-1 standard, showed that a metal-on-metal lumbar disc implant can operate under either boundary or mixed lubrication by adjusting the ball radius (Moghadas *et al.*, 2012a).

6.2.2 Lubricant

Because wear is a system and not merely a material property, the conditions of testing must be carefully chosen to replicate the clinical situation (Kurtz & Nevelos, 2012). Bovine serum was originally used as a substitute for the synovial fluid, to recreate the natural *in-vivo* conditions for synovial joints, such as knee and hip joints. It has been widely accepted as the optimal choice for laboratory wear studies of artificial joints (Wang *et al.*, 1998; Wang *et al.*, 1999; Scholes *et al.*, 2008; Scholes & Unsworth, 2009), because the obtained wear rate and wear mechanism closely match the clinical performance. In contrast, the intervertebral disc does not contain a synovial capsule, thus no synovial fluid. This leads to the concern whether bovine serum is applicable for wear testing of artificial disc replacement. To select the ideal lubricant for *in-vitro* wear tests, the chosen lubricant should possess a similar viscosity and composition to the body's natural lubricant (see Table 6.3).

Table 6.3: Some of the major composition of human interstitial fluid, blood plasma, bovine serum, and human synovial fluid (Fogh-Andersen *et al.*, 1995; Joshi & Joshi-Mendhurwar, 2005; Harsha & Joyce, 2011; Aaronson *et al.*, 2012)

Constituent	Human interstitial fluid (g/L)	Blood plasma (g/L)	Bovine serum (g/L)	Synovial fluid (g/L)
Protein	20.6	64-83	60-75	17-21.5
Albumin/Globulin ratio	0.01	1.8-2.0	0.93-1.21	1.27-1.7
Sodium	3.09	3.10-3.33	3.5-3.56	3.3
Calcium	0.06	0.09-0.10	0.05	0.06
Potassium	0.12	0.14-0.20	0.21	0.16

The intervertebral disc is likely to be lubricated by interstitial fluid that fills the tissue space of the spine (Kurtz & Nevelos, 2012). It is a clear, colourless, extravascular body fluid that bathes cells in all body tissues, and provides a means of delivering oxygen and nutrients to cells, intercellular communication, as well as removal of cell metabolic wastes (Graham, 2006; Roselli & Diller, 2011). This body fluid is formed by filtration from blood plasma through slit-pores of capillary membranes, and returns to the cardiovascular system via the lymphatic system (Roselli & Diller, 2011). Therefore, its composition should be similar to that of blood plasma with a lower protein content. The actual

composition of interstitial fluid is tissue specific or body area specific, and depends upon the local cell metabolism and substance exchange rate (between the tissue cells and the blood plasma). Up to now, the protein concentration of interstitial fluid taken from the spinal column is still unknown, but it has been reported that the interstitial fluid from upper limb has a protein concentration around 20.6 g/L (Fogh-Andersen *et al.*, 1995). On the other hand, interstitial fluid is proposed to be a Newtonian fluid with a viscosity that lies between the viscosity of water and the viscosity of blood plasma (Fogh-Andersen *et al.*, 1995). The viscosity of water, at 37°C body temperature, was reported as 0.695 mPa·s (Khurana, 2007); the viscosity of human blood plasma was found to be 1.2 mPa·s (Khurana, 2007) or 1.229 ± 0.086 mPa·s (Dintenfass, 1985), at body temperature.

Currently, a solution of bovine calf serum diluted with deionised water to a protein concentration of 20 g/L is recommended as the lubricant for wear testing of artificial intervertebral discs (ISO 18192-1, 2011). This lubricant attempts to mimic the natural interstitial fluid in the content of total protein concentration, however the albumin to globulin ratio is not considered. Bovine serum is a Non-Newtonian fluid and shows a shear thinning behaviour that is a reduction of the viscosity with increasing rate of shear in steady flow (Mattei *et al.*, 2010). Despite the difference in rheological properties and albumin-globulin

ratio, most of the contemporary wear and lubrication studies (Shaheen & Shepherd, 2007; Grupp *et al.*, 2010; Kraft *et al.*, 2012; Moghadas *et al.*, 2012a) of disc replacement were undertaken using a bovine serum lubricant. As an organic material, bovine serum shows important batch to batch differences. It also faces addition problems such as protein degradation and precipitation formation, which are not expected to happen under natural *in-vivo* conditions (Harsha & Joyce, 2011).

6.3 Materials & methods

6.3.1 Test Specimens

Four NuNec[®] cervical discs (as described in section 3.2.2) were used for *in-vitro* simulations; three for wear tests (discs 1 to 3) and one as a load soak control (disc 4). A similar number of samples have been used in previous wear studies (Scholes *et al.*, 2001; Tipper *et al.*, 2001).

6.3.2 Disc fixture

To attach the disc prosthesis to the spine simulator, custom-designed fixtures were required. Disc fixtures were designed according to the dimensions of the artificial disc and the vertical working space between the top and lower plates of the Bose spine simulator (Fig. 6.1). The vertical clearance between the top

plate and the centre of rotation (COR) of the spine simulator (*i.e.* the cross-point of lateral bending axis and flexion-extension axis) is 16 mm. In order to prevent the creation of any undesirable bending moment during testing, the COR of the artificial disc (*i.e.* the centre of the sphere from which the ball component is created) must match the COR of the spine simulator. This can be done by adjusting the height of the disc fixtures (Fig. 6.2).

Disc fixtures were made from 316L stainless-steel powder by 3T Rapid Product Development Ltd. (Newbury, Berkshire, UK) using direct metal laser sintering technology. Each pair of fixtures consisted of two parts with the inner contour produced to accommodate the end plates of the artificial disc, as shown in Fig. 6.3. The dimensions of the inner contour in the anterior-posterior and lateral directions are 12 mm and 14 mm, respectively. Fixation was achieved by a press-fit of the disc prosthesis into the fixture with the addition of locking pins. Cylindrical locking pins (4 mm diameter and 10 mm length) were used to restrict micro-motion during testing. Note that the original fixation cams of the disc prosthesis were removed before testing, to accommodate the locking pins. The detail engineering drawing of the disc fixture can be found in Appendix C.

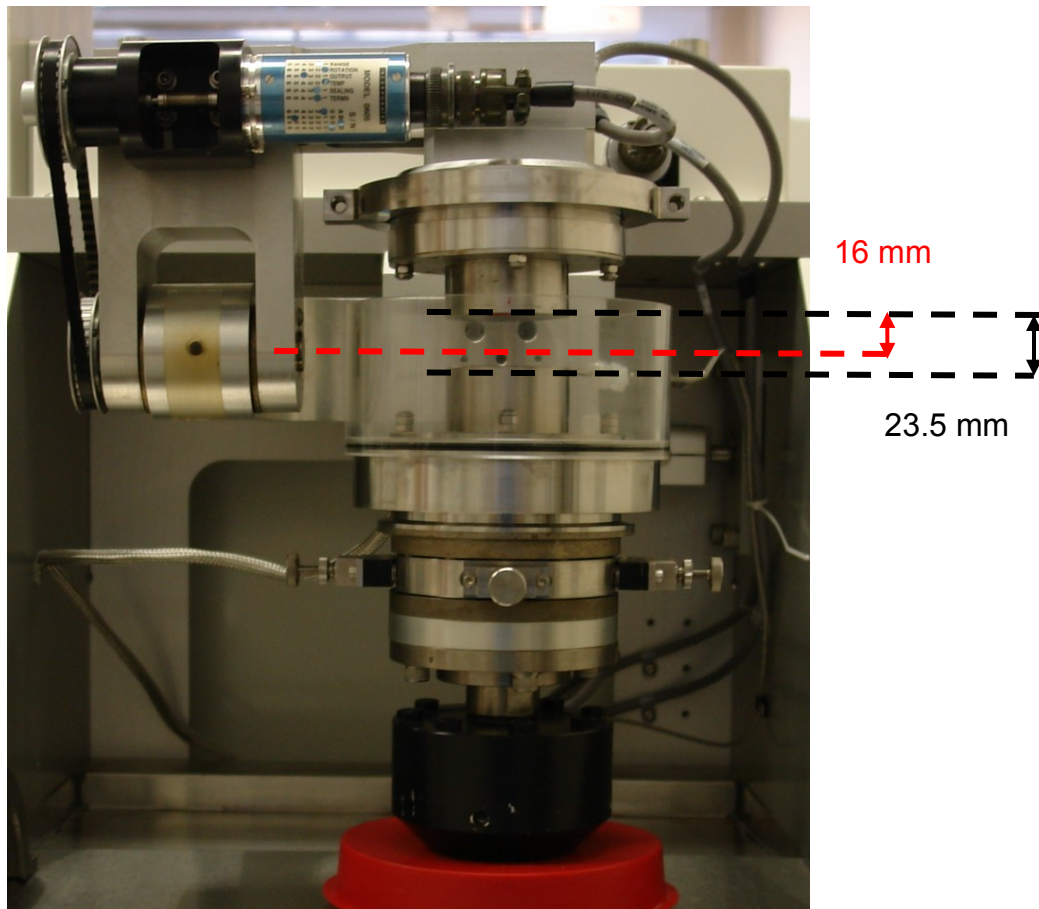


Fig. 6.1: Vertical distances from the top plate to the COR of the spine simulator (16 mm) and the lower plate (23.5 mm). Black dashed lines represent the top and lower plate levels, respectively. The red dashed line represents the level of the COR.

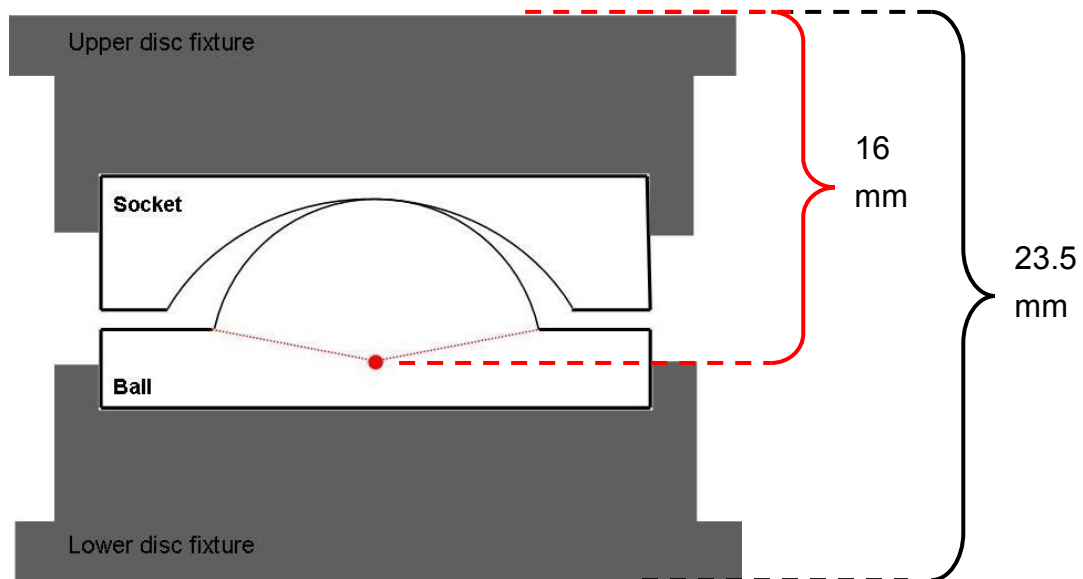


Fig. 6.2: Schematic diagram of the disc fixtures. The red dot represents the COR of the ball component.

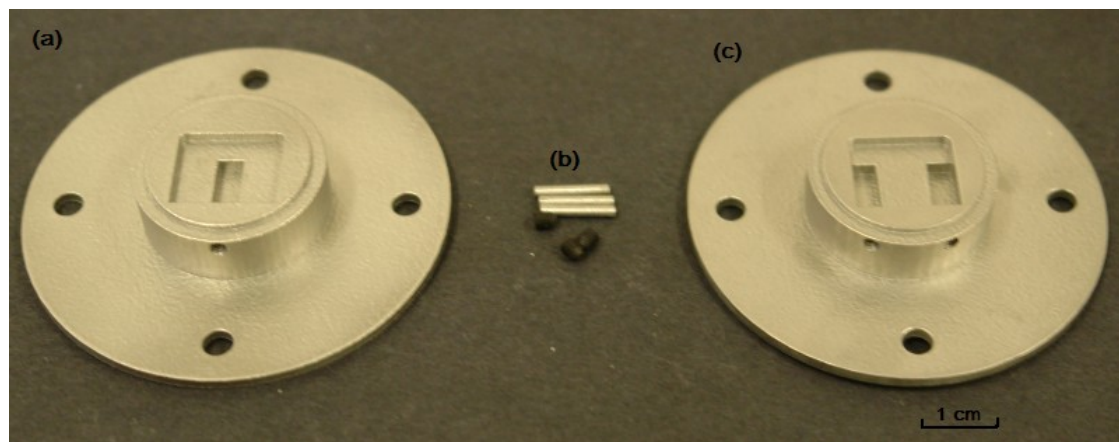


Fig. 6.3: a) lower ball fixture, b) locking pins and c) upper socket fixture.

6.3.3 Wear testing

All wear tests were performed using the Bose SDWS-1 Spine Simulators (Bose Corporation, ElectroForce Systems Group, Minnesota, USA), controlled

by Win test software. The dynamic load soak control was performed using a Bose 3330 materials testing machine (Bose Corporation, ElectroForce Systems Group, Minnesota, USA) which was also controlled by Win test software. For more information of the test equipment, please refer to section 3.3.5 and section 3.3.6.

6.3.3.1 Fixation and alignment

The specimens were mounted on custom-designed fixtures (refer to Fig. 6.3) to allow the correct alignment and orientation within the simulator. By moving the lower plate in the horizontal plane via the screw locks (refer to Fig. 3.12), the upper disc fixture was aligned parallel to the lower disc fixture, with a 0° inclined angle. The instantaneous COR of the artificial disc was positioned at the COR of the spine simulator. By rotating the top plate in the axial direction, the radiopaque markers of the ball and socket components were aligned in the vertical plane. After correct alignment, the screw locks were hand tightened to restrict the translation in the horizontal plane.

6.3.3.2 Loading and motions

For the wear tests, a sinusoidally varying load (50-150 N at 1 Hz) was applied to the disc prosthesis, together with the motions of $\pm 7.5^\circ$ flexion/extension, $\pm 6^\circ$ lateral bending and $\pm 4^\circ$ rotation, all at 1 Hz. The angular motions were out of

phase in accordance with ISO 18192-1 (2011): the lateral bending was 90° relative to the flexion/extension axis; the axial rotation and the lateral bending were 180° out of phase (as show in Fig. 6.4). Disc 4 was only assigned a dynamic axial load without motion, which is used as a reference point to correct for fluid uptake during the wear simulations.

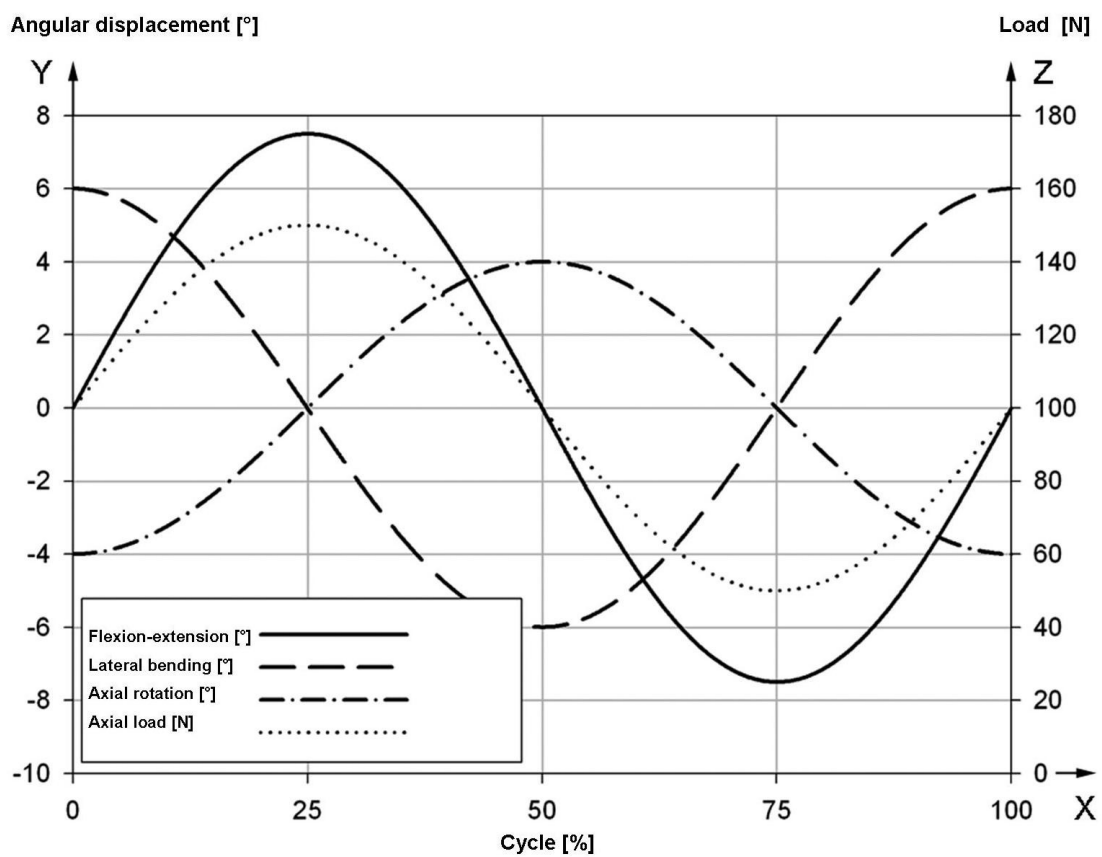


Fig. 6.4: Angular displacement and load curves of the spine simulator (adapted from ISO 18192-1, 2011)

6.3.3.3 Bovine serum based lubricant

Simulations were performed using a newborn calf serum based lubricant with a protein content of 20 ± 2 g/L, at 37°C (ISO 18192-1:2011). A 0.3 g/L concentration of sodium azide was also added to retard bacterial growth. The detailed procedure for lubricant preparation can be found in section 3.4.3. With the intention to maintain the same protein concentration; lubricant lost by evaporation was replenished twice a day with de-ionized water. Moreover, the serum lubricant was completely replaced every 0.5 million cycles (roughly 7 days), before protein denature occurred.

6.3.3.4 Gravimetric wear measurement

Prior to the commencement of the wear testing, each disc replacement was prepared according to the procedure presented in section 3.4.1. The disc specimens were then tested for 5 million cycles. At each measurement interval (0, 0.25, 0.5, 1, 2, 3, 4 and 5 million cycles) (ISO 18192-1:2011), the mass of the specimens were measured following the cleaning, drying and weighting protocol (outlined in section 3.4.2). To adjust for the effect of fluid absorption, the change in mass of the control disc was subtracted from that of the wear tested disc.

6.3.3.5 Surface characterization

Surface examination was performed before and after the wear tests using a white light non-contacting MicroXAM 2 interferometer (Omniscan Ltd., Penycase, UK) and following the procedure outlined in section 3.3.7. During the surface examination, the essential surface parameters were recorded. The arithmetic surface roughness (S_a), root mean square surface roughness (S_q) and surface skewness (S_{sk}) were obtained.

6.3.4 Frictional torque

Frictional tests were performed using the same single station Bose Spine Simulator equipped with a multi-axial load cell (refer to section 3.3.5). Frictional tests were only performed on discs 1 to 3, before and after the wear simulation. Each specimen was tested under a constant axial compressive load of 150 N, combined with a single degree of sinusoidal motion for 100 cycles. The motions of 0 to +7.5° flexion, 0 to +6° lateral bending and 0 to +4° axial rotation were each individually applied. Each motion was tested within a range of frequencies from 0 - 2 Hz, at 0.25 Hz increments. An average peak frictional torque (T) was calculated based on the values from the last 10 cycles during each simulation (Moghadas *et al.*, 2012a).

To determine the lubrication regime under which the NuNec[®] disc was acting, Stribeck analysis was used. The friction factor (f) was plotted against the Sommerfeld number (Z) as shown in Fig. 6.5.

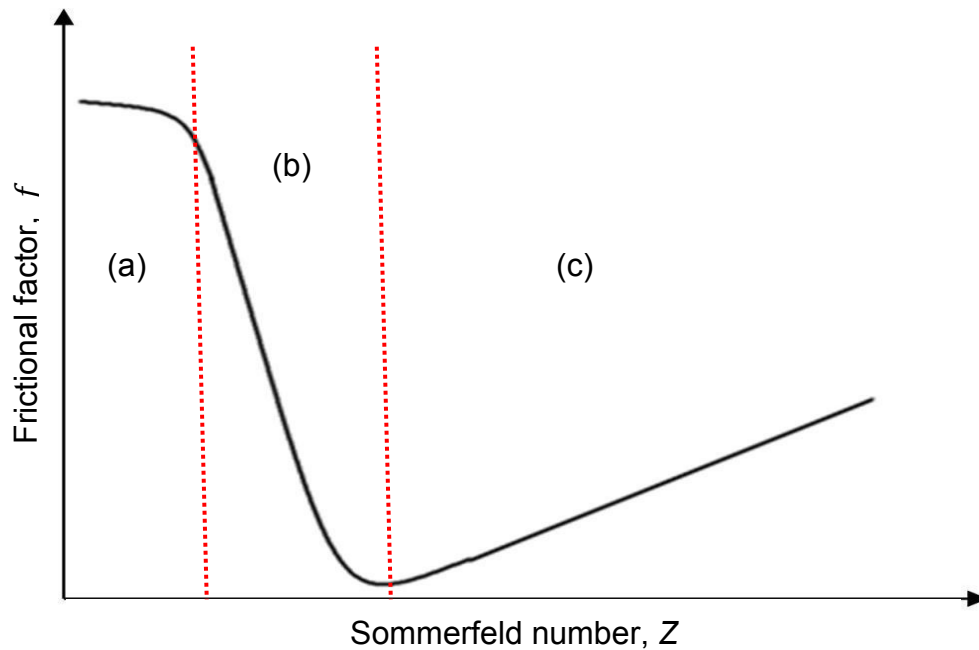


Fig. 6.5: A typical Stribeck curve (author's own drawing, adapted from Jin & Fisher, 2008). Region a) indicates boundary lubrication; b) indicates mixed lubrication; and c) indicates fluid-film lubrication.

The frictional torque and Sommerfeld number were calculated using Eqs. 1 and 2, respectively (Jin & Fisher, 2008; Joyce, 2009).

$$f = \frac{T}{rL} \quad (1)$$

where r is the ball radius and L is the applied load. The ball radius of NuNec[®] disc was found to be 6.3 mm (in section 4.3.4.1):

$$Z = \frac{\eta ur}{L} \quad (2)$$

where η is the lubricant viscosity and u is the entraining velocity which can be obtain from:

$$u = \frac{\omega r}{2} \quad (3)$$

where ω is the angular velocity (in radians) and can be expressed as follow:

$$\omega = \frac{2\theta h \pi}{180} \quad (4)$$

where θ is the angular displacement in each motion (e.g. 7.5° for flexion) and h is the test frequency.

The viscosity of the lubricant was measured using an AR-G2 cone-on-plate rheometer (TA instruments, West Sussex, UK) and following the procedure outlined in section 3.3.8. The viscosity was found to vary with shear rate, and shear-thinning behaviour was observed (Fig. 6.6). By applying a Newtonian model, a constant viscosity value can be obtained. Four repeated measurements were taken and the average viscosity of the diluted new born calf serum was found to be 1.03 ± 0.12 mPa·s.

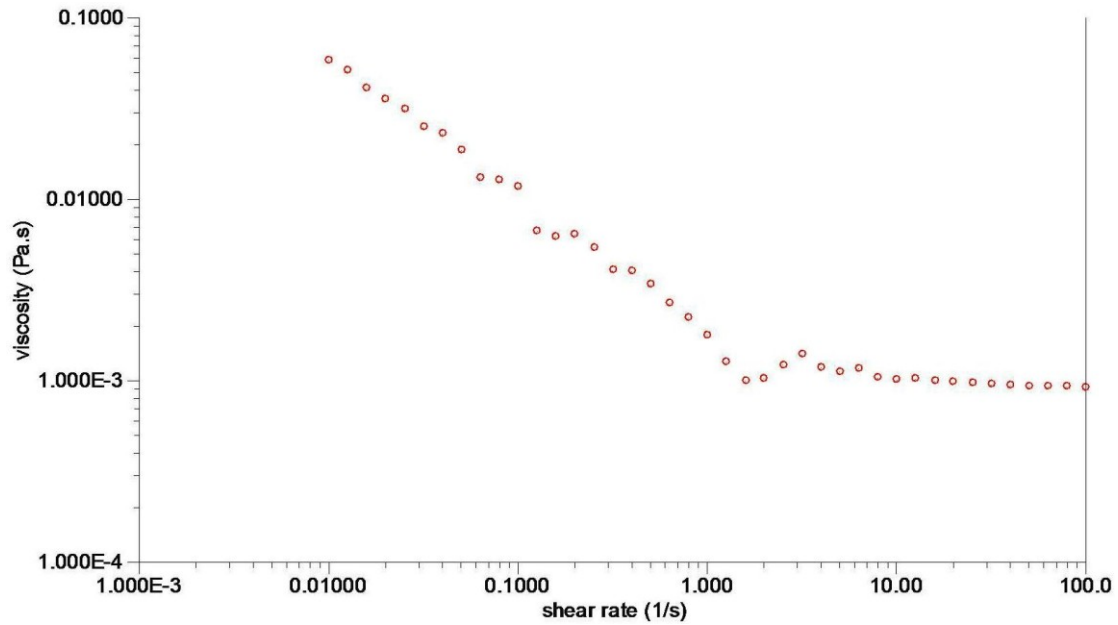


Fig. 6.6: Variation of viscosity against shear rate. Axes are on log 10 based scale.

6.3.5 Statistical analysis

The post-wear friction data was compared with the pre-wear results by plotting the 95 % confidence intervals (CI), assuming the variation of the friction results for each datum point is normally distributed around the true value. The upper and lower limits of the CI were calculated based on Eq. 5 (Sheldon, 2009). The obtained mean frictional torque of each datum point (\bar{X}) plus or minus the product of t-critical value ($t_{\alpha/2, n-1}$) and the standard error (S_E) was calculated using:

$$\bar{X} \pm t_{\alpha/2, n-1} \times S_E \quad (5)$$

where, S_E was defined as follow:

$$S_E = \frac{s}{\sqrt{n}} \quad (6)$$

where, s is the obtained standard deviation of each datum point, and n is the number of measurements (*i.e.* the number of disc specimens in this case). For a 95% confidence level with 3 measurements, the t-critical value was found be to 4.303 (Sheldon, 2009).

In this study, error bars were used to represent the 95% CI, which means that between these intervals there is a 95% of probability of finding the true mean value. If the confidence regions overlap with each other, it indicates there is no significant difference; no overlap indicates a significant difference. This method has been used previously to determine the variation of frictional torques of a metal-on-polymer based lumbar disc replacement after the bearing material was reversed (Moghadas *et al.*, 2012b).

6.4 Results

6.4.1 Wear results

For the PEEK-on-PEEK bearing combination subjected to *in-vitro* wear simulation, the accumulated mass loss was plotted against the number of

cycles for each individual disc (Fig. 6.7). There was no mass gain of the control specimen, but rather there was mass loss due to the hydroxyapatite coating break off during each cleaning procedure. After 5 million cycles, the coating was completely removed (see Fig. 6.8).

After correcting the mass loss using the control disc, the mean PEEK mass loss from the discs (specimens 1 to 3) was plotted against the number of cycles, as shown in Fig. 6.9. An initial run-in phase with a higher wear rate was observed (from 0 to 2 million cycles); this was followed by a steady-state phase with a reduced wear rate. The wear rates, for each wear phase, are summarised in Table 6.4. The corresponding volumetric wear rates were calculated, by taking into account the density of 1.3 g/mm^3 for PEEK (Grupp *et al.*, 2012; PEEK™ 450G datasheet, 2012). Over the entire wear test period, the total mean mass loss of PEEK was $12.5 \pm 0.4 \text{ mg}$ and the corresponding mean volumetric loss was $9.6 \pm 0.3 \text{ mm}^3$.

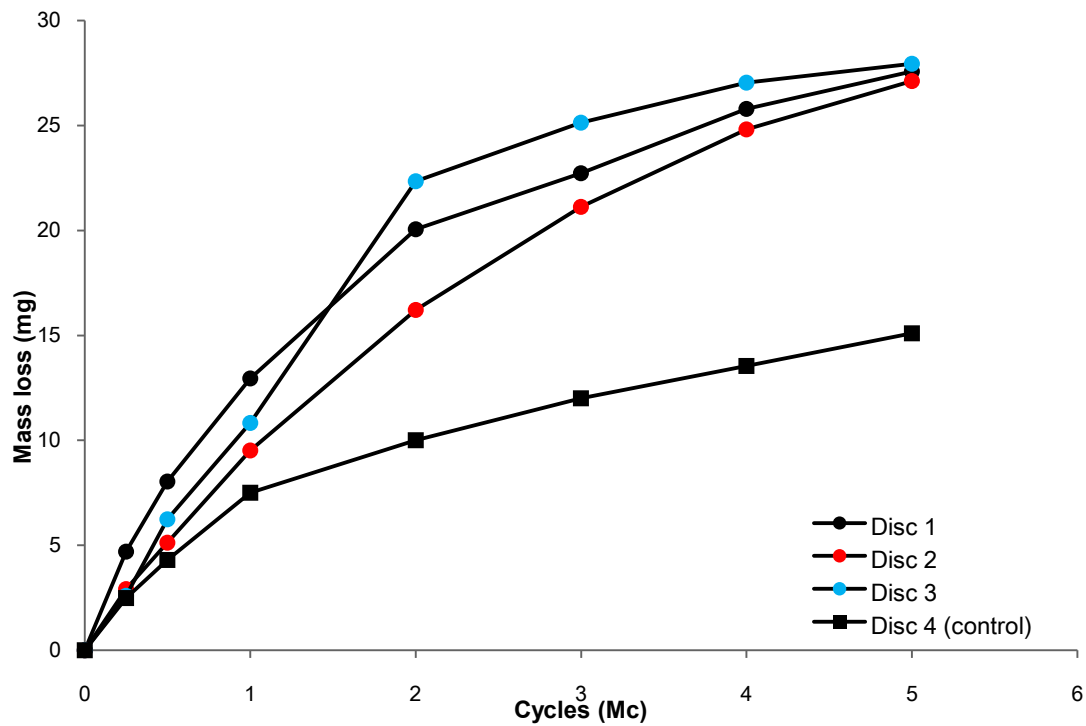


Fig. 6.7: Cumulative mass loss against number of cycles, for each disc. Discs 1-3 are the testing specimens and disc 4 is the load soak control specimen.

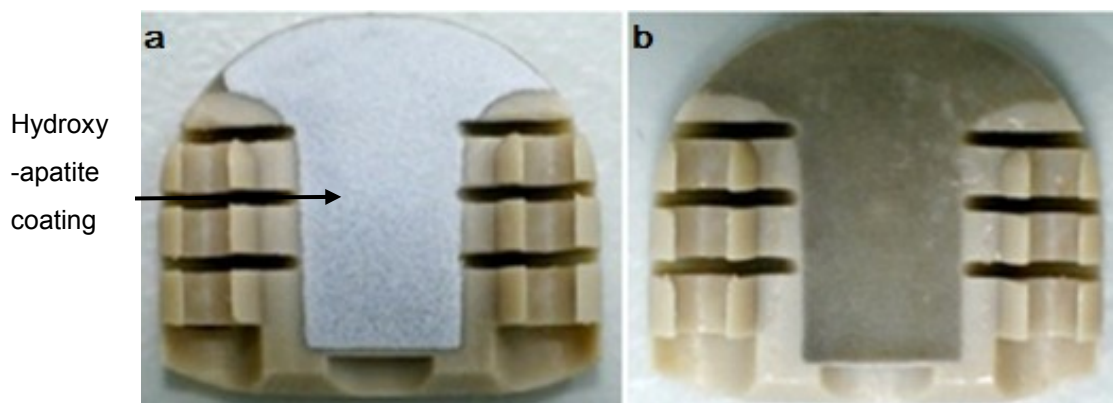


Fig. 6.8: Disc 1 superior end plate a) pre-wear and b) after 5 million cycles wear test. Note the light grey hydroxyapatite coating was completely removed.

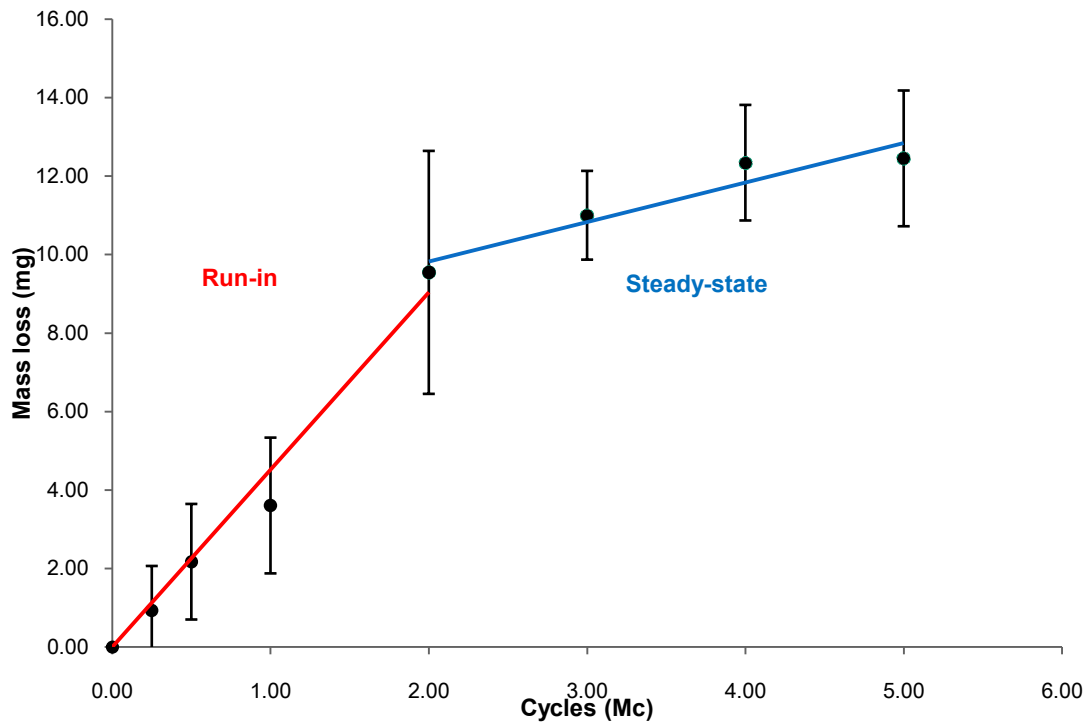


Fig. 6.9: Mean PEEK mass loss against number of cycles for discs 1 to 3. Error bars represent the standard deviation. Two regression lines have been fitted by $y = 4.7x - 0.3$ ($R^2 = 0.98$) and $y = x + 7.8$ ($R^2 = 0.91$) to show the initial run-in phase and steady-state phase.

Table 6.4: The mass loss rate for each individual disc, under different wear stages. The mean mass loss and mean volume loss are also presented.

Number of cycles ($\times 10^6$)	Disc 1 (mg/10 ⁶ cycles)	Disc 2 (mg/10 ⁶ cycles)	Disc 3 (mg/10 ⁶ cycles)	Mean \pm SD.(mg/10 ⁶ cycles)	Mean \pm SD (mm ³ /10 ⁶ cycles)
0-2 (run-in)	5.0	3.1	6.2	4.8 \pm 1.5	3.7 \pm 1.2
2-5 (steady-state)	0.8	1.9	0.2	1.0 \pm 0.9	0.7 \pm 0.7
0-5 (overall)	2.50	2.40	2.6	2.5 \pm 0.1	1.9 \pm 0.1

6.4.2 Surface topology

Prior to wear testing, fine machining marks were observed on the bearing surfaces (Fig. 6.10). However, these had been removed with some burnishing after testing. The characteristics of these wear patterns were consistent for all tested discs. Closer examination of the articulation surfaces (Fig. 6.11) shows the change in surface topography, with wear tracks seen on the bearing surface for the same disc. The change in surface profile is summarised in Table 6.5. The surface roughness parameters (S_a and S_q) were reduced in both components after 5 million cycles, while the surface profile (S_{sk}) of socket component was reversed from positive to negative skewness.

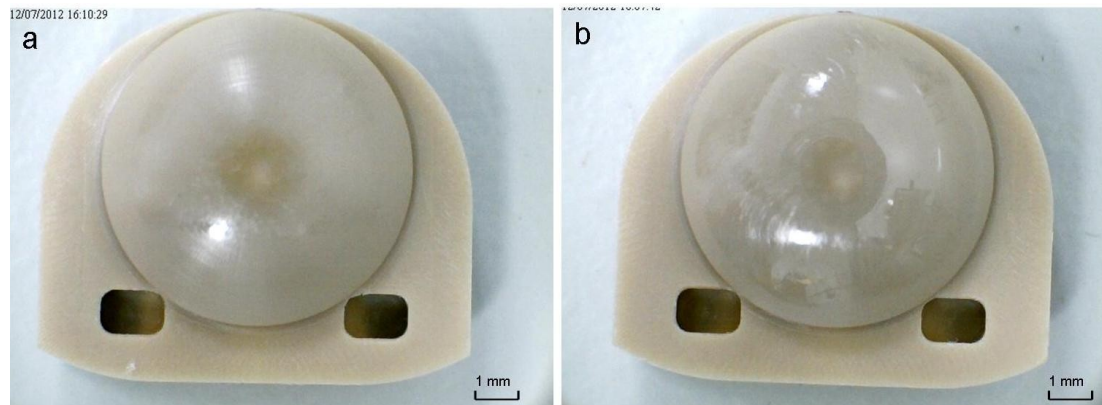


Fig. 6.10: Disc 1 ball part a) pre-wear and b) after 5 million cycles.

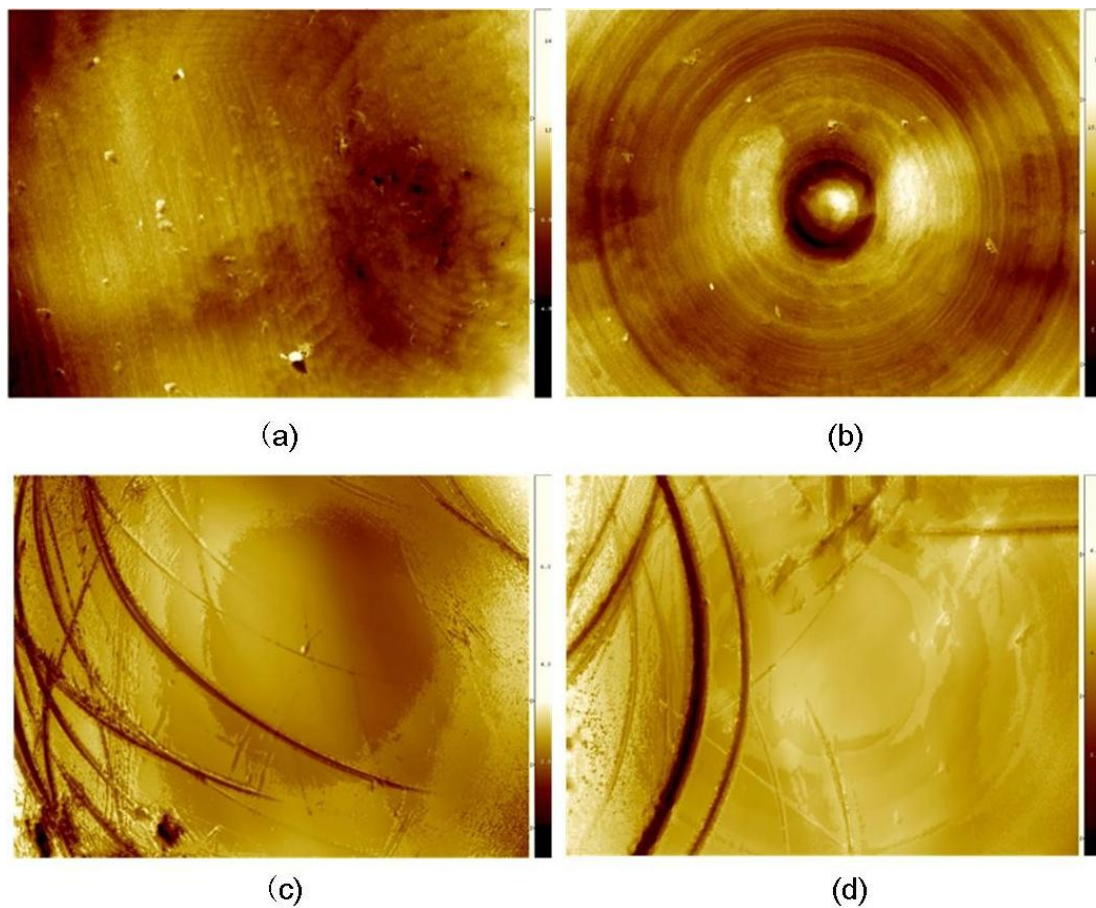


Fig. 6.11: Surface scan of disc 1 a) ball pre-wear, b) socket pre-wear, c) ball after 5 million cycles, and d) socket after 5 million cycles. Area of view is 639 x 859 μm at the pole of the specimen.

Table 6.5: Surface roughness values (mean \pm SD.) during wear testing for discs 1 to 3.

Parameters	Socket component		Ball component	
	Pre-wear	Post-wear	Pre-wear	Post-wear
S_a (μm)	0.967 ± 0.056	0.412 ± 0.035	0.949 ± 0.058	0.267 ± 0.033
S_{rms} (μm)	1.273 ± 0.058	0.599 ± 0.069	1.190 ± 0.066	0.350 ± 0.037
S_{sk}	0.408 ± 0.228	-1.453 ± 1.498	-0.303 ± 0.121	-0.362 ± 0.465

6.4.3 Frictional results

The frictional torque results are presented in Figs. 6.12 to 6.14. The mean maximum frictional torques, prior to the wear tests and at the end of the wear tests, occurred during flexion and were 3.71 ± 0.22 and 3.58 ± 0.13 N·m, respectively. Statistical analysis showed that there was no significant difference between pre-wear and post-wear mean friction torques at each test frequency, for every motion, as the 95% confidence intervals overlapped each other.

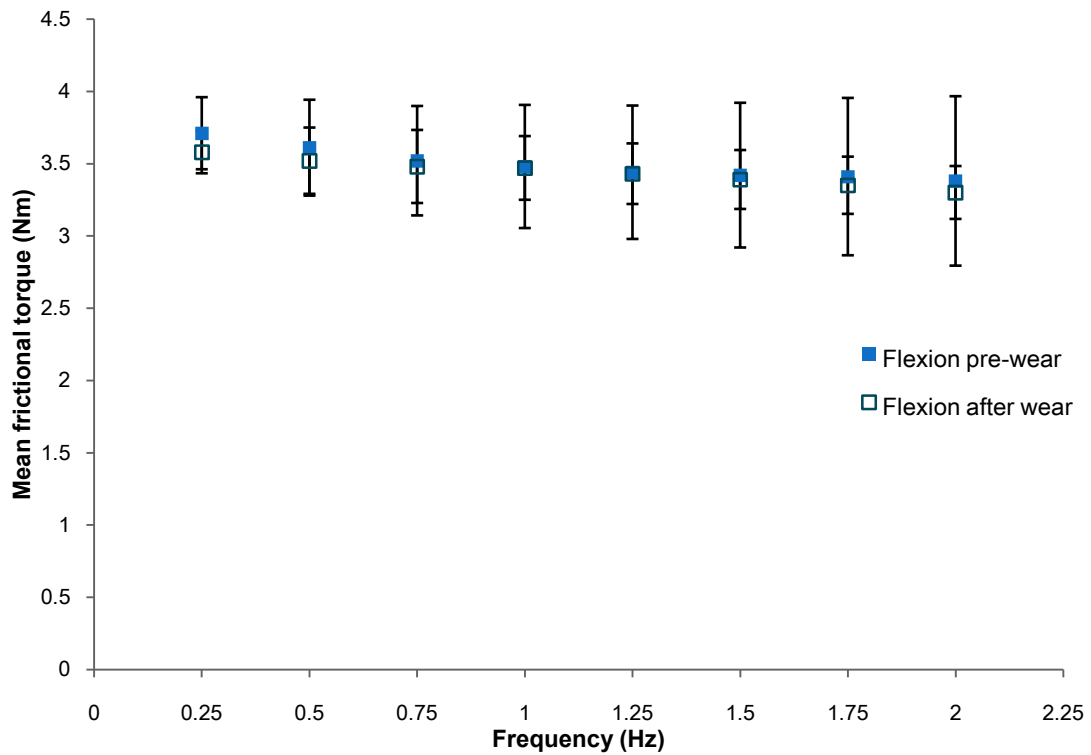


Fig. 6.12: Mean frictional torques of discs (1 to 3), under flexion motion (0 to +7.5°), before and after wear testing, plotted against frequency. Error bars represent 95% confidence intervals.

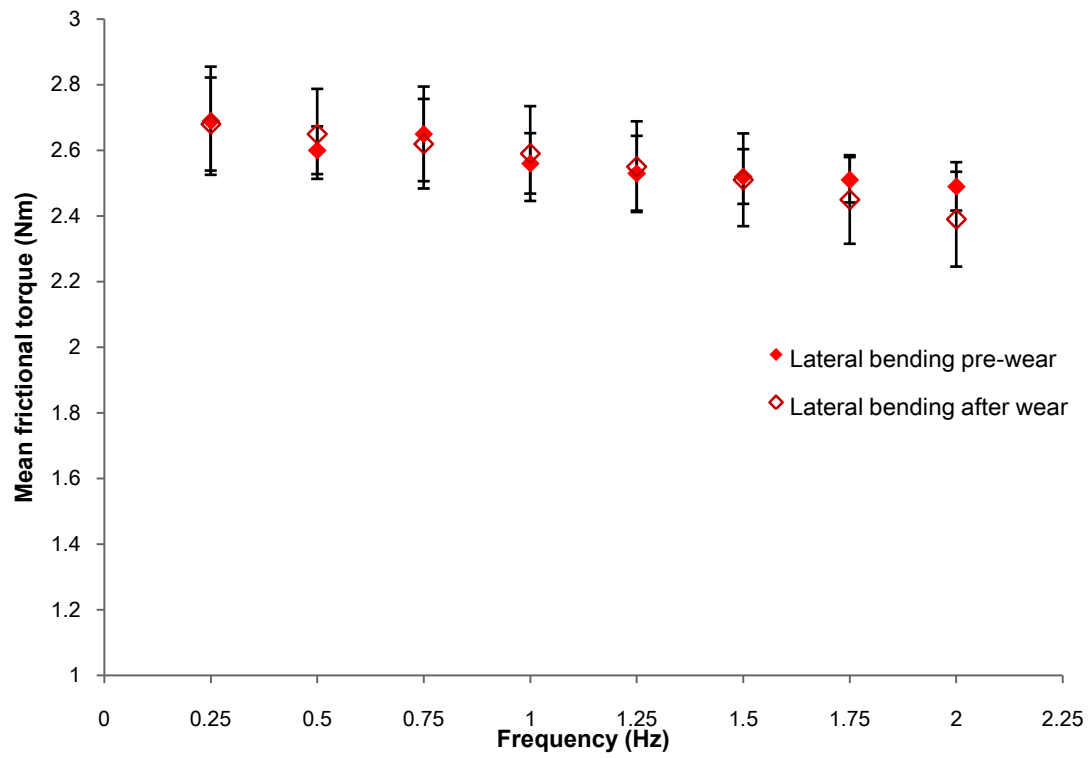


Fig. 6.13: Mean frictional torques of discs (1 to 3), under lateral bending motion (0 to +4°), before and after wear testing, plotted against frequency. Error bars represent 95% confidence intervals.

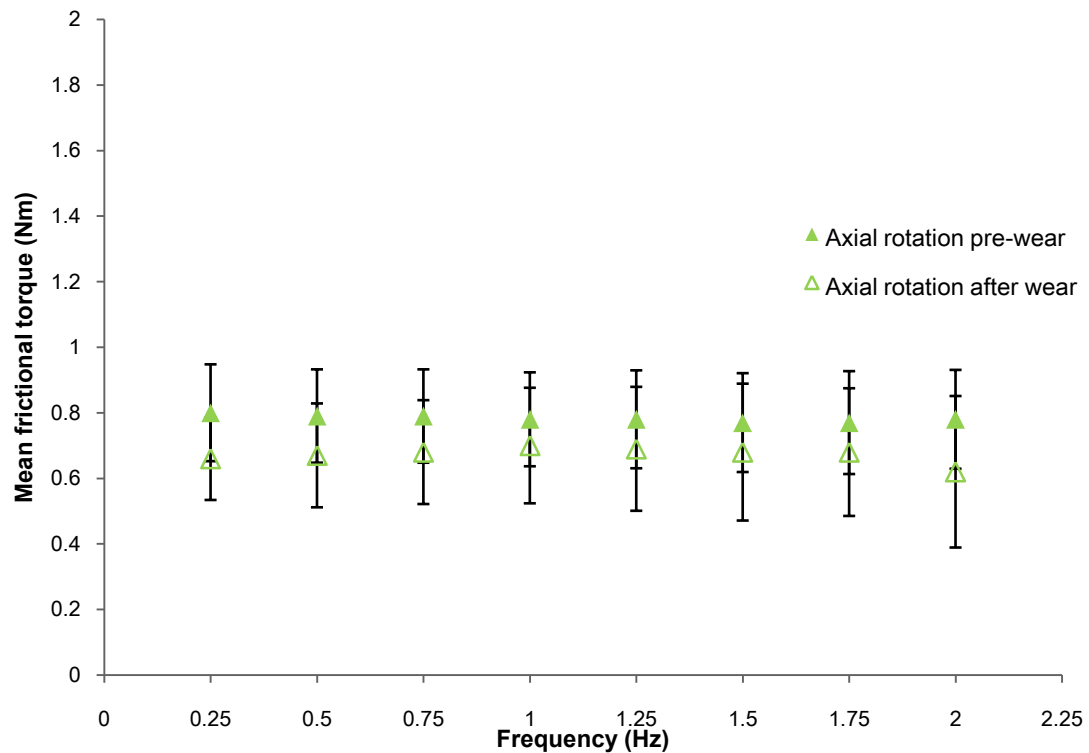


Fig. 6.14: Mean frictional torques of discs (1-3), under rotation motion (0 to +2°), before and after wear testing, plotted against frequency. Error bars represent 95% confidence intervals.

6.4.4 Stribeck plot

To investigate the lubrication regimes, Stribeck curves were plotted. The mean friction factors for discs 1-3 were plotted against the corresponding Sommerfeld number for each motion (Figs. 6.15-6.17).

Prior to wear simulation, under flexion motion or lateral bending motion, a slightly downward trend was seen as Sommerfeld number increased which

indicates boundary or mixed lubrication. For axial rotation, boundary lubrication dominated. A fairly constant trend was observed for the friction factor with increasing Sommerfeld number. After 5 million wear cycles, there were no obvious changes in the Stribeck curves for each motion; the disc replacements still operated under a boundary to mixed lubrication regime.

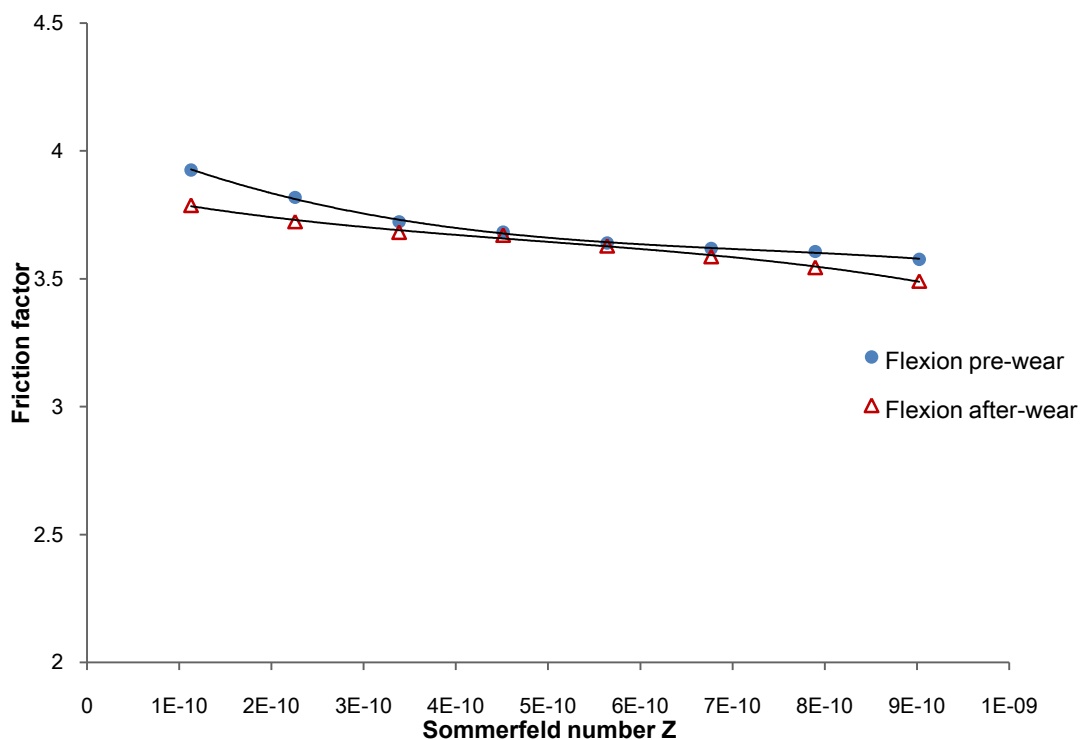


Fig. 6.15: Stribeck plot for disc samples under flexion motion (0 to +7.5°). A

third order polynomial has been fitted to the data points.

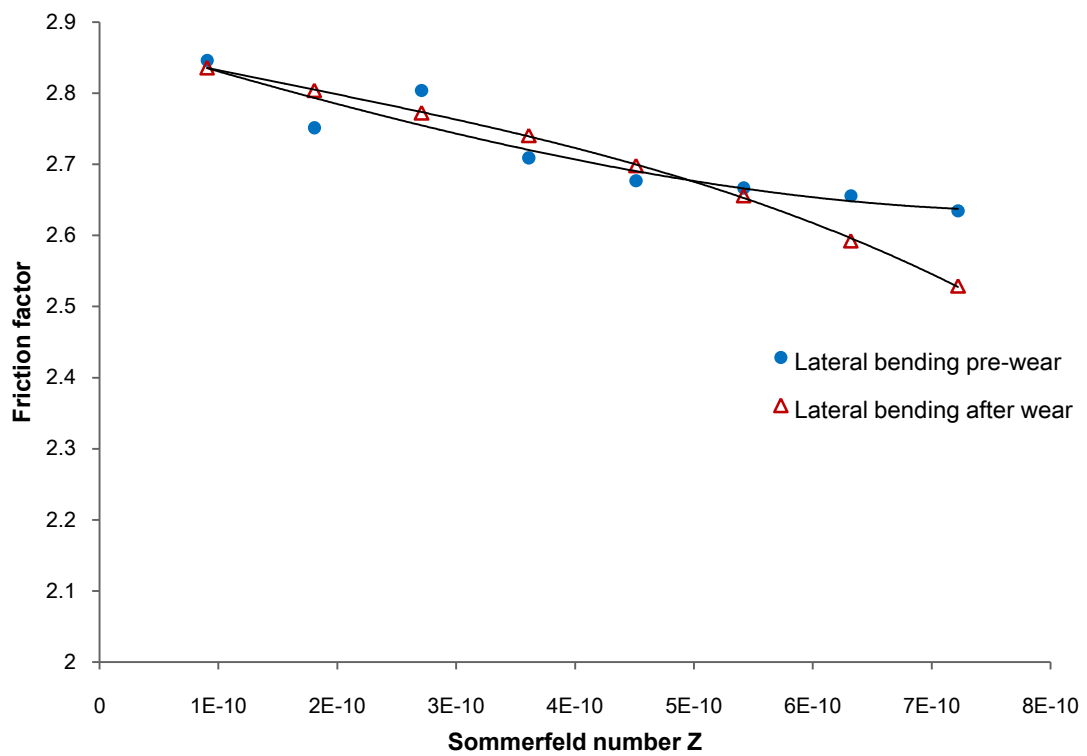


Fig. 6.16: Stribeck plot for disc samples under lateral bending motion (0 to +4°).

A third order polynomial has been fitted to the data points.

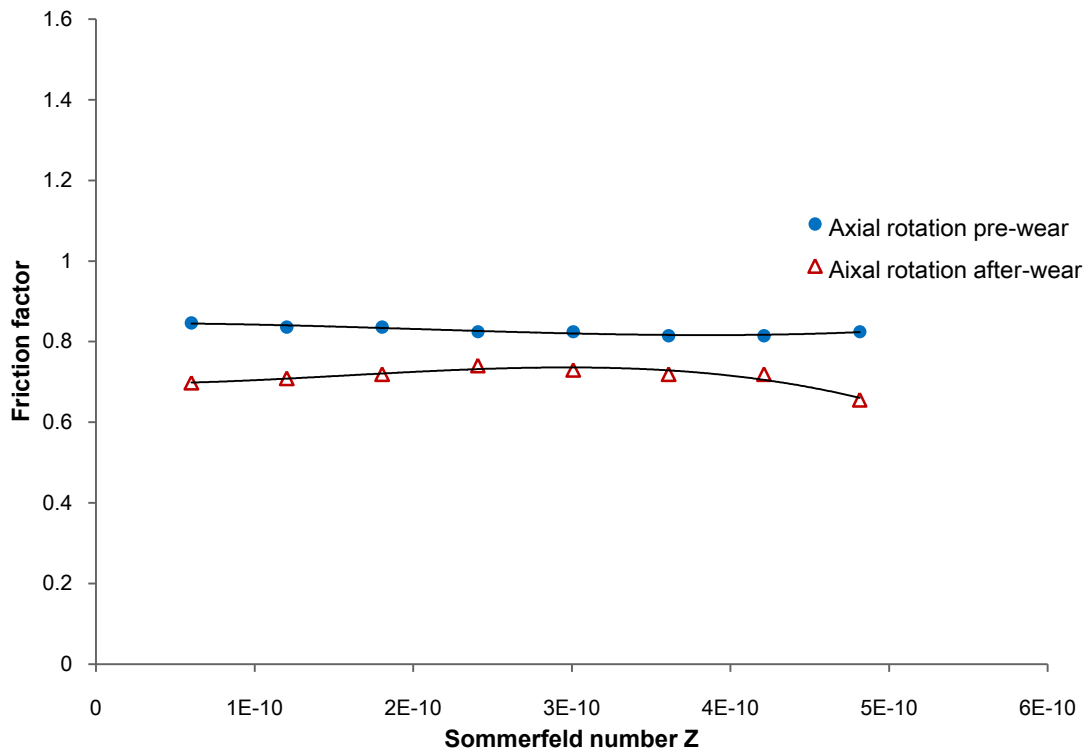


Fig. 6.17: Stribeck plot for disc samples under axial rotation motion (0 to +2°).

A third order polynomial has been fitted to the data points.

6.5 Discussion

6.5.1 Wear

The measured wear rates of 4.8 ± 1.5 (run-in) and 1.0 ± 0.9 (steady-state) mg/million cycles, correspond well to literature spine simulator studies. Grupp *et al.* (2010) determined a wear rate of 1.4 ± 0.4 mg/million cycles during steady-state conditions, for a generic PEEK self-mating cervical disc using an Activ® C cervical disc as the prototype. They conducted a 10 million cycle laboratory wear simulation using an Endolab multi-station spine simulator,

under the 2008 version of the ISO 18192-1 protocol, in a bovine serum based lubricant with 30 g/l protein content. In another wear study, under identical test conditions as Grupp *et al.* (2010), a higher test frequency of 2 Hz was used; a PEEK based generic cervical disc had a steady-state wear rate of 1.44 mg/million cycles and a run-in wear rate of 5.09 mg/million cycles (Kraft *et al.*, 2011). Brown *et al.* (2009) previously reported a relative low wear rate of 0.4 mg/million cycles (steady-state) for the same NuNec[®] cervical disc arthroplasty. In their study, a MTS multi-station spine simulator was used and followed the 2008 version of ISO 18192-1 protocol. However, the actual composition of lubricant, the test frequency and the disc size were not disclosed, thus it is difficult to identify the reasons for the difference found.

The gravimetric wear rates of cervical disc replacements with an UHMWPE against CoCrMo bearing combination have been reported as 1.0 ± 0.1 mg/million cycles and 2.8 mg/million cycles (as shown in Table 6.1), in spine simulator wear studies. These values correspond to volumetric wear rates of 1.07 and 3.0 mm³/million cycles, respectively. In comparison, a lower volumetric wear rate of 0.7 ± 0.7 mm³/million cycles of PEEK self-mating bearing articulation was observed in this study. Therefore, a PEEK based bearing is likely to generate less volume of wear particles than UHMWPE against CoCrMo. It is worth mentioning that a preliminary pin-on-disc screen

study (Scholes & Unsworth, 2010) showed the complete opposite wear results. It showed that a PEEK based self-mating articulation had a wear factor 4 times larger than that of UHMWPE against CoCrMo. This inconsistency is due to the adoption of different testing conditions and different motion profiles. The Pin-on-disc wear study involved applying a 2 MPa static compressive loading, combined with reciprocation and rotating-pin motion, and was conducted in 15 g/L protein content bovine serum (as shown in Table 6.2).

After 5 million cycles, mild burnishing was found on the bearing surfaces (Fig. 6.10b). This was consistent with the observed surface topology change. The surface roughness of the ball and socket components was reduced (Table 6.4) which indicated a smoother contact surface. Examination of all the articulating surfaces indicated that the main mechanisms of wear were abrasion and adhesion. Examination of the wear traces (Fig. 6.11) indicates that third body abrasion also occurred and was likely to have been caused by PEEK wear debris or the hydroxyapatite coating particles that became detached during the testing and cleaning process. No other surface damage was observed on the articulation surfaces after 5 million cycles.

Further examination of the socket surface showed that it was initially positively skewed with many asperities, thus these could have led to the high abrasive

wear during the run-in phase. After 5 million cycles many of these asperities have been flattened or removed, so the socket surface showed a negative skewed and a smooth surface profile. Topography such as this, facilitates a higher contact area, which may be more suitable for lubricated sliding. This may explain the observed low wear rate after steady-state wear was reached. Disintegration of the bearing surfaces (pitting and delamination) observed by other studies (Grupp, 2010; Kraft *et al.*, 2011) after run-in wear stage, was not seen in this study.

The main wear mechanism was abrasion wear rather than fatigue wear. Fatigue wear mainly depends on the contact stress and the bearing material, which in turn depends on the prosthesis design (Jin & Fisher, 2008). The maximum Hertz contact stress of NuNec[®] cervical disc arthroplasty of the smallest size is found to be 32.1 MPa (refer to section 4.4.1). The experienced contact stresses between the bearing surfaces of other comparable studies (Grupp *et al.*, 2010; Kraft *et al.*, 2011) were unknown, due to lack of information of the bearing design (ball radius and radial clearance).

6.5.2 Frictional torque

In this chapter, friction torque was used to describe the friction component rather than friction coefficient. It has previously been discussed that the use of

a coefficient of friction is not strictly correct for a ball and socket joint replacement, due to the unknown pressure distribution (Hall *et al.*, 1994). The obtained maximum frictional torque is in the similar order of magnitude as lumbar disc studies. For metal-on-metal based lumbar discs, a maximum frictional torque of 9.5 N·m was previously reported (Moghadas *et al.*, 2012a). Another frictional torque study conducted by Moghadas *et al.* (2012b) showed that for metal-on-polymer based lumbar discs, the maximum frictional torques were 3.21 N·m (a metal socket articulates against a polymer ball) and 1.78 N·m (a polymer socket articulates against a metal ball). Frictional torque generated at the bearing surface will transmit to either the fixation interface or the facet joints, depending on the bearing design. For a constrained bearing design with a fixed centre of rotation (*e.g.* NuNec[®] cervical disc), the frictional torque is sustained by the implant-bone interface. In contrast, it was found for the mobile bearing design (*e.g.* Bryan[®] cervical disc) that the frictional force is offset by a reaction force in the facet joint (Sears *et al.*, 2006).

Thermal degradation of the bearing surface due to frictional heat generation is not a concern. The temperature rise between the bearing surfaces was previously measured by Kraft *et al.* (2012). For a PEEK based self-mating bearing combination, under the same testing condition as used in this thesis,

the maximum temperature was found to be 45°C (*i.e.* 8°C temperature rise) which is well below the glass transition temperature of PEEK (143°C).

The Stribeck analysis showed that this cervical disc will operate under boundary or mixed lubrication regime, both before and after wear testing to 5 million cycles. This finding is in agreement with the theoretical lubrication analysis conducted in chapter 4. Under natural cervical spine operating conditions, NuNec[®] cervical disc will operate under boundary lubrication regime with a lambda ratio value less than unity.

In comparison with lumbar disc lubrication studies (Moghadas *et al.*, 2012a), similar lubrication regimes were obtained. Metal-on-metal based lumbar discs also expected to operate under either boundary or mixed lubrication. Under these situations, surface asperities are either directly or partial contacted, hence the wear and friction are increased. A high wear rate generally means a large amount of wear debris generation. This is undesirable for disc replacement designs, since it may lead to adverse tissue response (*e.g.* inflammation and osteolysis) and reduces the longevity of the disc replacement (Ingham & Fisher, 2005).

6.5.3 Hydroxyapatite

The hydroxyapatite coating from the discs was lost during the experiments as a result of the cleaning process. The loss of the hydroxyapatite coating was not as a result of the wear testing as coating was also lost from the control disc where there was no motion. Clearly the loss of the hydroxyapatite coating is not something that would occur *in-vivo*, but it does raise a question about alternative methods of cleaning that may need to be developed for wear testing of implants that have hydroxyapatite. The loss of hydroxyapatite coating may be due to the Virkon disinfectant solution used during cleaning procedure. This solution contains sulfamic acid which can lead to dissolution of hydroxyapatite (Wu *et al.*, 1975).

6.6 Chapter summary

In this chapter, the tribological performance of the NuNec® cervical disc was assessed. The PEEK-on-PEEK self-mating bearing combination showed a steady state wear rate of 1.0 ± 0.9 mg/million cycles. The corresponding volumetric wear rate was 0.7 ± 0.7 mm³/million cycles. This all-polymer based cervical disc replacement is likely to operate under a boundary or mixed lubrication regime, and the main wear mechanism is abrasive wear. The hydroxyapatite coating from the discs was lost during the experiments.

Alternative methods of cleaning may need to be developed for wear testing of implants that have an hydroxyapatite coating, or implants may need to be tested without the coating.

Chapter 7

Overall Discussion & Conclusions

PEEK was initially proposed as a potential bearing material for total hip replacement. However, undesirable wear outcomes were obtained from hip simulator studies (Wang *et al.*, 1998; Wang *et al.*, 1999). In these experiments, an unreinforced PEEK socket articulated against an alumina ceramic head. Under this configuration, the obtained wear rate is roughly equal to 6 times that of the traditional hip bearing combination (UHMWPE against CoCrMo). Recently, more attention has been given on adoption of this promising material for low load demand applications, such as cervical disc replacement. A new bearing combination of a PEEK based self-mating articulation has been introduced, with great potential to overcome current wear debris induced issues, for example osteolysis (Ingham & Fisher, 2005; Brown, 2006) and metal ion accumulation (Zeh *et al.*, 2007; Hallab, 2008).

PEEK is proved to be biocompatible in either bulk form or particulate form (Toth, 2012). Its wear particles were found to be non-cytotoxic and less inflammatory than UHMWPE particles with similar size and shape (Hallab *et al.*, 2012). Apart from biocompatibility, other essential material attributes, for cervical disc application, include good mechanical strength and good wear resistance.

The research conducted in this thesis is aimed to further evaluate PEEK as a potential bearing material for cervical disc replacement. The theoretical lubrication and contact stress analysis conducted in chapter 4, shows that PEEK based cervical discs are likely to operate under a boundary lubrication regime, regardless of the radial clearance used. Extensive surface asperity contact is expected to happen, with the generation of wear debris likely. In the case of NuNec[®] cervical disc, the maximum contact stress between the bearing surfaces was found to be 32.1 MPa. This stress is well below the yield strength or fatigue strength of PEEK 450G. Thus, the structural safety of this device is assured.

As mentioned in section 5.2.1, polymers are susceptible to the effect of radiation sterilisation and ageing. According to the work conducted in chapter 5, it confirms that sterilisation combined with thermal ageing, induce negligible deterioration effects on the flexural strength of PEEK. The obtained average flexural fatigue strength is in the range of 99.4 to 107.4 MPa. In comparison, UHMWPE was reported to have a flexural fatigue strength of 31 MPa; after gamma sterilisation, this fatigue strength was further reduced to 18 MPa (Sauer *et al.*, 1996).

Good wear resistance is essential for the clinical success of disc replacement. In chapter 6, the tribological performance of the NuNec[®] cervical disc was assessed, with the intention to provide a better understanding of the performance of PEEK based cervical disc replacement. The major findings of this study are listed at below:

- The measured frictional torques is in the same order of magnitude as metal-on-metal based lumbar disc replacements.
- Stribeck analysis shows that this all-polymer based cervical disc replacement is likely to operate under a boundary or mixed lubrication regime.
- For the NuNec[®] cervical disc with the smallest footprint, a steady state wear rate of 1.0 ± 0.9 mg/million cycles (*i.e.* 0.7 ± 0.7 mm³/million cycles) is obtained. This wear rate is comparable to the reported wear rate of UHMWPE against CoCrMo bearing combination.
- The main wear mechanism is abrasion wear rather than fatigue wear. Disintegration of the bearing surfaces (*e.g.* pitting and delamination) was not seen.

In future studies, it may be interesting to perform wear tests of NuNec[®] cervical disc with different footprints, thus a full understanding of the relationship between implant size and wear rate can be obtained. An *in-vitro* hip simulator

study conducted by Lesile *et al.* (2008) shows that metal-on-metal based hip replacement with different bearing sizes (*i.e.* femoral head diameter) result in different run-in wear rates. This may due to the fact that different bearing sizes lead to different contact stress distribution. As a consequence, different wear mechanisms may occur.

Glossary

ACRONYMS:

AR: Axial Rotation

ASTM: American Society for Testing and Materials

CI: Confidence Interval

CMM: Coordinate Measuring Machine

CoCrMo: Cobalt Chromium Molybdenum Alloy

COR: Centre of Rotation

DSC: Differential Scanning Calorimetry

F/E: Flexion/Extension

FS: Fusion Surgery

FTIR: Fourier Transform Infrared Spectroscopy

GAG: Glycosaminoglycan

Hertz: Hertzian

ICI: Imperial Chemical Industries

IFI: Instrumental Falling Weight Impact

ISO: International Standard Organization

JKR: Johnson Kendall Roberts

LB: Lateral Bending

PAN: Poly-acryl-nitrile

PEEK: Poly-ether-ether-ketone

rhBMP-2: Bone Morphogenetic Protein-2

SEM: Scanning Electron Microscopy

TDR: Total Disc Replacement

UHMWPE: Ultra High Molecular Weight Polyethylene

WAXD: Wide Angle X-ray Diffraction

MATHMATIC SYMBOLS:

S_a : Arithmetical mean roughness (3D)

S_q : Root mean square roughness (3D)

λ_c : Profile filter which is used to separate waviness and roughness

R_1 : Radius curvature of ball component

R_2 : Radius curvature of socket component

c : Radial clearance equals to the difference between the R_2 and R_1

E' : Equivalent elastic modulus for the two bearing material

R : Equivalent radius for ball and socket

E : Young's modulus of the material

ν : Poisson's ratio of the material

F : Applied force (in chapter 3) or flexural yielding load (in chapter 5)

P_{max} : Maximum contact stress

P : Loading stress component of the JKR contact model

P' : Adhesion stress component of the JKR contact model

a : Real contact radius for JKR contact model

γ : Work of adhesion per unit area

h_{\min} : Minimum lubrication film thickness

η : Viscosity of the lubricant

u : Entraining velocity of the disc

E^* : Equivalent modulus of elasticity

λ : Lambda ratio

σ : Compound surface roughness

ω : Angular velocity in radians

δ : Flexural yielding displacement

l : Span length for three-point flexural bending

b : Width of the PEEK 450G specimen

d : Thickness of the PEEK 450G specimen

y_i : Dependent variable

x_i : Independent variable

$\hat{\sigma}_{\beta_1}$: Standard errors of gradient of the obtained Stress-life fatigue curve

$\hat{\sigma}_{\beta_0}$: Standard errors of intercept of the obtained Stress-life fatigue curve

$\hat{\sigma}_e$: Unbiased mean error

y_i : Actual stress level

\hat{y}_i : Predicted stress level according to the obtained linear regression line

M_z : Bending moment in z-axis

M_x : Bending moment in x-axis

M_y : Bending moment in y-axis

S_{sk} : Surface skewness (3D)

T : Average peak frictional torque

f : Friction factor

Z : Sommerfeld number

r : Radius of the ball component of the NuNec[®] disc

θ : Angular displacement in each motion (extension-flexion, lateral bending, and axial rotation)

h : Test frequency

\bar{X} : Mean frictional torque of each datum point

$t_{\alpha/2, n-1}$: t-critical value

S_E : Standard error

s : Standard deviation of each datum point

n : Number of measurements

Appendix A

*The real contact radius for
ball-on-socket based cervical TDRs
(see section 4.5)*

Please note:

For Johnson-Kendall-Roberts contact model, the real contact radius (a) is defined as below

$$a = \sqrt[3]{\frac{3R}{4E'} \left(F + 3\gamma\pi R + \sqrt{6\gamma\pi R F + (3\gamma\pi R)^2} \right)}$$

By using the parameter values from table 4.1, we can obtain the real contact radius when under 150 N load.

Step 1:

$$E' = \frac{E}{2(1-\nu^2)} = \frac{3.7 \times 10^6}{2(1-0.36^2)} = 2.125 \times 10^6 \text{ (Pa)}$$

$$R = \frac{R_1(R_1 + c)}{c} = \left(\frac{6.3(6.3 + 0.7)}{0.7} \right) / 1000 = 0.063(m)$$

Step 2:

$$\frac{3R}{4E'} \left(F + 3\gamma\pi R + \sqrt{6\gamma\pi R F + (3\gamma\pi R)^2} \right)$$

→

$$\frac{3 \times 0.063}{4 \times 2.125 \times 10^6} \left(150 + 3 \times 0.088 \times \pi \times 0.063 + \sqrt{6 \times 0.088 \times \pi \times 0.063 \times 150 + (3 \times 0.088 \times \pi \times 0.063)^2} \right)$$

$$= 3.423 \times 10^{-9} (m)$$

Step 3:

$$a = \sqrt[3]{\frac{3R}{4E'} \left(F + 3\gamma\pi R + \sqrt{6\gamma\pi R F + (3\gamma\pi R)^2} \right)}$$

→

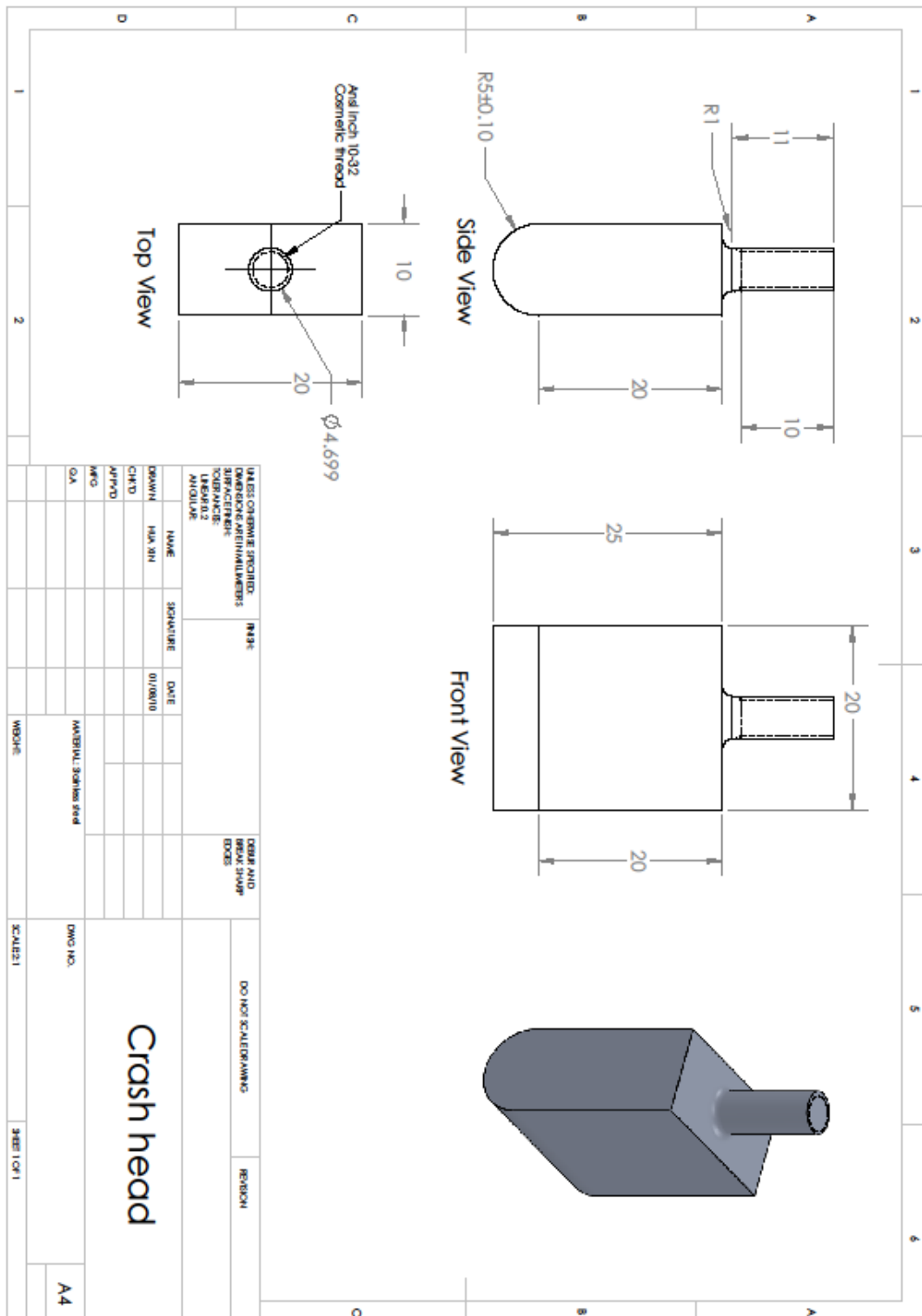
$$a = \sqrt[3]{3.423 \times 10^{-9}} = 1.507 \times 10^{-3} (m) \approx 1.51(mm)$$

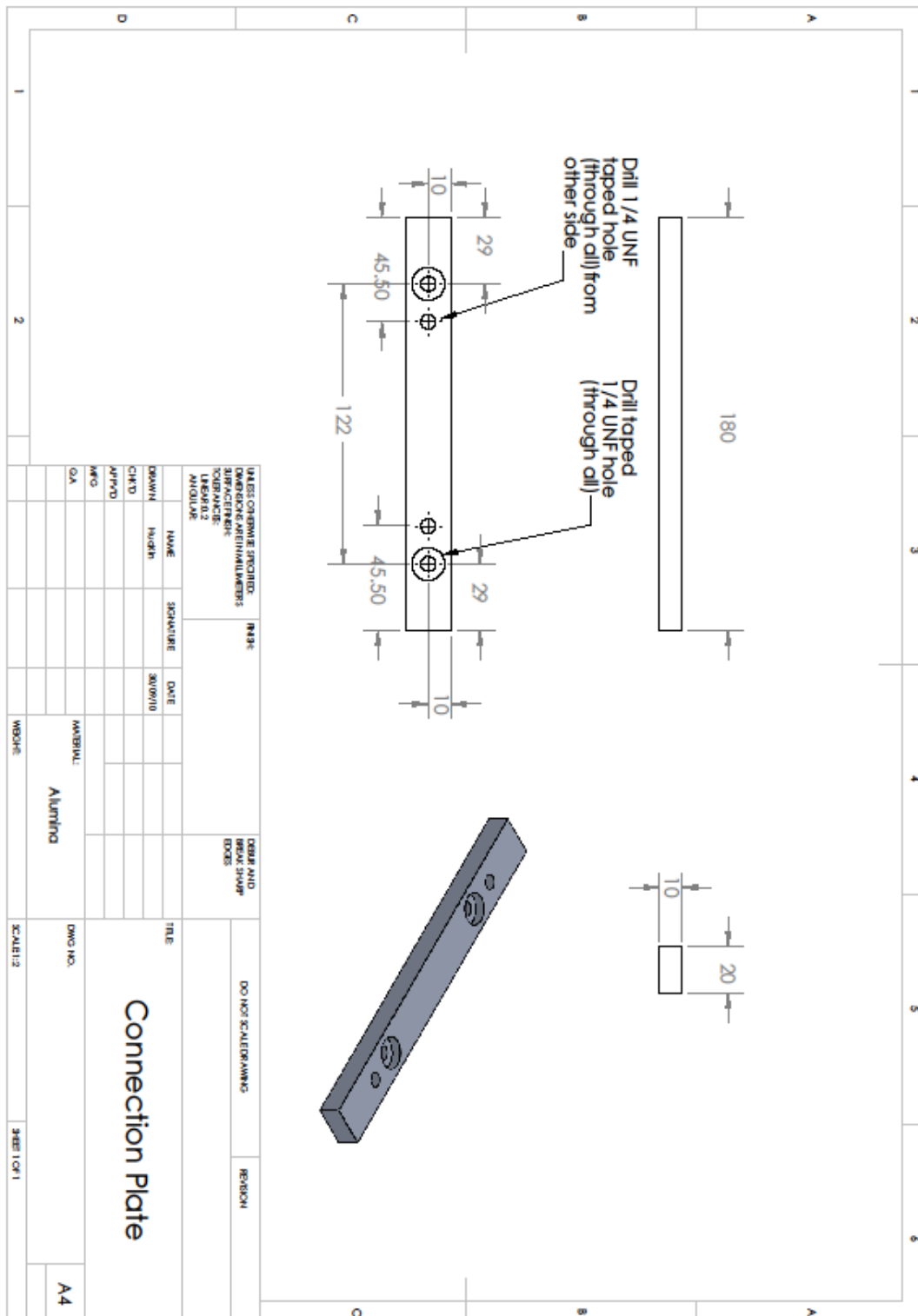
Appendix B

*The engineering drawings of the
three-point bending test rig
(see section 5.3.3)*

Please note:

This aluminium test rig is designed according to ISO 178 (2003) standard, and consists of one crash-head, two upright supporters, and one connection plate.





Appendix C

*The engineering drawings of the
NuNec[®] disc fixtures
(see section 6.3.2)*

Please note:

This stainless steel disc fixture consists of two essential parts (ball fixture and socket fixture). Ball fixture is for the upper NuNec[®] disc component with a concave articulating surface; socket fixture is for the lower NuNec[®] disc component with a convex articulating surface

Reference

Aaronson, P.I., Ward, J.P.T. and Connelly, M.J. (2012) **The Cardiovascular System at a Glance**. 4th ed. Oxford: Blackwell Publishing. pp. 18-20.

Abu, Bakar M.S., Cheng, M.H.W., Tang, S.M. *et al.* (2003) Tensile properties, tension-tension fatigue and biological response of polyetheretherketone-hydroxyapatite composites for load-bearing orthopedic implants. **Biomaterials**, 24 (13): 2245-2250.

Adams, G.G. (2012) "Chapter 4-1: Contact Mechanics" In: Bruce, R.W. (ed.) **Handbook of Lubrication and Tribology, Volume II: Theory and Design**. 2nd ed. Florida: CRC Press. pp. 1-18.

Anderson, P.A., Rouleau, J.P., Bryan, V.E. *et al.* (2003) Wear analysis of the Bryan cervical disc prosthesis. **Spine**, 28 (20): S186-S194.

Anderson, P.A. and Rouleau, J.P. (2004) Intervertebral Disc Arthroplasty. **Spine**, 29 (23): 2779-2786.

ASTM F2003-02 (2008) "Standard Test Methods for Accelerated Aging of Ultra-High Molecular Weight Polyethylene after Gamma Irradiation in Air" American Society for Testing and Materials, Pennsylvania, USA.

Available from <http://www.astm.org/Standards/F2003.htm>

ASTM F2026 (2010) "Standard specification for PEEK polymers for surgical implant application" American Society for Testing and Materials, Pennsylvania, USA.

Available from <http://www.astm.org/Standards/F2026.htm>

ASTM F2346 (2005) "Standard Test Methods for Static and Dynamic Characterization of Spinal Artificial Discs" American Society for Testing and Materials, Pennsylvania, USA.

Available from <http://www.astm.org/Standards/F2346.htm>

ASTM F2423 (2005) "Standard Guide for Functional, Kinematic, and Wear Assessment of Total Disc Prostheses" American Society for Testing and Materials, Pennsylvania, USA.

Available from <http://www.astm.org/Standards/F2423.htm>

ASTM F2778 (2009) "Standard Test Method for Measurement of Percent Crystallinity of Polyetheretherketone (PEEK) Polymers by means of Specular Reflectance Fourier Transform Infrared Spectroscopy (R-FTIR)" American Society for Testing and Materials, Pennsylvania, USA.

Available from <http://www.astm.org/Standards/F2778.htm>

Auerbach, J.D., Jones, K.J., Fras, C.I. *et al.* (2008) The prevalence of indications and contraindications to cervical total disc replacement. **Spine**, 8 (5): 711-716.

Baker, D.A., Hastings, R.S. and Pruitt L. (2000) Compression and tension fatigue resistance of medical grade ultra high molecular weight polyethylene: the effect of morphology, sterilization, aging and temperature. **Polymer**, 41 (2): 795-808.

Bao, Q.B., Songer, M., Pimenta, L. *et al.* (2007) Nubac Disc Arthroplasty: Preclinical Studies and Preliminary Safety and Efficacy Evaluations. **SAS Journal**, 1 (1): 36-45.

Béland, S. (1990) **High Performance Thermoplastic Resins and Their Composites**. New Jersey: Noyes Publications. pp. 10-36.

Bhushan, B. (1998) "Chapter 21: Tribology- friction, wear, and lubrication" In: Dorf, R.C. (ed.) **The Engineering Handbook**. Florida: CRC Press. pp. 1-6.

Brillhart, M. and Botsis, J. (1992) Fatigue fracture behaviour of PEEK: 2. Effects of thickness and temperature. **Polymer**, 33 (24): 5225-5232.

Brillhart, M. and Botsis, J. (1994) Fatigue crack growth analysis in PEEK. **International Journal of Fatigue**, 16 (2): 134-140.

Brillhart, M., Gregory, B.L. and Botsis, J. (1991) Fatigue fracture behaviour of PEEK: 1. Effects of load level. **Polymer**, 32 (9): 1605-1611.

Brown, S.A. (2006) "Chapter 2: Synthetic biomaterials for spinal applications" In: Kurtz, S.M. and Edidin, A.A. (ed.) **Spine Technology Handbook**. Burlington: Elsevier Academic Press. pp.11-32.

Brown, T., Bao, Q.B. and Hallab, N. (2009) "Biotribological Assessment of NuNec, a PEEK on PEEK Cervical Disc Replacement According to ISO and ASTM Recommendations" In **9th SAS meeting. London, 28 April – 1 May 2009**. Abstract No. 94 (p.100).

BS 3518-1 (1993) "Methods of Fatigue Testing-Part 1: guide to general principles" British Standards Institution, UK.

Available from <http://shop.bsigroup.com/en/SearchResults/?q=3518-1:1993>

Buggy, M. and Dillon, G. (1991) Flexural fatigue of carbon fibre-reinforced PEEK laminates. **Composites**, 22 (3): 191-198.

Cartwright, K. and Devine, J. (2005) **Investigation into the effect of gamma sterilization (200kGy) and accelerated ageing on the properties of PEEK-OPTIMA**. Thornton Cleveleys: Invibio Ltd.

Available from http://calvaryspine.com/pdfs/Ageing_and_Gamma.pdf

Cassinelli, E.H., Hall, R.A. and Kang, J.D. (2001) Biochemistry of intervertebral disc degeneration and the potential for gene therapy applications. **Spine**, 1 (3): 205-214.

Charles, H.R., Souad, R. and Chrisine, C. (2001) In vivo biocompatibility testing of PEEK polymer for a spinal implant system: A study in rabbits. **Journal of Biomedical materials Research**, 62 (4): 488-498.

Clellow, J.P., Pylios, T. and Shepherd, D.E.T. (2008) Soft layer bearing joints for spine arthroplasty. **Materials & Design**, 29 (10): 1981-1985.

Cohen, A. (1983) Comparing Regression Coefficients across Subsamples: A Study of the Statistical Test. **Sociological Method & Research**, 12 (1): 77-94.

Cripton, P.A., Kroeker, S.G. and Saari, A. (2006) "Chapter 5: Musculature Actuation and Biomechanics of the Spine" In: Kurtz, S.M. and Edidin, A.A. (ed.) **Spine Technology Handbook**. Burlington: Elsevier Academic Press. pp. 99-144.

Curtis, D.C., Moore, D.R., Slater, B. *et al.* (1998) Fatigue testing of multi-angle laminates of CF/PEEK. **Composites**, 19 (6): 446-452.

Delamarter, R.B., Murrey, D., Janssen, M.E. *et al.* (2010) Results at 24 months from the prospective, randomized, multicenter-Investigational devices exemption trial of Prodisc-C versus anterior cervical discectomy and fusion

with 4-year follow-up and continued access patients. **SAS Journal**, 4 (4): 122-128.

Dintenfass, L. (1985) **Blood Viscosity**. Lancaster: MTP Press Limited. pp. 20-21.

Dintwa, E., Tijskens, E. and Ramon, H. (2008) On the accuracy of the Hertz model to describe the normal contact of soft elastic spheres. **Granular Matter**, 10 (3): 209-221.

Dvorak, J., Antinnes, J.A., Panjabi, M., *et al.* (1992) Age and gender related normal motion of the cervical spine. **Spine**, 17 (10): 393-398.

Faghihnejad, A. and Zeng, H. (2013) "Chapter 1: Introduction" In Zeng, H. (ed.) **Polymer Adhesion, Friction, and Lubrication**. New Jersey: John Wiley & Sons Inc. pp. 1-18.

Fogh-Andersen, N., Altura, B.M., Altura, B.T. *et al.* (1995) Composition of interstitial fluid. **Clinical Chemistry**, 41 (10): 1522-1525.

Galbusera, F., Bellini, C.M., Brayda-bruno, M. *et al.* (2008) Biomechanical studies on cervical total disc arthroplasty: a literature review. **Clinical Biomechanics**, 23 (9): 1095-1104.

Goodman, S.B. (2007) Wear particles, periprosthetic osteolysis and the immune system. **Biomaterials**, 28 (34): 5044-5048.

Goryacheva, G. (1998) **Contact Mechanics in Tribology**. Burlington: Kluwer Academic Publishers. pp. 1-60.

Graham, J. (2006) "Chapter 13: Standard Test Methods for Spine Implants" In Kurtz, S.M. and Edidin, A.A. (ed.) **Spine Technology Handbook**. Burlington: Elsevier Academic Press. pp. 397-439.

Grupp, T.M., Meisel, H.J., Cotton, J.A. *et al.* (2010) Alternative bearing materials for intervertebral disc arthroplasty. **Biomaterials**, 31(3): 523-532.

Guerin, H.A. and Elliott, D.M. (2006) "Chapter 3: Structure and Properties of Soft Tissues in the Spine" In Kurtz, S.M. and Edidin, A.A. (ed.) **Spine Technology Handbook**. Burlington: Elsevier Academic Press. pp. 35-63.

Hall, R.M., Unsworth, A., Wroblewski, B.M. *et al.* (1994) Frictional characterization of explanted Charnley hip prostheses. **Wear**, 175 (1-2): 159-166.

Hallab, N.J. (2008) "Intervertebral disc joint replacement technology" In Revell, A.P. (ed.) **Joint Replacement Technology**. Cambridge: Woodhead Publishing Limited. pp. 515-544.

Hallab, N.J. , McAllister, K., Brady, M. *et al.* (2012) Macrophage reactivity to different polymers demonstrates particle size- and material-specific reactivity: PEEK-OPTIMA particles versus UHMWPE particles in the submicron, micron, and 10 micron size ranges. **Journal Biomedical Materials Research**, 100b (2): 480-492.

Hamrock B.J. and Dowson, D. (1997) Isothermal EHL at point contacts, part III-fully flooded results. **Journal of Lubrication Technology**, 99 (2): 264-276.

Harsha, A.P. and Joyce, T.J. (2011) Challenges associated with using bovine serum in wear testing orthopaedic biopolymers. **Proceedings of the**

Institution of Mechanical Engineers, Part H: Journal of Engineering in Medicine, 225(10): 948-958.

Hattori, S., Oda, H., Kawai, S., *et al.* (1981) Cervical Intradiscal Pressure in Movements and Traction of the Cervical Spine. **Zeitschrift Fur Orthopadie**, 119: 568-569.

Heller, J.G., Sasso, R.C., Papadopoulos, S.M., *et al.* (2008) Comparison of Bryan cervical disc arthroplasty with anterior cervical decompression and fusion. **Spine**, 34 (2): 101-107.

Hemmerlinch, K.J. (1998) General aging theory and simplified protocol for accelerated aging of medical devices. **Medical Plastic and Biomaterials Magazine**. July/August , p. 16-23.

Hilibrand, A.S. and Robbins, M. (2004) Adjacent segment degeneration and adjacent segment disease: the consequence of spinal fusion? **Spine**, 4 (6): s190-s194.

Howling, G.I., Sakoda, H., Antonarulrajah, A., *et al.* (2003) Biological response to wear debris generated in carbon based composites as potential bearing surfaces for artificial hip joints. **Journal of Biomedical Material Research B - Applied Biomaterials**, 67 (2): 758-764.

Hukins, D.W.L., Mahomed, A. and Kukureka, S.N. (2008) Accelerated aging for testing polymeric biomaterials and medical devices. **Medical Engineering & Physics**, 30 (10): 1270-1274.

Hutchings, I.M. (1992) **Tribology: Friction and Wear of Engineering Materials**, Arnold, E. (ed.). London: CRC Press. pp. 70-75.

Ingham, E. and Fisher, J. (2005) The role of macrophages in osteolysis of total joint replacement. **Biomaterials**, 26 (11): 1271-1286.

ISO 14242-2 (2000) "Implants for surgery – Wear of total hip joint prostheses – Part 2: Methods of measurement" International Organization for Standardization, Geneva, Switzerland.

Available from: http://www.iso.org/iso/catalogue_detail.htm?csnumber=25376

ISO 178 (2003) "Plastics-Determination of flexural properties" International Organization for Standardization, Geneva, Switzerland.

Available from http://www.iso.org/iso/catalogue_detail.htm?csnumber=45091

ISO 18192-1 (2011) "Implants for Surgery – Wear of Total Intervertebral Spinal Disc Prostheses Part 1: Loading and Displacement Parameters for Wear Testing and Corresponding Environmental Conditions" International Organization for Standardization, Geneva, Switzerland.

Available from http://www.iso.org/iso/catalogue_detail.htm?csnumber=57235

ISO 3274 (1996) "Geometric Product Specification (GPS) – Surface texture: Profile method – Nominal characteristics of contact (stylus) instruments" International Organization for Standardization, Geneva, Switzerland.

Available from

http://www.iso.org/iso/home/store/catalogue_tc/catalogue_detail.htm?csnumber=1916

ISO 4287 (1998) "Geometrical Product Specification (GPS) – Surface texture: Profile method – Terms, definitions and surface texture parameters" International Organization for Standardization, Geneva, Switzerland.

Available from

http://www.iso.org/iso/home/store/catalogue_tc/catalogue_detail.htm?csnumber=10132

Jaekel, D.J., Medel, F.J. and Kurtz, S.M. (2009) Validation of Crystallinity Measurements of Medical Grade PEEK Using Specular Reflectance FTIR-microscopy. **Medical PEEK Lexicon** [online].

Available from http://www.medicalpeek.org/pub_reports/view/70

Jeffery, M.T. (2012) "Chapter 7: Biocompatibility of Polyaryl-ether-ether-ketone Polymers" In Kurtz, S.M. (ed.) **PEEK Biomaterial Handbook**. Oxford: Willian Andrew. pp. 81-92.

Jin, Z.M., Dowson, D. and Fisher, J. (1997) Analysis of fluid film lubrication in artificial hip joint replacements with surfaces of high elastic modulus. **Proceedings of the Institution of Mechanical Engineers, Part H: Journal of Engineering in Medicine**, 211 (3): 247-256.

Jin, Z. and Fisher, J. (2008) "Chapter 2: Tribology in joint replacement" In Revell, A.P. (ed.) **Joint Replacement Technology**. Cambridge: Woodhead Publishing Limited. pp. 31-56.

Jin, Z., Medley, J.B. and Dowson, D. (2003) Fluid film lubrication in artificial hip joints. **Tribological Research and Design for Engineering Systems**, 221 (3): 237-256.

Johnson, G.R. (2008) "Biomechanics of joints" In Revell, A.P. (ed.) **Joint Replacement Technology**. Cambridge: Woodhead Publishing Limited. pp. 1-30.

Jones, D.P., Leach, D.C. and Moore, D.R. (1985) Mechanical properties of poly(ether-ether-ketone) for engineering applications. **Polymer**, 26 (9): 1385-1393.

Joshi, V.D. and Joshi-Mendhurwar, S. (2005) **Physiology: Prep Manual for Undergraduates. 3rd ed.** New Delhi: Elsevier India.

Joyce, T. (2009) "Chapter 6: Biopolymer Tribology" In Sinha, K.S. and Briscoe B.J. (ed.) **Polymer Tribology**. London: Imperial College Press. pp. 227-266.

Khurana, I. (2007) **Textbook of Human Physiology for Dental Students**. New Delhi: Elsevier India. pp. 212-214.

Kraft, M., Koch, D. and Bushelow, M. (2011) Evaluation of PEEK on PEEK as a new articulation concept for cervical total disc replacement devices. In **Annual meeting of the German spine society**. Hamburg, 2011. Poster 97.

Available from http://www.medicalpeek.org/pub_reports/view/143

Kraft, M., Koch, K.D. and Bushelow, M. (2012) An investigation into PEEK-on-PEEK as a bearing surface candidate for cervical total disc replacement. **Spine**, 12 (7): 603-611.

Kurtz, S.M. (2012a) **PEEK Biomaterial Handbook**. Oxford: William Andrew. pp. 9-23.

Kurtz, S.M. (2012b) **PEEK Biomaterials Handbook**. Oxford: William Andrew Publishing. pp 75-79.

Kurtz, S.M. and Devine, J.N. (2007) PEEK biomaterials in trauma, orthopedic and spinal implants. **Biomaterials**, 28 (32): 4845-4869.

Kurtz, S.M. and Nevelos, J. (2012) "Chapter 16 - Arthroplasty Bearing Surfaces" In Kurtz, S.M. (ed.) **PEEK Biomaterials Handbook**. Oxford: William Andrew Publishing. pp. 261-275.

Kurtz, S.M. (2006) "Chapter 11: Total Disc Arthroplasty" In Kurtz, S.M. and Edidin, A.A. (ed.) **Spine Technology Handbook**. Burlington: Elsevier Academic Press. pp. 303-370.

Kurtz, S.M. and Edidin, A.A. (2006) **Spine Technology Handbook**. Burlington: Elsevier Academic Press. pp. 1-9.

Lambert, B.J., Tang, F.W. and Rogers, W.J. (2001) "Chapter 2.6.1 temperature based accelerated ageing" In Ward, S. (ed.) **Polymer in medical applications**. Shrewsbury: Rapra technology limited. pp. 15-17.

Lesile, I., Williams, S., Brown, C. *et al.* (2008) Effect of bearing size on the long-term wear, wear debris and ion levels of large diameter metal-on-metal hip replacements- An in vitro study. **Journal of biomedical materials research: B applied biomaterials**, 87 (1): 163-172

Louis-Ugbo, Pedlow, F.X. and Heller, J.G. (2012) "Chapter 1: Anatomy of the cervical spine" In Benzel, E.C. (ed.) **The Cervical Spine**. 5th ed. Philadelphia: Lippincott William & Wilkins. pp.1-33.

Lu, S., Buchanan, F.J. and Orr, J.F. (2002) Analysis of variables influencing the accelerated ageing behaviour of ultra-high molecular weight polyethylene (UHMWPE). **Polymer Testing**, 21(6): 623-631.

Ludema, K.C. (2012) "Chapter 1-1: Tribology" In Bruce, R.W. (ed.) **HandBook of Lubrication and Tribology, Volume II: Theory and Design**. 2nd ed. Florida: CRC Press. pp. 1-6.

Maniadakis, N and Gray, A. (2000) The economic burden of back pain in the UK. **Pain**, 84 (1): 95-103.

Massey, L.K. (2005) **The Effect of Sterilization Methods on Plastics and Elastomers**. 2nd ed. NewYork: William Andrew Publishing. pp. 1-15.

Mattei, L., Puccio, F.D., Piccoigallo, B. *et al.* (2011) Lubrication and wear modelling of artificial hip Joints: A review. **Tribology international**, 44(5): 532-549.

McCarberg, B.H., Stanos, S. and D'Arcy, Y. (2012) **Back and Neck Pain**. New York: Oxford University Press. pp. 1-5.

Mcminn, R.M.H., Hutchings, R.T. and Logan, B.M. (1998) **Human Anatomy-Concise Handbook**. London:Manson Publishing Ltd. pp. 15-17, 77-81.

Moghadas, P.M, Mahomed, A., Hukins, D.W.L. *et al.* (2012a) Friction in metal-on-metal total disc arthroplasty: Effect of ball radius. **Journal of Biomechanics**, 45 (3): 504-509.

Moghadas, P.M., Shepherd, D.E.T., Hukins, D.W.L. *et al.* (2012b) Polymer-on-metal or metal-on-polymer total disc arthroplasty: does it make a difference? **Spine**, 37 (21): 1834-1838.

Myshkin, N.K. and Kovalev, A.V. (2009) "Chapter 1: Adhesion and friction of polymers" In Sinha, S.K. and Briscoe, B.J. (ed.) **Polymer Tribology**. London: Imperial College Press. pp. 3-37.

Nabhan, A., Ahlhelm, F., Pitzen, T. *et al.* (2007) Disc replacement using Prodisc-c versus fusion: a prospective randomised and controlled raddiological and clinical study. **European Spine Journal**, 16 (3): 423-430.

- Nachemson, A.L. (1981) Disc Pressure Measurements. **Spine**, 6: 93-97.
- Nikolar, K.M. and Alexander, V. K. (2009) "Chapter 1: Adhesion and Friction of Polymers" In Sinha, K.S. and Briscoe, B.J. (ed.) **Polymer Tribology**. London: Imperial College Press. pp.3-37.
- Nisitani, H., Noguchi, H. and Kim, Y.H. (1992) Evaluation of fatigue strength of plain and notched specimens of short carbon-fiber reinforced polyetheretherketone in comparison with polyetheretherketone. **Engineering fracture mechanics**, 43 (5): 685-705.
- Oskouian, R., Whitehill, R., Samii, A. *et al.* (2004) The future of spinal arthroplasty: a biomaterial perspective. **Neurosurg Focus**, 17 (3): 10-14.
- Panjabi, M.M., Crisco, J.J., Vasavada, A. *et al.* (2001) Mechanical Properties of the Human Cervical Spine as Shown by Three-Dimensional Load-Displacement Curves. **Spine**, 26 (24): 2692-2700.
- PEEK Materials Properties Guide (2012) **Victrex Ltd.** Available from http://www.victrex.com/docs/literature-docs/Victrex_PROPERTIES-GUIDE_EN_Metric.pdf
- PEEK Optima-LT1 product specification (2009) **Invibio Ltd.** Available from <http://www.invibio.com/resource-library/brochures-preview.php?id=30>
- PEEK Processing Guide (2012) **Victrex Ltd.** Available from <http://www.victrex.com/docs/literature-docs/Processing%20Guide.pdf>
- PEEKTM 450G datasheet (2012) **Victrex Ltd.** Available from <http://www.victrex.com/en/peek-450g-polymer.php>

Pruitt, L.A. and Chakravartula, A.M. (2011) **Mechanics of Biomaterials – Fundamental Principles for Implant Design**. NewYork:Cambridge University Press. pp. 456-460.

Rae, P.J., Brown, E.N. and Orlor, E.B. (2007) The mechanical properties of poly(ether-ether-ketone) (PEEK) with emphasis on the large compressive strain response. **Polymer**, 48 (2): 598-615.

Ratner, B.D. (2012) “Degradation of materials in the Biological Environment” In Ratner, B.D., Hoffman A.S. and Schoen, F.J. *et al.* (ed.) **Biomaterial Science: an introduction to materials in medicine**. 3rd ed. Oxford: Elsevier academic press. pp. 675-715.

Reitman, M., Jaekel, D., Siskey, R. *et al.* (2012) “Chapter 4: Morphology and crystalline architecture of polyaryletherketones” In Kurtz S.M. (ed.) **PEEK Biomaterial Handbook**. Oxford: William Andrew Publishing. pp. 49-59.

Richaud, E., Ferreira, P., Audouin, L. *et al.* (2010) Radiochemical ageing of poly-ether-ether-keone. **European Polymer Journal**, 46 (4): 731-743.

Ritchie, R.O. (2003) “Fatigue of polymer” In Ritchie, R.O. and Murakami Y. **Comprehensive structural integrity- Volume 4: cyclic loading and fatigue**. Perganmon: Elsevier. pp. 390-394.

Rivard, C.H., Rhalmi, S. and Coillard, C. (2001) In vivo biocompatiblity testing of PEEK polymer for a spinal implant system: a study in rabbits. **Journal of Biomaterial Marerials Research**, 62 (4): 488-498.

Roberts, S., Evans, H.,Trivedi, J. *et al.* (2006) Histology and pathology of the human intervertebral disc. **The Journal of Bone and Joint Surgery**, 88a (2): 10-14.

Robertson, J.T., Papadopoulos, S.M. and Traynelis, V.C. (2005) Assessment of adjacent-segment disease in patients treated with cervical fusion or arthroplasty : a prospective 2-year study. **Journal of Neurosurgery: Spine**, 3 (6): 417-423.

Roselli, R.J. and Diller, K.R. (2011) **Biotransport: Principles and Applications**. New York: Springer. pp. 139-140.

Saib, K.S., Evan, W.J. and Isaac, D.H. (1993) The role of microstructure during fatigue crack growth in poly(aryl-ether-ether-ketone) (PEEK). **Polymer**, 34 (15): 3198-3203.

Salvia, P., Champagne, O., Feipel, V. *et al.* (2006) Clinical and goniometric evaluation of patients with spasmodic torticollis. **Clinical Biomechanics**, 21 (4): 323-329.

Sauer, W.L., Weaver, K.D. and Beals, N.B. (1996) Fatigue performance of ultra-high molecular-weight polyethylene: effect of gamma radiation sterilization. **Biomaterials**, 17 (20): 1929-1935.

Schambron, T., Lowe, A. and McGregor, H.V. (2010) Effects of environmental ageing on the static and cyclic bending properties of braided carbon fibre/PEEK bone plates. **Composites Part B-Engineering**, 39 (7-8): 1216-1220.

Scholes, S.C. and Unsworth, A. (2007) The wear properties of CFR-PEEK-Optima articulating against ceramic assessed on a multidirectional pin-on-plate machine. **Proceedings of the Institution of Mechanical Engineers, Part H: Journal of Engineering in Medicine**, 221(3): 281-289.

Scholes, S.C. and Unsworth, A. (2000) Comparison of friction and lubrication of different hip prostheses. **Proceedings of the Institution of Mechanical Engineers, Part H: Journal of Engineering in Medicine**, 214 (1): 49-57.

Scholes, S.C., Green, S.M. and Unsworth, A. (2001) The wear of metal-on-metal total hip prostheses measured in a hip simulator. **Proceedings of the Institution of Mechanical Engineers, Part H: Journal of Engineering in Medicine**, 215 (6): 523-530.

Scholes, S.C. and Unsworth, A. (2009) Wear studies on the likely performance of CFR-PEEK/CoCrMo for use as artificial joint bearing materials. **Journal of Materials Science: Materials in Medicine**, 20 (1): 163-170.

Scholes, S.C. and Unsworth, A. (2010) The wear performance of PEEK-Optima based self-mating couples. **Wear**, 268 (3-4): 380-387.

Sears, W.R., Mccombe, P.F. and Sasso, R.C. (2006) Kinematics of cervical and lumber total disc replacement . **Seminars in Spine Surgery**, 18 (2): 117-129.

Shaheen, A. and Shepherd, D.E.T. (2007) Lubrication regimes in lumber total disc arthroplasty. **Proceedings of the Institution of Mechanical Engineers, Part H: Journal of Engineering in medicine**, 221 (6): 621-627.

Sheldon, M.R. (2009) **Introduction to probability and statistics for engineers and scientists**. 4th ed. London: Elsevier Academic Press. pp. 247-251.

Sınmazçelik, T. and Yılmaz, T. (2007) Thermal aging effects on mechanical and tribological performance of PEEK and short fiber reinforced PEEK composites. **Materials & Design**, 28 (2): 641-648.

Sobieraj, M.C., Murphy, J.E., Brinkman, J.G. *et al.* (2010) Notched fatigue behavior of PEEK. **Biomaterials**, 32 (35): 9156-9162.

Sobieraj, M.C. and Rimnac, C.M. (2012) "Chapter 5: Fracture, fatigue and notch behavior of PEEK" In Kurtz, S.M. (ed.) **PEEK Biomaterial Handbook**. Oxford: William Andrew Publishing. pp. 61-71.

Stuart, G. (2012) "Chapter 3: Compounds and composite materials" In Kurtz, S.M. (ed.) **PEEK Biomaterial Handbook**. Oxford: William Andrew Publishing. pp. 23-48.

Tang, S.M., Cheang, P., AbuBakar, M.S. *et al.* (2004) Tension-tension fatigue behaviour of hydroxyapatite reinforced polyetheretherketone composites. **International Journal of Fatigue**, 26 (1): 49-57.

Teoh, S.H. (2000) Fatigue of biomaterials: a review. **International Journal of Fatigue**, 22 (10): 825-837.

Tipper, J.L., Firkins, P.J., Besong, A.A. *et al.* (2001) Characterization of wear debris from UHMWPE on zirconia ceramic, metal-on-metal and alumina ceramic-on-ceramic hip prostheses generated in a physiological anatomical hip joint simulator. **Wear**, 250 (1-12): 120-128.

Toth, J.M., Wang, M., Estes, B.T. *et al.* (2006) Polyetheretherketone as a biomaterial for spinal applications. **Biomaterials**, 27 (3): 324-334.

Urban, J.P.G. and Roberts, S. (2003) Degeneration of the intervertebral disc. **Arthritis Research & Therapy**, 5 (3): 120-130.

Utzschneider, S., Becker, F., Grupp, T.M. *et al.* (2010) Inflammatory response against different carbon fiber-reinforced PEEK wear particles compared with UHMWPE in vivo. **Acta Biomaterialia**, 6 (11): 4296-4304.

Van Ooij, A., Oner, F.C. and Verbout, A.J. (2003) Complication of artificial disc replacement: a report of 27 patients with the SB Charité disc. **Journal of Spinal Disorder Technique**, 16 (4): 369-383.

Walsh, K., Crudds, M. and Coggon, D. (1992) Low back pain in eight areas of Britain. **Journal of Epidemiology and Community Health**, 46 (3): 227-230.

Wang, A., Lin, R., Polineni, V.K. *et al.* (1998) Carbon fiber reinforced poly-ether-ether-ketone composite as a bearing surface for total hip replacement. **Tribology International**, 31 (11): 661-667.

Wang, A., Lin, R., Stark, C. *et al.* (1999) Suitability and limitations of carbon fiber reinforced PEEK composites as bearing surfaces for total joint replacements. **Wear**, 225-229 (2): 724-727.

Wenzel, S.A. and Shepherd, D.E.T. (2007) Contact stresses in lumbar total disc arthroplasty. **Bio-Medical Materials and Engineering**, 17 (3): 169-173.

White, J.R. (2006) Polymer ageing: physics, chemistry or engineering? Time to reflect. **Comptes Rendus Chimie**, 7 (11-12): 1396-1408.

Windberger, U., Bartholovitsch, A., Plasenzotti *et al.* (2003) Whole blood viscosity, plasma viscosity and erythrocyte aggregation in nine mammalian species: reference values and comparison of data. **Experimental physiology**, 88 (3): 431-440.

Wu, M.S., Higuchi, W.I., Fox, J.L. *et al.* (1975) Kinetics and Mechanism of Hydroxyapatite crystal dissolution in weak acid buffers using the rotating disc method. **Journal of Dental Research**, 55 (3): 496-505.

Xin, H., Shepherd, D.E.T. and Dearn, K.D. (2012) PEEK (Poly-ether-ether-ketone) based cervical total disc arthroplasty: contact stress and lubrication analysis. **The Open Biomedical Engineering Journal**, 6: 73-79.

Xin, H., Shepherd, D.E.T. and Dearn, K.D. (2013a) Strength of poly-ether-ether-ketone: Effects of sterilisation and thermal ageing. **Polymer Testing**, 32 (6): 1001-1005.

Xin, H., Shepherd, D.E.T. and Dearn, K.D. (2013b) A Tribological assessment of a PEEK based self-mating total cervical disc replacement. **Wear**, 303 (1-2): 473-479.

Zechmeister, I., Winkler, R. and Mad, P. (2011) Artificial total disc replacement versus fusion for the cervical spine: a systematic review. **European Spine Journal**, 2 (2): 177-184.

Zeh, A., Planert, M., Siegert, G. *et al.* (2007) Release of cobalt and chromium ions into the serum following implantation of the metal-on-metal Maverick-Typer artificial lumbar disc (Medtronic Sofamor Danek). **Spine**, 32 (3): 348-352.

Zhang, G. and Schlarb, A.K. (2009) Correlation of the tribological behaviors with the mechanical properties of poly-ether-ether-ketones (PEEKs) with different molecular weights and their fiber filled composites. **Wear**, 266 (1-2): 337-344.

Zhang, S., Awaja, F., James, N. *et al.* (2011) Autohesion of plasma treated semi-crystalline PEEK: Comparative study of argon, nitrogen and oxygen treatments. **Colloids and Surfaces A: Physicochemical and Engineering Aspects**, 374 (1-3): 88-95.

Zhao, C.Q., Wang, L.M., Jiang, L.S. *et al.* (2007) The cell biology of intervertebral disc aging and degeneration. **Ageing Research Reviews**, 6 (3): 247-261.

Zurovsky, Y., Mitchell, G. and Hattingh, J. (1994) Composition and Viscosity of interstitial fluid of rabbits. **Experimental Physiology**, 80 (2): 203-207.